

2010-06-25

An Experimental Study on PEO Polymer Electrolyte Based All-Solid-State Supercapacitor

Yijing Yin

University of Miami, j.in@umiami.edu

Follow this and additional works at: https://scholarlyrepository.miami.edu/oa_dissertations

Recommended Citation

Yin, Yijing, "An Experimental Study on PEO Polymer Electrolyte Based All-Solid-State Supercapacitor" (2010). *Open Access Dissertations*. 440.

https://scholarlyrepository.miami.edu/oa_dissertations/440

This Open access is brought to you for free and open access by the Electronic Theses and Dissertations at Scholarly Repository. It has been accepted for inclusion in Open Access Dissertations by an authorized administrator of Scholarly Repository. For more information, please contact repository.library@miami.edu.

UNIVERSITY OF MIAMI

AN EXPERIMENTAL STUDY ON PEO POLYMER ELECTROLYTE BASED
ALL-SOLID-STATE SUPERCAPACITOR

By

Yijing Yin

A DISSERTATION

Submitted to the Faculty
of the University of Miami
in partial fulfillment of the requirements for
the degree of Doctor of Philosophy

Coral Gables, Florida

June 2010

©2010
Yijing Yin
All Rights Reserved

UNIVERSITY OF MIAMI

A dissertation submitted in partial fulfillment of
the requirements for the degree of
Doctor of Philosophy

AN EXPERIMENTAL STUDY ON PEO POLYMER ELECTROLYTE BASED
ALL-SOLID-STATE SUPERCAPACITOR

YIJING YIN

Approved:

Xiangyang Zhou, Ph.D.
Assistant Professor of Mechanical and
Aerospace Engineering

Terri A. Scandura, Ph.D.
Dean of the Graduate
School

Hongtan Liu, Ph.D.
Professor of Mechanical and
Aerospace Engineering

Na Li, Ph.D.
Assistant Professor of
Mechanical and
Aerospace Engineering

Chenzhong Li, Ph.D.
Assistant Professor of Biomedical
Engineering at Florida International University

YIJING YIN

(Ph.D., Mechanical and Aerospace Engineering)

An Experimental Study on PEO Polymer

(June 2010)

Electrolyte based All-Solid-State Supercapacitor

Abstract of a doctoral dissertation at the University of Miami.

Dissertation supervised by Professor Xiangyang Zhou.

No. of pages in text. (179)

Supercapacitors are one of the most important electrochemical energy storage and conversion devices, however low ionic conductivity of solid state polymer electrolytes and the poor accessibility of the ions to the active sites in the porous electrode will cause low performance for all-solid-state supercapacitors and will limit their application. The objective of the dissertation is to improve the performance of all-solid-state supercapacitor by improving electrolyte conductivity and solving accessibility problem of the ions to the active sites.

The low ionic conductivity (10^{-8} S/cm) of poly(ethylene oxide) (PEO) limits its application as an electrolyte. Since PEO is a semicrystal polymer and the ion conduction take place mainly in the amorphous regions of the PEO/Lithium salt complex, improvements in the percentage of amorphous phase in PEO or increasing the charge carrier concentration and mobility could increase the ionic

conductivity of PEO electrolyte. Hot pressing along with the additions of different lithium salts, inorganic fillers and plasticizers were applied to improve the ionic conductivity of PEO polymer electrolytes. Four electrode methods were used to evaluate the conductivity of PEO based polymer electrolytes. Results show that adding certain lithium salts, inorganic fillers, and plasticizers could improve the ionic conductivity of PEO electrolytes up to 10^{-4} S/cm. Further hot pressing treatment could improve the ionic conductivity of PEO electrolytes up to 10^{-3} S/cm. The conductivity improvement after hot pressing treatment is elucidated as that the spherulite crystal phase is converted into the fringed micelle crystal phase or the amorphous phase of PEO electrolytes.

PEO electrolytes were added into active carbon as a binder and an ion conductor, so as to provide electrodes with not only ion conduction, but also the accessibility of ion to the active sites of electrodes. The NaI/I₂ mediator was added to improve the conductivity of PEO electrolyte and provide pseudocapacitance for all-solid-state supercapacitors. Impedance, cyclic voltammetry, and galvanostatic charge/discharge measurements were conducted to evaluate the electrochemical performance of PEO polymer electrolytes based all-solid-state supercapacitors.

Results demonstrate that the conductivity of PEO electrolyte could be improved to 0.1 S/cm with a mediator concentration of 50wt%. A high conductivity in the PEO electrolyte with mediator is an indication of a high electron exchange rate between the mediator and mediator. The high electron exchange rates at mediator carbon interface and between mediator and mediator are essential in order to obtain a high response rate and high power. This automatically solves the accessibility problem. With the addition of NaI/I₂ mediator, the specific capacitance increased more than 30 folds, specific power increased almost 20 folds, and specific energy increased around 10 folds. Further addition of filler to the electrodes along with the mediator could double the specific capacitor and specific power of the all-solid-state supercapacitor. The stability of the corresponded supercapacitor is good within 2000 cycles.

I would like to express my deep and sincere gratitude to many people who made this Ph.D. thesis possible. Special thanks are due to my advisor, Dr. Xiangyang Zhou, for accepting me as his Ph.D. student, for his insight resolving the problems encountered throughout research and thesis writing, and his invaluable comments during my graduate study. I would like to thank Dr Azzam Mansour and Naval Research Laboratory. In addition I would like to thank all of my Ph.D. committee members, Dr. Hongtan Liu, Dr. Na Li and Dr. Chenzhong Li.

I would like to thank the Department of Mechanical and Aerospace Engineering and the Graduate school at University of Miami for financial support. I would like to thank my very good friend Juanjuan Zhou, who has been a great colleague through the last two years but an even better friend. The quality of my dissertation benefited greatly from our long thought provoking conversations as well as from our friendship. Many thanks to all the other group members from clean energy Lab. I would like to thank all of my family and friends who have supported me for the last three years on this great journey that has been my Ph. D.

TABLE OF CONTENTS

LIST OF FIGURES.....	vii
LIST OF TABLES.....	xii
CHAPTER 1 INTRODUCTION	1
1.1 A critical analysis of all-solid-state supercapacitors	1
1.2 The opportunities and approaches.....	4
1.2.1 Is it possible to further increase the conductivity of PEO based polymer electrolytes?.....	4
1.2.2 What are the possible benefits of combining some mediators in polymer electrolytes?.....	7
1.3 Objectives.....	11
CHAPTER 2 LITERATURE REVIEW	12
2.1 History and current study of supercapacitors	12
2.2 Principle of supercapacitor.....	17
2.2.1 Electrical double layer capacitor (EDLC).....	17
2.2.2 Pseudocapacitor.....	20
2.2.3 Solid electrolytes versus liquid electrolytes	26
2.3 Polymer electrolytes.....	29
2.4 PEO-based polymer electrolytes.....	36
2.5 Methods for improving PEO-based electrolytes	42
2.6 Electrode materials.....	47
2.6.1 Carbon electrode	47
2.6.2 Polymer electrode.....	47
2.6.3 Metal oxides.....	48
2.7 Characterization methods.....	49
2.7.1 Electrochemical characterizations.....	50
2.7.2 Instrumental analysis.....	53
2.8 Summary	62
CHAPTER 3 EXPERIMENTAL	64

3.1 Materials.....	64
3.2 Fabrication of PEO/LiX (X=AlO ₂ ⁻ , ClO ₄ ⁻ , TFS ⁻) base SCs	66
3.2.1 Preparation mesoporous SiO ₂ and TiO ₂ with sol-gel method	66
3.2.2 Preparation of PEO/LiX(X=AlO ₂ ⁻ , ClO ₄ ⁻ , TFS ⁻) polymer electrolyte	67
3.2.3 Add iodide/iodine/ (I ⁻ /I ₂) mediators into PEO/LiX gel	69
3.2.4 Preparation of electrode and electrode assembly	70
3.3 Characterization and evaluation of PEO electrolyte-based supercapacitors	72
3.3.1 Phys-chemical property Characterization	72
3.3.2 Electrochemical performance evaluation	74
Chapter 4 PEO/LiX(X=AlO ₂ ⁻ , ClO ₄ ⁻ , TFS ⁻) BASED POLYMER ELECTROLYTE	79
4.1 Effect of different anions.....	79
4.1.1 Conductivity measurement results	79
4.1.2 XRD analysis.....	82
4.2 Effect of fillers	87
4.2.1 Conductivity measurement results	87
4.2.2 FTIR analysis	88
4.2.3 XRD analysis.....	92
4.2.4 DSC analysis	93
4.2.5 SEM analysis.....	97
4.3 Effect of hot pressing	99
4.3.1 Conductivity results of PEO/LiTFS electrolytes.....	99
4.3.2 Conductivity results of PEO/LiAlO ₂ electrolytes	116
4.4 Effect of mediator concentration.....	118
4.5 Discussions.....	122
4.6. Conclusions	129
Chapter 5 PEO/LiX/AC BASED SUPERCAPACITOR.....	132
5.1 Effect of different lithium salts	133
5.2 Effect of filler and mediator	137
5.2.1 Effect of filler	137
5.2.2 Effect of mediator.....	142
5.2.3 Synergic effect of mediator and filler	145
5.3 Effect of scan rate.....	147
5.4 Effect of cycle number	152

5.5 Surface morphology and chemical analysis	154
5.6 Discussions.....	156
5.7 Conclusions.....	162
REFERENCES.....	165

LIST OF FIGURES

Figure 1. 1 A schematic illustration of the charge process in a porous RuO ₂ electrode.	4
Figure 1. 2 Temperature dependence of conductivity for P(EO) ₆ :LiN(CF ₃ SO ₂) ₂ during various heating and cooling runs[6].....	6
Figure 1. 3 Transfer processes for Fe(III)/Fe(II) and I ₃ ⁻ /I ⁻ : Step 1, approach of the reactants. Step 2, the moment of collision. Step 3, electron transfer. Step 4, the separation of products.	9
Figure 1. 4 Schematic of solid state electrochemical supercapacitor.	9
Figure 2. 1 Sketch of Ragone plot for various energy storage and conversion devices[10,11].	12
Figure 2. 2 Schematic of a liquid electrolyte based EDLC.....	17
Figure 2. 3 The electrochemical double layer extends from the electrode surface into bulk of liquid electrolyte.....	20
Figure 2. 4 A current vs. potential dependence for (a) pseudocapacitor [10]; and (b) EDL capacitance.....	22
Figure 2. 5 Chemical structure schematic of polymer electrolyte and polyelectrolyte.....	32
Figure 2. 6 Diagrammatic representation of a chemical gel network with junction points (a), and a physical gel network having junction zones (b) [99].	34
Figure 2. 7 A segment of a polyethylene oxide chain.....	36
Figure 2. 8 Cation motion in a polymer electrolyte assisted by polymer chains only [98].	40
Figure 2. 9 Cations motion in a polymer electrolyte facilitated by the ionic cluster [98].....	41
Figure 2. 10 Hierarchy of equivalent circuit (a) Simple capacitor (b) Capacitor with equivalent series resistance (ESR) (c) Capacitor with equivalent series resistance and equivalent parallel resistance (EPR) (d) Capacitor with equivalent series resistance and equivalent parallel resistance (EPR) in series with a Warburg element (e) Parallel combination of n C and EPR (f) parallel C, EPR elements connected with pore-resistance elements, Rp [19].....	53

Figure 2. 11 Schematic DSC curve demonstrating the appearance of several common features	57
Figure 3. 1 Preparation procedure for PEO/LiX/SiO ₂ (X=AlO ₂ ⁻ , ClO ₄ ⁻ , TFS ⁻) electrolyte.	69
Figure 3. 2 Preparation procedure for Mediator enhanced PEO/LiX/AC (X=AlO ₂ ⁻ , ClO ₄ ⁻ , TFS ⁻) based electrode.	70
Figure 3. 3 Schematic of supercapacitors for electrochemical tests.	71
Figure 3. 4 Schematic of the fixture for a standard four-point conductivity measurements.	75
Figure 3. 5 Schematic of the Two-electrode Through-plane conductivity measurements.	77
Figure 4. 1 The crystal structure of Lithium salt (a) LiAlO ₂ , (b) LiClO ₄ , and(c) LiTFS.	82
Figure 4. 2 XRD spectrum of a PEO/LiAlO ₂	83
Figure 4. 3 XRD spectrum of a PEO/LiTFS.	84
Figure 4. 4 The morphology of PEO/LiX polymer electrolytes X= (a) LiAlO ₂ (×1300); (b) LiAlO ₂ (×10,000); (c) LiClO ₄ (×1180), (b) LiClO ₄ (×240000)and (c) LiTFS (×1180). (f) LiTFS (×5000).	87
Figure 4. 5 Baseline corrected spectra comparing pure PEO (black) and PEO/LiAlO ₂ (blue) electrolytes. The C-O-C stretching (1100 cm ⁻¹) is indicated by the red arrows and the downshift (1020 cm ⁻¹) due to the polyether-salt interactions is indicated with the green arrows.	89
Figure 4. 6 XRD spectrum of a PEO/LiAlO ₂ , PEO/LiAlO ₂ /SiO ₂ and PEO/LiAlO ₂ /TiO ₂ electrolytes.	93
Figure 4. 7 DSC curves of PEO/LiAlO ₂ , PEO/LiAlO ₂ /SiO ₂ and PEO/LiAlO ₂ /TiO ₂ electrolytes at cycle 1(a)T _g curves; (b)T _m curve	95
Figure 4. 8 Table-top SEM images of pristine and hot pressed PEO/LiAlO ₂ composite electrolytes: (a) without filler; (b) with SiO ₂ filler; (c) with TiO ₂ filler. .	97
Figure 4. 9 Conductivity of pristine and hot pressed PEO/LiTFS/EC electrolytes vesus storage time	102
Figure 4. 10 Unaltered FTIR spectra of PLE, PLE-20 and PLE-60.	106

Figure 4. 11 Baseline corrected and rescaled FTIR spectra of PLE, PLE-20, and PLE-60.	107
Figure 4. 12 XRD spectra for PEO/LiTFS electrolytes (The upper spectra is for a pristine sample, others are for hot pressed samples).....	111
Figure 4. 13 XRD spectra for PEO/LiTFS electrolytes (The upper spectra is for a pristine PLE sample, the middle one is for a sample that was hot pressed for 20 min, and the bottom one is for a sample that was hot pressed for 60 min).	112
Figure 4. 14 DSC curves of PEO/LiTFS electrolyte (a) T_g curve; (b) T_m curve (solid red line is the pristine sample, blue dash line is hot pressed 5 min sample, black dash dot line is hot pressed 15 min sample, green dash dot dot line is hot pressed 35 min sample).....	114
Figure 4. 15 Scanning electrical microscopy (SEM) images of the PEO/LiTFS electrolytes (a) pristine PLE (x650); (b) pristine PLE (x24000); (c) hot pressed PLE (x650); (d) hot pressed PLE (x24000).	115
Figure 4. 16 Conductivity of PEO/LiX (X=TFS ⁻ , AlO ₂ ⁻) electrolytes with filler and NaI/I ₂ mediator.....	121
Figure 4. 17 XRD spectrum for PEO/LiTFS doped with 50% NaI/I ₂	122
Figure 4. 18 XRD spectrum for PEO/LiAlO ₂ doped with 50% NaI/I ₂	122
Figure 4. 19 The fringed micelle model of the two phase structure of polymer.	125
Figure 4. 20 (a) Plate-like re-entry model of lamellar crystal; (b) folded chain lamellae tied together by inter-lamellar amorphous chains.....	125
Figure 4. 21 Schematic phase diagram of PEO/LiTFS polymer electrolytes. There are crystalline, amorphous (L), pure salt, and pure polymer phases.	128
Figure 5. 1 CV results of symmetric PEO/LiX/AC (X=AlO ₂ ⁻ , ClO ₄ ⁻ , TFS ⁻) composite electrode supercapacitor (Potential range: 0~0.8 V, scanning rate: 35 mV/s).....	134
Figure 5. 2 Nyquist plots for symmetric PEO/LiX/AC (X=AlO ₂ ⁻ , ClO ₄ ⁻ , TFS ⁻) composite electrode supercapacitor (1~100,000Hz).....	136
Figure 5. 3 SEM images of the PEO/LiX/AC (X=AlO ₂ ⁻ , ClO ₄ ⁻ , TFS ⁻) composite electrode surfaces.	137
Figure 5. 4 CV results of symmetric PEO/LiTFS/AC, PEO/LiTFS/AC/SiO ₂ , and PEO/LiTFS/AC/TiO ₂ electrode supercapacitor (Potential range: 0~0.8 V, scanning	

rate: 20 mV/s).....	139
Figure 5. 5 Nyquist plots for PEO/LiTFS/AC polymer electrode supercapacitor and PEO/LiTFS/AC/SiO ₂ polymer electrode supercapacitors.....	139
Figure 5. 6 CV results of symmetric PEO/LiAlO ₂ /AC electrode based supercapacitors. (Potential range: 0~0.8 V, scanning rate: 35 mV/s).....	140
Figure 5. 7 Nyquist plots for symmetric PEO/LiAlO ₂ /AC electrode based supercapacitor.....	141
Figure 5. 8 CV results of symmetric polymer electrode supercapacitor with or without mediator. (Potential range: 0~0.8 V, scanning rate: 35 mV/s).	142
Figure 5. 9 Nyquist plots for PEO/LiAlO ₂ /AC electrodes with iodine/iodide (I ⁻ / I ₂) mediator.....	144
Figure 5. 10 CV results of symmetric PEO/LiAlO ₂ /AC/NaI/I ₂ electrode supercapacitor with or without filler. (Potential range: 0~0.8 V, scanning rate: 35 mV/s).....	146
Figure 5. 11 Nyquist plots for polymer electrode supercapacitors with various inorganic filler in the composite electrode. PEO/LiAlO ₂ /C electrodes were loaded with addition of filler and iodine/iodide (I ⁻ / I ₂) mediators.	147
Figure 5. 12 CV results as a function of potential scan rate for PEO/LiAlO ₂ /AC-Nafion-PEO/LiAlO ₂ /AC supercapacitors.	148
Figure 5. 13 CV results as a function of potential scan rate for PEO/LiAlO ₂ /AC/NaI/I ₂ -Nafion-PEO/LiAlO ₂ /AC/NaI/I ₂ supercapacitors.	150
Figure 5. 14 CV results as a function of potential scan rate for PLE/AC-Nafion- PLE/AC supercapacitors.	150
Figure 5. 15 CV results as a function of potential scan rate for PLE/AC/NaI/I ₂ - Nafion- PLE/AC/NaI/I ₂ supercapacitors.	151
Figure 5. 16 Ragone plots (specific power versus specific energy) for supercapacitors with and without mediator.....	151
Figure 5. 17 Specific capacitance as a function of charge/discharge cycle numbers for PEO/LiTFS/AC-Nafion-PEO/LiTFS/AC supercapacitor.....	152
Figure 5. 18 Specific capacitance as a function of charge/discharge cycle numbers for PLE/AC/NaI/I ₂ -Nafion- PLE/AC/NaI/I ₂ supercapacitor.....	153
Figure 5. 19 Specific capacitance as a function of charge/discharge cycle numbers for PEO/LiAlO ₂ /AC/NaI/I ₂ -Nafion- PEO/LiAlO ₂ /AC/NaI/I ₂ supercapacitor.	153

Figure 5. 20 SEM morphology of PEO/LiAlO ₂ /SiO ₂ composite membrane and PEO/LiAlO ₂ /SiO ₂ (TiO ₂)/AC composite electrode.....	156
Figure 5. 21 Limiting current density plotted versus scan rate (the electrode potential is 0.8 V).....	161

LIST OF TABLES

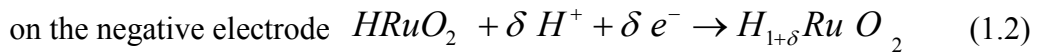
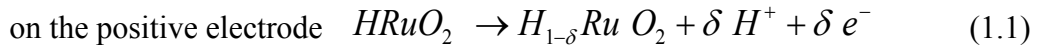
Table 2.1 Comparisons of Capacitor, Supercapacitor and Battery[10-15].....	13
Table 2. 2 Advantage and disadvantage of EDLC and Pseudocapacitor [18].....	21
Table 2. 3 Comparisons between liquid electrolyte and solid electrolyte based supercapacitors.....	28
Table 2. 4 Commonly used solid polymer electrolytes	31
Table 2. 5 Summary of PEO/LiX (X=AlO ₂ ⁻ , ClO ₄ ⁻ , TFS ⁻) polymer electrolyte.	39
Table 2. 6 FTIR peak for PEO based polymer electrolyte.	60
Table 3. 1 Materials used in the experiment.....	64
Table 4. 10 In-plane conductivity and through-plane conductivity of PEO/LiX (X=AlO ₂ ⁻ , ClO ₄ ⁻ , TFS ⁻) polymer electrolytes ($\sigma_{\text{in-plane}}$ is the in-plane conductivity and $\sigma_{\text{through-plane}}$ is the through-plane conductivity).....	80
Table 4. 2 In-plane conductivity of PEO/LiAlO ₂ based composite electrolytes	87
Table 4. 3 Thermal transitions parameter of the sample for DSC measurements	96
Table 4. 4 In-plane conductivity measurement result for PEO/LiTFS/EC electrolytes under hot pressing treatment.....	101
Table 4. 5 In-plane conductivity measurement result for PEO/LiTFS electrolytes under the high temperature treatment.....	103
Table 4. 6 Through-plane conductivity measurement result for PEO/LiTFS electrolytes	105
Table 4. 7 Assignment of the FTIR peaks to the vibration modes of molecules.....	109
Table 4. 8 Thermal Transitions Parameter of the PEO/LiTFS electrolytes for DSC Measurements.....	113
Table 4. 9 Conductivity data for PEO/ LiAlO ₂ electrolytes	117
Table 4. 10 Composition and in-plane conductivity of PEO/LiX (X=AlO ₂ ⁻ , ClO ₄ ⁻ , TFS ⁻) electrolytes doped with NaI/I ₂ mediator.....	120
Table 4. 11 Regression parameters for Eq. 4.2.....	121
Table 5. 1 Composition of components in the PEO/LiX/AC (X=AlO ₂ ⁻ , ClO ₄ ⁻ , TFS ⁻) composite electrodes. The mass of the Nanofoam carbon paper is not included.	134
Table 5. 2 Summary of the electrochemical performance for PEO/LiX/AC	

(X=AlO ₂ ⁻ , ClO ₄ ⁻ , TFS ⁻) composite electrode supercapacitor (Direct paint sample, with electrode surface area of 1cm ²).	136
Table 5. 3 Compositions of the PEO/LiTFS/AC electrodes with or without filler.	138
Table 5. 4 Summary of the series resistance, specific capacitance, and specific power for supercapacitors with and without filler in the composite electrode	138
Table 5. 5 The compositions of the PEO/LiAlO ₂ /AC composite electrodes	140
Table 5. 6 Summary of the specific capacitance and specific power for supercapacitors	140
Table 5. 7 The compositions of the PEO/LiAlO ₂ /AC/NaI/I ₂ composite electrodes	142
Table 5. 8 Specific capacitance and specific power for supercapacitors with or without mediator.	144
Table 5. 9 The compositions of PEO/LiAlO ₂ /AC composite electrodes	146
Table 5. 10 Specific capacitance and specific power for PEO/LiAlO ₂ /AC/NaI/I ₂ electrode supercapacitor	147
Table 5. 11 Linear fitting result for curve of current density versus scan rate in Figure 5.22	161

CHAPTER 1 INTRODUCTION

1.1 A critical analysis of all-solid-state supercapacitors

As far as we know, the liquid electrolyte based supercapacitors with the highest specific power and energy are those with RuO_2 electrodes. These systems have been studied for more than 30 years since Conway's original work in the 1970's [1]. These systems not only provide a very high specific capacitance and energy but also very good reversibility and very high cycle life ($\sim 10^6$). This outstanding performance is thought to originate from highly reversible faradaic reactions of these metal oxides as follows:



Here, $0 < \delta < 1$, while RuO_2 and H_2RuO_2 represent the positive and negative electrodes in a completely charged state. This a process of electron accepting/donating via valence changes during a charging/discharging process. According to most commonly accepted view of this process [1], there are several points worth mentioning.

1) The reactions around the oxidation states of Ru^{2+} , Ru^{3+} , Ru^{4+} , and probably Ru^{6+} are highly reversible. These reactions involving electron exchange or accepting/denoting must be facile reactions to ensure a good reversibility.

2) The participation of protons in these reactions is very important. Many authors actually use “proton intercalation” to describe this process, implicating a similarity to the Li^+ intercalation in the carbon electrode in a rechargeable Li-ion battery. However, there is a major difference between these two situations because in a Li-ion battery, voltage is stable during discharge and specific energy is very high (up to 400 Wh/kg) whereas the voltage of a supercapacitor is proportional to the amount of charge. Nevertheless, “proton intercalation” does partially neutralize the charged surface and slow down the reduction of voltage in terms of a unit amount of discharge. Thus, the accessibility of protons to the active sites of a porous RuO_2 electrode is essential. The active sites on the surface can be charged whereas those in the bulk of RuO_2 can't be charged and hence are not utilized.

3) Because “proton intercalation” is a necessary process, a fast transport of protons from the electrolyte on to the surface of the porous RuO_2 electrode is essential. As shown in Figure 1.1, the active sites on the surface interfacing with the

electrolyte can be easily accessed by the protons. The active sites in the pores are less easily accessible. Because the lattice water can relay protons per a structural diffusion [2], the internal sites may be accessible but with a lot of difficulty. Thus, in a crystalline ruthenium oxide electrode, the energy is stored only in its surface layers. However, in the amorphous phase $\text{RuO}_2 \cdot x\text{H}_2\text{O}$, charge and discharge proceed both on the surface and in the bulk but with a very low charge/discharge current. That is why the specific capacitance of a $\text{RuO}_2 \cdot x\text{H}_2\text{O}$ electrode (768 F/g) is considerably larger than that obtained with crystalline RuO_2 films (380 F/g) [3]. In the case of a RuO_2 based supercapacitor with a solid state electrolyte only 170 F/g was realized [4], although the authors had made great progress to impregnate Nafion electrolyte into amorphous RuO_2 and to magnify the contact area.

4) In comparison to liquid electrolytes, solid electrolytes have quite a few disadvantages. First, the ionic conductivity of solid electrolytes is generally much lower than that of liquid electrolytes. For example, the commonly used H_2SO_4 solution has a conductivity of ~ 0.8 S/cm while Nafion can barely reach to 0.2 S/cm when it is well-treated and fully hydrated. Secondly, due to lack of viscosity or fluidity, solid-state electrolytes are usually much more difficult to permeate into the

small pores of a porous electrode and to form an intimate contact with the electrode surface. Thirdly, because a small extent of irreversible side reaction between the electrodes and electrolyte is inevitable, the adverse products of the side reactions tend to stay at the interface between the solid-state electrolytes and electrodes. These products may be removed via diffusion or convection in a liquid electrolyte. The side reaction and the products will result in degradation of the supercapacitor.

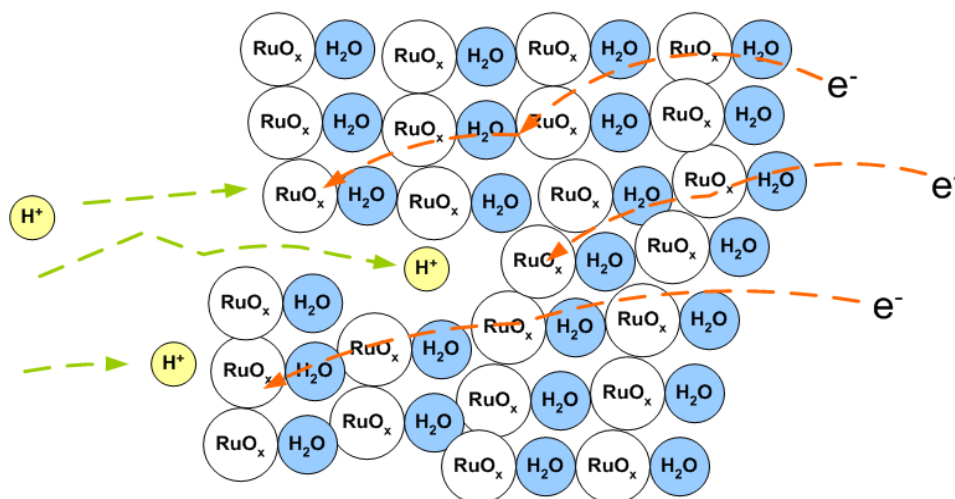


Figure 1. 1 A schematic illustration of the charge process in a porous RuO_2 electrode.

1.2 The opportunities and approaches

1.2.1 Is it possible to further increase the conductivity of PEO based polymer electrolytes?

Having a polar ether group and significant segmental mobility, poly(ethylene oxide) (PEO) has an outstanding compatibility as a solid solvent for a wide range of

salts and especially a high lithium ion stability. PEO also has a very good film forming characteristic and can be made in a variety of size and shapes. PEO can be easily and readily synthesized and modified in a laboratory or can be easily obtained at a low cost. However, the conductivity of a pristine PEO-lithium salt polymer is low (10^{-8} S/cm). The conductivity of PEO electrolytes can be improved with the following methods: 1) to use lithium salts with high solubility in PEO; 2) to add plasticizers that increase the amount of amorphous phase in which the solubility and ionization of lithium salts is significantly increased; 3) to add microscopic fillers that may inhibit formation of polymer crystals and result in fast ion transport paths via an interaction between the fillers and electrolyte; 4) to apply uniaxial strain to enable some helical conduction channels in the stretching direction. A possible method that remains unexplored is heat treatment. It is well known that the conductivity of amorphous PEO is much greater than that of crystalline PEO. Increasing temperature can increase the conductivity not only by increasing the mobility via a thermal activation but also by increasing the solubility of the salt. It is also well known that during a natural cooling process, pre-melted PEO may take a very long time to form crystalline phases [5]. Thus, it is possible that in a PEO electrolyte synthesized using

a solution casting method, the ratio of amorphous phase to crystalline phase can be increased by a melting and cooling cycle. Therefore, a higher conductivity can be obtained.

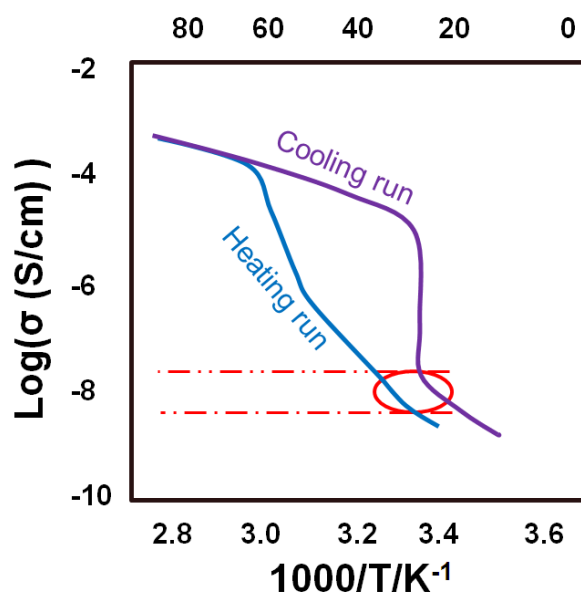


Figure 1. 2 Temperature dependence of conductivity for $P(EO)_6:LiN(CF_3SO_2)_2$ during various heating and cooling runs[6].

M. Marzantowicz [6] studied the crystallization and conductivity of PEO:LiTFSI polymer electrolytes in various heating and cooling runs in the temperature range from -60 to 100 °C. As observed in a heating and cooling cycle as shown in Figure 1.2, the room temperature conductivity after a heating and cooling cycle is still one order of magnitude greater than the initial room temperature conductivity of the same PEO polymer electrolytes. If one order of magnitude conductivity increasement after heating/cooling run is repeatable, this will be an effective way to

improve the conductivity of two phase polymer electrolytes, especially PEO.

1.2.2 What are the possible benefits of combining some mediators in polymer electrolytes?

1.2.2.1 Effect on conductivity

Mediators refer to compounds that can undergo facile oxidation/reduction reactions. Good examples of mediators or redox pairs include NaI/I_2 and $\text{K}_3\text{Fe(CN)}_6/\text{K}_4\text{Fe(CN)}_6$. For the transport of mediators or redox pairs in electrolytes, two elementary processes are in operation: 1) the physical migration of the species, and 2) the exchange reaction which causes an apparent displacement. The second process is also called transfer diffusion. The mechanism can be expressed by [7]:



where A is the reduced state of a species, AX is the oxidized state of the species, X is a molecule, ion, radical, or energy quantum. The net effect is that A and AX exchange their positions and translate a step to the left and right, respectively. Figure 1.3 illustrates the transfer diffusion of Fe(III)/Fe(II) and I_3^-/I^- . [8] The apparent diffusivity of the mediators in liquid solutions (water or organic solvents) is given by: [6]

$$D_{AX}^* = D_{AX} + \frac{k\delta_{AX}^2\pi}{6}C_A \quad (1.4)$$

where D_{AX} is the diffusivity for conventional or physical diffusion, k is the reaction rate for Equation 1.4, C_A is the concentration of A . In liquid solutions, the transfer diffusion related conductivity of ferrocene and ferricinium can reach to 0.3-0.6 S/cm while the conductivity of I_3^-/Γ can be 0.05-0.1 S/cm at 1 M. Both types of mediators have potential to enable a high conductivity in solid electrolytes. Conductivity, σ , of a species is related with the diffusivity, D , via the Nernst-Einstein equation, [9]

$$\sigma = \frac{(zF)^2}{RT}C_A D_{AX}^* \quad (1.5)$$

where Z is charge on AX , F is Farady's constant, R is gas constant, T is absolute temperature.

Transport processes of mediators and ions in polymer electrolytes are more complicated than those in liquid electrolytes. The transport processes in polymer electrolytes that are enclosed in pores of electronic conducting materials are poorly understood. Interaction between the ions and functional groups and radicals in the solid electrolytes may result in an "anomaly" of the transport processes or unexpected high conductivity.

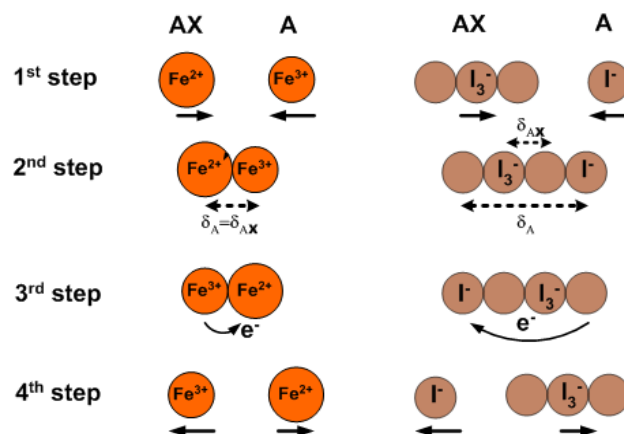


Figure 1. 3 Transfer processes for Fe(III)/Fe(II) and I₃⁻/I⁻ : Step 1, approach of the reactants. Step 2, the moment of collision. Step 3, electron transfer. Step 4, the separation of products.

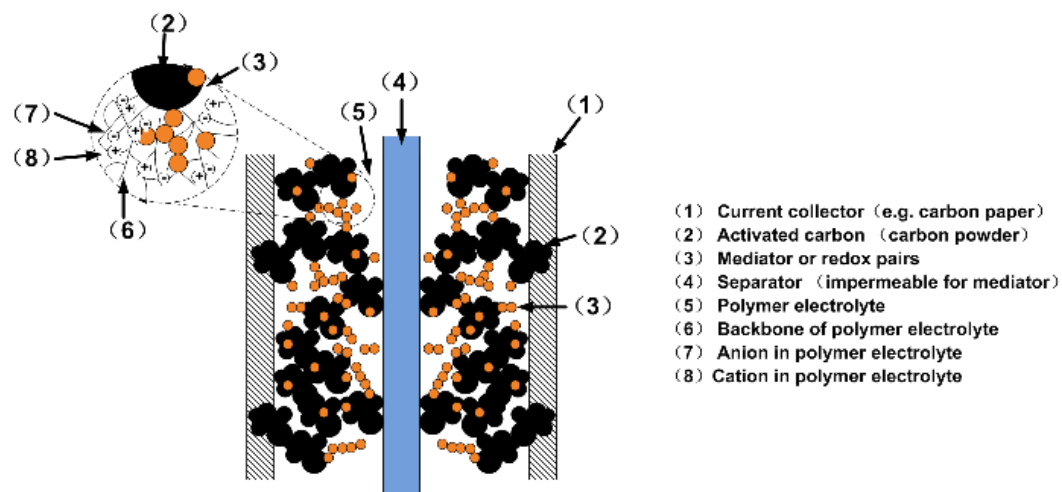


Figure 1. 4 Schematic of solid state electrochemical supercapacitor.

1.2.2.2 Effect on charge/discharge

A new design of supercapacitor is shown in Figure 1.4. The supercapacitor consists of two composite electrodes and a Nafion membrane as the separator. The composite electrodes contain both PEO polymer electrolytes and carbon powder or

activated carbon. Mediators are dissolved or dispersed in the PEO polymer electrolyte. The charge process of the supercapacitor is schematically illustrated in Figure 1.5. In the negative electrode, electrons first reach the surface of porous carbon, then transfer to mediator via a reduction reaction, and then transfer to other mediators in the bulk of the electrolyte. Thus, the mediators can store some charges and provide pseudocapacitance. Two other possible benefits can be identified also. First, each mediator is surrounded by the polymer electrolyte and in the vicinity of the ions in the PEO electrolyte. Thus, the access of ions to the mediators is maximized. The problem with the accessibility of the proton to the active sites in the RuO_2 electrode as shown in Figure 1.1 is mitigated. Secondly, in the RuO_2 electrode, the charge process is limited by the transport of protons or the conductivity of proton. In the case of mediators, the approach of the charged mediator and ions with opposite charge can move towards each other. Thus, the effective conductivity is the summation of the ions and the mediators. After all, it is possible that by dispersing mediators into PEO polymer electrolytes, not only the total capacitance and energy can be increased but also the maximum power that is inversely proportional to the effective internal resistance during charge/discharge can be maximized.

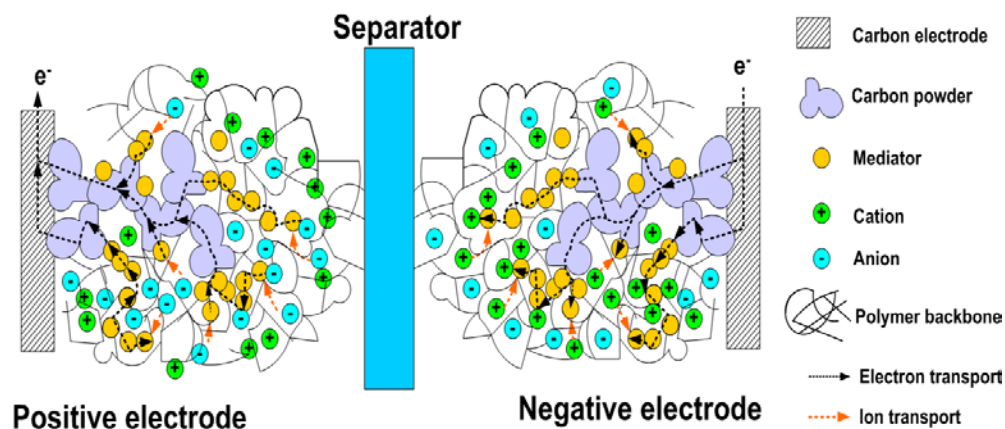


Figure 1.5 Illustration of formation of “molecular capacitor” and charging process in proposed supercapacitor.

1.3 Objectives

Three major objectives of this study is: 1) to evaluate and clarify the effects of hot pressing treatment, dispersed mediators, anions, and fillers on the conductivity of PEO polymer electrolytes elucidate the mechanisms of conduction in the PEO electrolytes and; 2) to evaluate and clarify the effects of mediator on the electrochemical performance of PEO polymer electrolyte based all-solid-state supercapacitors; and 3) to demonstrate that a significant improvement of performance can be realized using these approaches.

CHAPTER 2 LITERATURE REVIEW

2.1 History and current study of supercapacitors

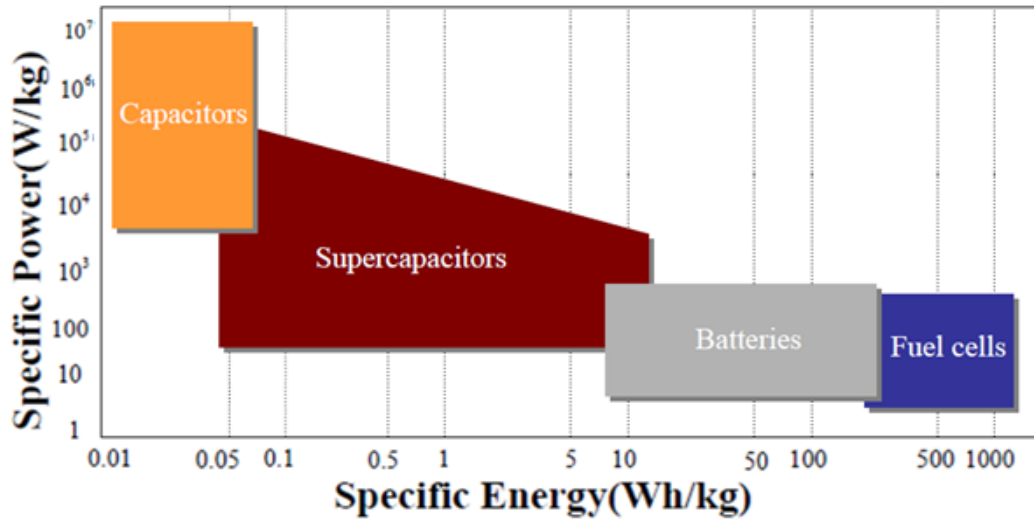


Figure 2. 1 Sketch of Ragone plot for various energy storage and conversion devices[10,11].

The supercapacitor is one of the major electrochemical energy storage and conversion devices for which the major performance parameters, specific power and energy, are often represented using a Ragone diagram as shown in Figure 2.1[10, 11]. Generally speaking, when an electrochemical energy storage device can achieve a high power by varying its operational parameters, its energy output is low and vice versa. Supercapacitors (SCs) actually fill in the gap between batteries that have high specific energy but low specific power and conventional capacitors or dielectrical capacitors that have high specific power but low specific energy. A list of

the properties and performance for fuel cells, batteries, SCs, and capacitors is given in Table 2.1.

Table 2.1 Comparisons of Capacitor, Supercapacitor and Battery[10-15]

Parameters	Fuel Cell	Rechargeable battery	Supercapacitor	Capacitor
Operate Temperature (°C)	+25 to +90	-20 to +65	-40 to +85	-20 to +100
Charge Time	1 - 1.5 hrs	0.3 ~ 10 hrs	1 ~ 30 sec	$10^{-6} \sim 10^{-3}$ sec
Discharge Time	10~300hrs	1 ~ 5 hrs	1 ~ 30 sec	$10^{-6} \sim 10^{-3}$ sec
Specific Energy (Wh/kg)	300 ~ 3,000	20 ~ 200	1 ~ 10	< 0.1
Specific Power (kW/kg)	1~100	50 ~ 200	1,000 ~ 2,000	> 10,000
Cycle Life	N/A	100~1000 partial discharge	> 100,000 full discharge	> 500,000 full discharge
Charge/Discharge Efficiency	N/A	0.7 ~ 0.85	0.90 ~ 0.95	~ 1.0

The fuel cell is the only one of these four electrochemical devices that relies on the supply of a fuel (hydrogen, methanol etc.) and an oxidant (oxygen or air) for power generation. The fuel cell is capable of storing large amounts of energy in terms of unit mass of the device but has small specific power. The opposite is true for capacitors. While their specific energy is low, they can release a large amount of energy in a short period of time (millisecond to second). This feature is very useful for enabling high acceleration in a propulsion system.

The specific power and energy of a battery are typically between those of a fuel cell and a capacitor. For rechargeable batteries or secondary batteries, although the specific energy is high, their charge/discharge cycle life is low, generally in the range of 10^2 to 10^3 evaluated usually at 30-50% discharge depth. However, in the case of capacitors, the cycle life is usually 10^6 at a full discharge. A supercapacitor not only provides comparable specific energy and power, but a much longer cycle life than a rechargeable battery.

In a conventional capacitor or a dielectric capacitor, energy is stored by the removal of charge carriers, typically electrons, from one metal plate and depositing them on another. This charge separation creates a potential difference between the two plates, which can be harnessed in an external circuit. The amount of charge stored is essentially a function of the size and material properties of the plates, while the voltage between the plates is limited by the dielectric breakdown of the substance separating the plates. Different materials sandwiched between the plates to separate them result in attaining different voltages.

In contrast to classic parallel-plate capacitors or dielectric capacitors, which store energy through induced electric fields in a dielectric medium with a thickness of

typically a few millimeters, the capacitance of supercapacitors originates from characteristic physico-chemical properties of electric double layer (or EDL), with a structure of charge distribution at the electrode/electrolyte interface with a thickness of a few nanometers. The strength of an electric field in the EDL can reach 10^9 V/m [13]. Ideal supercapacitors can realize a large number of charge/discharge cycles, a high cycling efficiency (typically >90%), and a long lifetime. However, research and development efforts have been focused on further increasing the power and energy, increasing the cycle life, mitigating self-discharge, enhancing the safety level and environmental compatibility, and reducing cost [16, 17].

The storage of electrical charge in the interface between a metal and an electrolytic solution has been studied by chemists since the nineteenth century, but the practical use of electric double layer capacitors (EDLCs) have only been in use since 1957, when the first patent was granted to Becker at General Electric Corp. for an electrolytic capacitor using porous carbon electrodes [1].

In 1971, Nippon Electric Company (NEC) produced the first commercially successful double-layer capacitors under the name “supercapacitor.” “Supercapacitor” is the commercial name of the device made by NEC, Japan. Since

then, a number of companies started producing electrochemical capacitors. In the late 70's and 80's, Conway and his coworkers made a great contribution to the capacitor research work based on RuO_2 , which has high specific capacitance and low internal resistance [18]. Those types of supercapacitors rely on both electric double layer and metal oxides that can undergo redox reactions or valence changes to store charges. This latter charge storage capability was referred to as pseudocapacitance.

By 1987, ELNA had begun producing their EDLCs under the name “Dynacap”. The “PRI Ultracapacitor,” developed from 1982, incorporated metal-oxide electrodes and was designed for military applications [19]. These commercial supercapacitors are widely used as power sources for activators, or as elements for long time constant circuits, or standby power for random access memory devices, and telephone equipments, etc. [20].

All these studies triggered a study by the U.S. Department of Energy in the context of hybrid development programs [21]. The U.S. Department of Energy ultracapacitor development program was initiated in 1989, and short term as well as long term goals were defined for 1998–2003 and after 2003, respectively [21].

Commercial productions of supercapacitors in the current markets are based on the high surface area porous carbon materials as well as based on noble metal dioxide systems [19].

2.2 Principle of supercapacitor

2.2.1 Electrical double layer capacitor (EDLC)

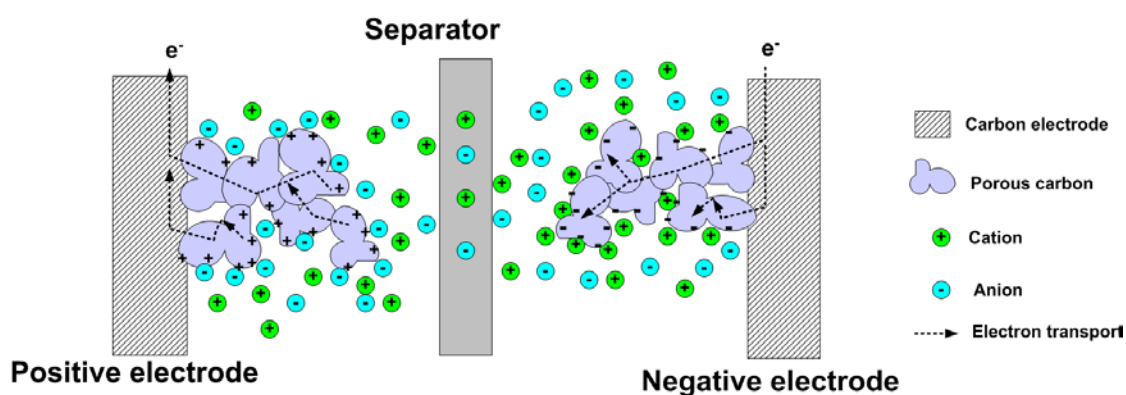


Figure 2. 2 Schematic of a liquid electrolyte based EDLC

As shown in Figure 2.2, a liquid electrolyte based EDLC consists of two porous electrodes with high surface area immersed in or impregnated with an electrolyte solution [22]. A semi-permeable membrane serves as a separator between both electrodes so as to prevent electrical contact. However, the separator still allows ions from the electrolyte to pass through. When the electrodes are charged, solvated ions of opposite charge are attracted to the electrodes, and are accumulated at the interfaces between the electrode and the electrolytic solution to

form an EDL. One electrode is positively charged and another is negatively charged. Thus, this charge storage process does not involve charge transfer between electrolyte and the electrode, or is non-faradic.

The first theoretical models for the EDL on electrode surfaces in liquid solution were developed by Helmholtz in 1879 [12, 16]. He proposed a simple charge separation at the interface. The interface separates two layers of opposite charges, one in the electrode and the other in the solution. The thickness of this Helmholtz layer equals the distance of closest approach of the charges in the liquid electrolyte towards the electrode [23-26]. The capacitance in the Helmholtz model does not change with the surface potential or concentrations [23-26]. Gouy (1910) developed a different EDL model in order to explain the effects of both electric potential and ionic concentration with the aid of Boltzmann distributions [23-26]. While ions in the double layer are not compact, as described in the Helmholtz model, the ions in Gouy's model are free to move. This is called the diffuse layer.

A combination of Helmholtz's and Gouy's models is illustrated in Figure 2.3, a schematic representation of a more realistic model for EDL. The first layer in the solid material is of one sign (positive or negative) and the other layer of the opposite

sign is in the electrolyte outside this solid electrode. The inner layer closest to the electrode, also called the compact layer or Helmholtz layer, consists of the solvent molecules and sometimes other specifically adsorbed ions or molecules. The inner layer can be further divided into an inner Helmholtz plane and an outer Helmholtz plane. The inner Helmholtz plane is where the electrical centers of the specifically adsorbed ions are located, while the outer Helmholtz plane represents the closest distance that the solvated ions can approach metal or the starting point of the diffuse layer. The charge layer (or inner Helmholtz plane) in the electrolyte was first considered static and the potential profile in the EDL decreased linearly with the distance from electrode surface. In an EDL, the total charge density in the solution is made up of the charge density from adsorbed ions in the inner layer and the excess charge density in the diffuse layer. Hence the capacitance of the double layer includes Helmholtz type compact double layer capacitance C_H and diffuse region of the double layer capacitance C_{diff} , and the total double layer capacitance is given by equation (2.1)

$$\frac{1}{C} = \frac{1}{C_H} + \frac{1}{C_{diff}} \quad (2.1)$$

The EDL can be affected by many factors, including the structures and properties of the electrodes and electrolyte. Because charging and discharging of EDLCs do not involve any major chemical reaction, electric double-layer capacitors are highly reversible and hence have a long charge/discharge cycle life (10^6).

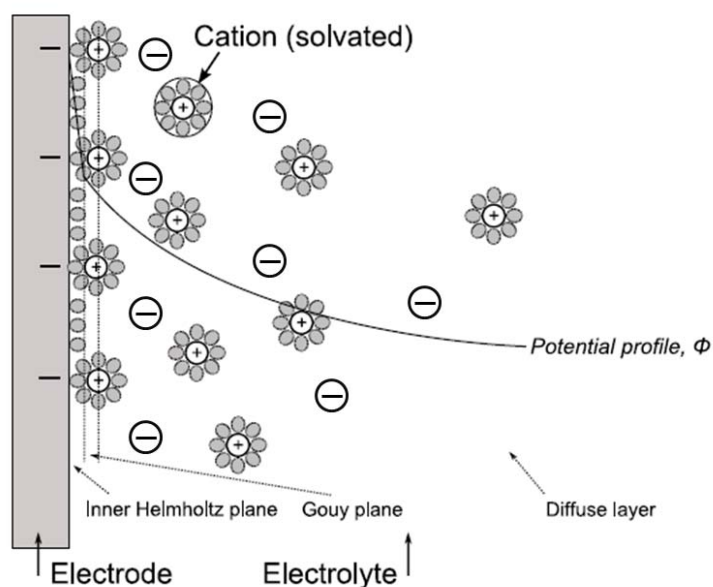


Figure 2. 3 The electrochemical double layer extends from the electrode surface into bulk of liquid electrolyte

2.2.2 Pseudocapacitor

Double-layer type electrochemical capacitors are complemented by capacitors based on so-called pseudocapacitance, which arises in some electro sorption processes and in redox reactions of electrode materials [18, 19]. The advantage

and disadvantage comparisons between electric double-layer capacitor and pseudocapacitor are listed in Table 2.2.

Table 2. 2 Advantage and disadvantage of EDLC and Pseudocapacitor [18].

Electric double layer capacitor	Pseudocapacitor
Narrow potential window (1-5 V)	Narrow potential window (1-5V)
~90 degree phase angle	Phase angle is a function of frequency, typically shows transmission-line behavior
Low specific energy	High specific energy
High charge/discharge rate and very high power	Kinetic limitations for high charge/discharge rates and hence power limited by kinetic factors
Indefinitely reversible	Highly reversible
Capacitance constant with voltage	Capacitance not constant with voltage

Several types of faradic processes may occur in the electrodes of pseudocapacitors: 1) reversible adsorption/desorption of hydrogen on the surface of the electrodes [10, 27]; 2) redox reactions related to oxidation state change or valence change when transition metal oxides, for example, RuO_2 and IrO_2 , are used as the active materials; 3) reversible processes of electrochemical doping–dedoping in electrodes based on conductive polymers [28], and 4) irreversible reactions that lead to degradation and self-discharge of the supercapacitors.

Pseudocapacitors with surface compounds

In pseudocapacitors there can occur reversible faradic surface redox reactions with chemical compounds that undergo electrosorption/desorption with a charge transfer [10, 27]. One of the most commonly used examples is electrosorption/desorption of hydrogen on Pt surface as can be expressed by

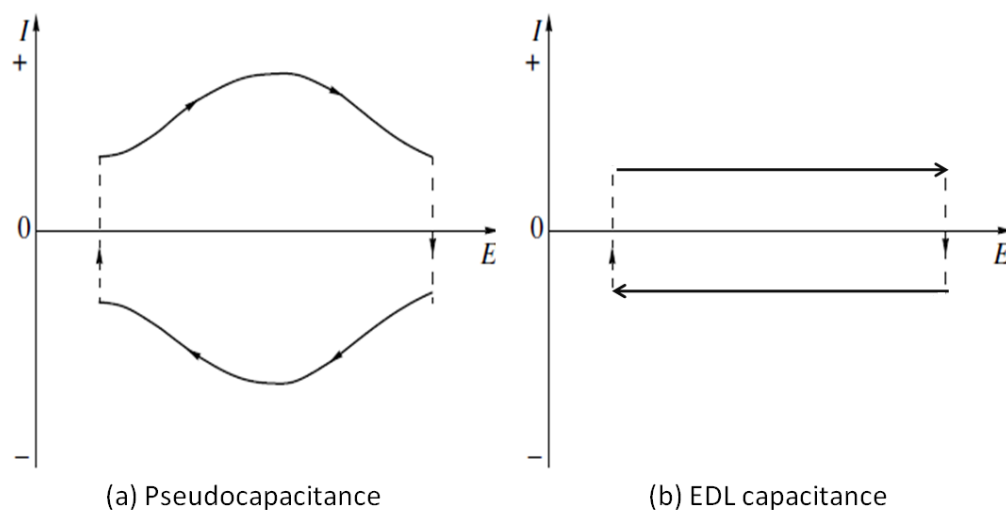
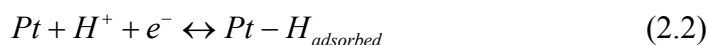


Figure 2. 4 A current vs. potential dependence for (a) pseudocapacitor [10]; and (b)

EDL capacitance.

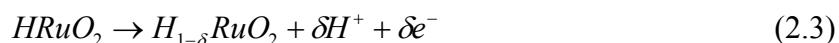
As opposed to the electrochemical reaction in a battery, where in an ideal case there exists an equilibrium potential of the electrochemical reaction, there is no definite potential of the adsorption reaction in pseudocapacitors. The capacitance

originated from these redox reactions is the charge required for a full coverage of the metal surface with a monolayer of adsorbed species. The shape of a cyclic voltammetric curve (CV) for this type of pseudocapacitor is dependent on the potential scan rate as shown in Figure 2.4a [10]. There is a certain critical potential scan rate above which the faradic process in pseudocapacitors becomes irreversible. One of the distinct features of this CV curve is its mirror symmetry, which shows an ideal charge/discharge process of a capacitor. However, the CV curve is different from that of an EDLC in that the current is not a constant with respect to potential.

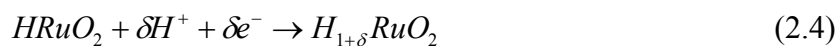
Pseudocapacitors based on metal oxides

One of the most frequently studied categories of electrode materials of pseudocapacitors is noble metal oxides such as RuO₂ and IrO₂. In the case of RuO₂, an oxide film grows on ruthenium during a prolonged cycling [29, 30]. The major electrochemical reactions occurring at interface between the metal oxide electrode and electrolyte is proposed as follows:

on the positive electrode



on the negative electrode



where $0 < \delta < 1$.

The redox process in the potential region from 0.1 to 0.3 V versus SHE occurs reversibly [29]. The high cost of oxides of noble metals restricts their broad practical use. That is why in the last few years other materials with similar properties have been studied. These may be mixed oxides of noble and other metals deposited onto metallic supports [31–34] or porous carbon supports [35, 36].

Pseudocapacitors Based on Conductive Polymers

In electron-conductive polymers, oxidation and reduction reactions of polymers that have a network of conjugated double bonds, such as polyacetylene, polyaniline, polypyrrole, are sufficiently reversible and proceed both under the action of chemical reagents and by electrochemical means. In the course of each reaction of this type they form a polycompound between the oxidized or reduced polymer and ions of the opposite sign (counterions) introduced (intercalated) into the polymer matrix. This process is traditionally called a doping by anions or cations. Use of

some electron-conductive polymers as electrodes for pseudocapacitors is based on the sufficient reversibility of redox reactions of their electrochemical doping–dedoping [10, 37]. The process of reversible electrochemical doping–dedoping may be represented by the following reactions:



Here, P_m is a polymer with a network of conjugated double bonds, m is the polymerization degree, A^- denotes anions, and M^+ represents cations. The doping reactions proceed from the left to the right, and the dedoping reactions, in the reverse direction. Reaction (2.5) is a reaction of oxidative p-doping, and Reaction (2.6) is a reaction of reductive n-doping. Most electron-conductive polymers can only be p-doped, some of them may be reversibly p-doped and n-doped at the same time, while only few are amenable to electrochemical n-doping at high reduction potentials.

In summary, the high values of specific capacitance attainable through supercapacitor technology are a result of EDL capacitance and pseudo-capacitance. EDL capacitance offers considerable charge storage capabilities thanks to possessing high surface-area materials as electrodes, and the fact that

charge separation occurs at atomic dimensions. Pseudocapacitance that arises from redox or ion sorption reactions further improves the achievable capacitance.

2.2.3 Solid electrolytes versus liquid electrolytes

One of criteria to classify different supercapacitors is the type of electrolyte used. The electrolyte materials for supercapacitors could be classified into liquid electrolytes, solid inorganic electrolytes, and polymer electrolytes. The liquid electrolyte for a supercapacitor could be further classified as an aqueous electrolyte (such as potassium hydroxide or sulfuric acid) and an organic electrolyte (such as acetonitrile or ethylene carbonate). Advantages of the aqueous electrolyte are the higher conductance (0.8 S/cm for H₂SO₄) and the fact that purification and drying processes during production are less stringent. The cost of aqueous electrolytes is usually much lower than that of suitable organic electrolytes. However, using an aqueous electrolyte limits the unit cell voltage of the supercapacitor to typically 1 V, thus reducing the available energy significantly more than organic electrolytes. Vaporization and icing of the liquid electrolyte also limits the use of the supercapacitors in a narrow range of

temperature (0-60°C for aqueous electrolytes). The most recent commercial supercapacitors use room temperature ionic liquids due to their higher ionic conductivities, and stable, non-flammable and non-volatile properties [38–41]. Although the most investigated and developed supercapacitors have been liquid electrolyte based supercapacitors, they suffer from other problems including leakage, combustion in the case of organic electrolytes, corrosion, poisoning and pollution to the environment, and fabrication and especially packaging difficulties.

Although solid electrolytes should include both low melting point salts and polymer materials that contain free and mobile ions, a vast majority of solid electrolytes are polymer electrolytes. Replacing the liquid electrolytes with polymer electrolytes may result in a leakage-free, corrosion-free, environmentally friendly, easy to fabricate, and easy to package supercapacitor. If the existing thin film technology is applied, the supercapacitor can be very compact and lightweight. However, a few reports on development and study of all-solid-state supercapacitors have been presented in literature [10]. In an effort to benchmark the current status of all-solid-state supercapacitors, the specific capacitance, power and energy of a list of all-solid-state supercapacitors are summarized in Table 2.3.

The electrolytes used in solid state supercapacitors could be inorganic salts (such as LiPOH), inorganic acids (phosphotungsten acid) or polymer electrolytes including Nafion 117 and Polyvinylidene fluoride (PVDF). In general, the specific capacitance, power, and energy for all-solid-state supercapacitors are significantly lower than those for liquid electrolyte based supercapacitors. Possible reasons for this can be: 1) the contact area between the electrolyte and electrode materials, especially porous electrode materials, in solid-state electrolyte supercapacitors is less than that in the liquid electrolyte supercapacitors, and 2) the ionic conductivity of solid electrolyte is less than that in the liquid electrolyte.

Table 2. 3 Comparisons between liquid electrolyte and solid electrolyte based supercapacitors.

Supercapacitor device	Specific capacitance on active materials	Specific power on device	Specific energy on device	Reference
Activated carbon electrode in liquid electrolyte	100-150 F/g	5 kW/kg	5 Wh/kg	[42]
Conductive polymer based electrode in liquid electrolyte	100-300	1-3 kW/kg	10-40 Wh/kg	[10, 42]
Typical RuO ₂ based electrode in liquid electrolyte	200-770 F/g	1-5 kW/kg	10-40 Wh/kg	[10, 42]
Ppy(DS)/PMMA-LiClO ₄ -EC/Ppy(DS)	20-60 F/g	0.2 kW/kg	3 Wh/kg	[43]
H ₃ PMo ₁₂ O ₄₀ ·nH ₂ O/Nafion /HRuO ₂ · nH ₂ O	112 F/g	0.2 kW/kg	3 Wh/kg	[44]

HRuO ₂ ·nH ₂ O/Nafion 117/HRuO ₂ ·nH ₂ O	170 F/g		5.5 Wh/kg	[45]
PANI composite/FEP-g-AA- SO ₃ H/PANI composite	98 F/g	0.25 kW/kg	5.0 Wh/kg	[46]
Activated C/Nafion+ PVDF/Activated Carbon	90-130 F/g		3.8-5.4 Wh/kg	[47]
Pani+DMS/EC+LiF/Pani/DMS	90 F/g	0.15 kW/kg	3.8 Wh/kg	[48]
RuO ₂ /LiPON/RuO ₂ /Pt	0.02 F/g			[49]
PANI/phosphotungsten acid/PANI	260 F/g	0.016 kW/kg	10 Wh/kg	[50]
Pyrrole/Nafion/Pyrrole	35 F/g	0.0037 kW/kg	3.4 Wh/kg	[51]

2.3 Polymer electrolytes

Polymer electrolytes are one of the most important components in all-solid-state electrochemical devices, including rechargeable batteries and supercapacitors. Polymer electrolytes have three important functions in supercapacitors and batteries: (1) they carry cations (mostly lithium ions), and (2) they serve as an electrode spacer or a separator [52, 53]. For the application of supercapacitors, the most emphasized properties in previous research are ionic conductivity and its behavior in a charge/discharge process, although the specific requirements are as follows:

- 1) Ion conductivity at an ambient temperature should be 10^{-3} S/cm or higher.
- 2) An applicable polymer electrolyte should have a wide potential window in which the charge/discharge can proceed without any side reaction or any process

giving rise to degradation of the performance and components of the supercapacitor.

3) An applicable polymer electrolyte should have good thermal stability because charge/discharge may release heat that may result in degradation of the supercapacitor.

4) Mechanical properties and manufacturability are important for its wide application.

5) Low costs are pursued for commercialization and implementation of the supercapacitor. The polymer electrolyte should be inexpensive and readily available.

Polymer electrolytes can be further divided into dry or solid polymer electrolytes, polymer gel electrolytes, and polyelectrolytes. Solid polymer electrolytes are defined as solvent free systems with an ionic conducting phase formed by dissolved salts in a polar polymer matrix. Gel electrolytes, also named as gelled polymer electrolytes, are usually obtained by incorporating a larger quantity of liquid plasticizer and/or solvents to a polymer matrix that is capable of forming a stable gel with the polymer host structure [40, 54]. The third category of polymer electrolytes may be called polyelectrolytes, which are different from the other two categories in that their

charged functional groups because they are covalently bonded to the polymer backbone [55]. Usually, the cations are mobile whereas anions are immobile. One of the subcategories of polyelectrolyte is perfluorosulfonic ionomers. The most widely applied ionomer electrolyte is perfluorosulfonic ionomers, including Nafion and its derivatives, which are well-known for fuel cell applications.

Dry (Solid) polymer electrolytes

Table 2. 4 Commonly used solid polymer electrolytes

Polymer electrolyte	Acronym	repeat unit	T _g (°C)	T _m (°C)
Poly(ethylene oxide)	PEO	$-(\text{CH}_2\text{CH}_2\text{O})_n-$	-64	65
Poly(propylene oxide)	PPO	$-(\text{CH}(\text{-CH}_3)\text{CH}_2\text{O})_n-$	-60	–
Poly[bis(methoxy ethoxyethox-ide)-phosphazene]	PMEP	$-[\text{N}=\text{P}(\text{-O}(\text{CH}_2\text{CH}_2\text{O})_2\text{CH}_3)_2]_n-$	-83	–
Poly(dimethylsiloxane)	PDMS	$-[\text{SiO}(\text{-CH}_3)_2]_n-$	-127	-40
Polyacrylonitrile	PAN	$-(\text{CH}_2\text{CH}(\text{-CN}))_n-$	125	317
Poly(methyl methacrylate)	PMMA	$-(\text{CH}_2\text{C}(\text{-CH}_3)(\text{-COOCH}_3))_n-$	105	–
Poly(vinyl chloride)	PVC	$-(\text{CH}_2\text{CHCl})_n-$	82	–
Poly(vinylidene fluoride)	PVF	$-(\text{CH}_2\text{CF}_2)_n-$	-40	~170

In dry polymer electrolytes, a salt is dissolved in the matrix of the polymer. To date, quite a few polymers have been used as the matrix of polymer electrolytes for various electrochemical devices. The most widely used dry polymer

electrolytes and their glass transition and melting temperatures between which the polymer electrolytes can be used are listed in Table 2.4. They are poly(ethylene oxide) (PEO) [56-64], Poly(propylene oxide) (PPO), poly(acrylonitrile) (PAN) [65-72], poly(methyl methacrylate) (PMMA) [73-76], poly(vinyl chloride)(PVC) [77-83] and poly(vinylidene fluoride) (PVdF) [84-90]. The most commonly used salts are lithium salts including LiClO_4 , LiBF_4 , LiPF_6 , LiAsF_6 , $\text{Li}(\text{CF}_3\text{SO}_3)$ (LiTFS), $\text{LiN}(\text{CF}_3\text{SO}_2)$ (LiTFSI), and $\text{LiC}(\text{CF}_3\text{SO}_2)_2$ that can readily be dissolved in high molecular weight polyether hosts such as PEO and PPO.

Polyelectrolytes

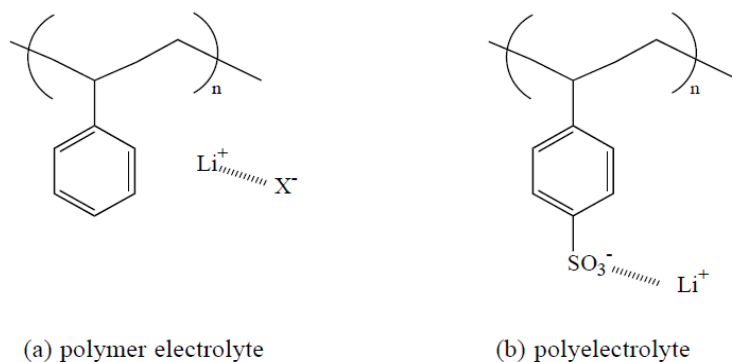


Figure 2. 5 Chemical structure schematic of polymer electrolyte and polyelectrolyte.

The difference between the polymer electrolyte and polyelectrolyte is the mobility of anions. The solid polymer electrolytes are a polymer matrix in which

both anions and cations from dissolved salts are mobile in the polymer matrix. However, in a polyelectrolyte, the anion of the salt is attached to the polymer matrix with covalent bond while the cation is movable in the electrolyte. This is schematically shown in Figure 2.5. Therefore, the polyelectrolyte is also called a single ion conductor and its cation transference number is close to 1.0, which is one of most important requirements for a rechargeable battery [91-93].

Ionomers have recently received much attention because they are single ion conductors with a high ionic conductivity (10^{-4} - 10^{-1} S/cm) [95]. Nafion, developed and commercialized by DuPont, is a perfluorosulfonated ionomer used as a separator or an electrolyte in a variety of electrochemical devices including sensors, fuel cells, batteries, and electro-organic synthesis systems [91]. Water facilitates the motion of protons through the polymer matrix and thus the water content and water dynamics determine proton exchange membrane properties, such as proton conductivity and transport of water [96]. Although Nafion and its derivatives have a high conductivity (10^{-3} - 10^{-1} S/cm), they are not suitable for use in the porous electrodes of a supercapacitor because the water in Nafion undergoes electrolysis at a voltage close to 1.2 V and sometimes even below 1.2 V. The

electrolysis of water that liberates hydrogen and oxygen is an irreversible process that depletes water in Nafion, thereby reducing conductivity, resulting in self discharge, and reducing the charge/discharge efficiency of a supercapacitor. Because of this, Nafion was rarely used as electrolyte in the porous electrode.

Polymer gel electrolytes

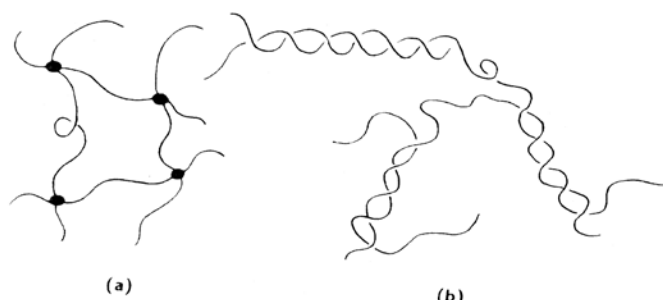


Figure 2. 6 Diagrammatic representation of a chemical gel network with junction points (a), and a physical gel network having junction zones (b) [99].

Generally, a polymeric gel is defined as a system which consists of a polymer network swollen with solvent [97]. Owing to their unique hybrid network structures, gels always simultaneously possess both the cohesive properties of solids and the diffusive transport properties of liquids. Some polymer gel electrolytes have high ionic conductivity of 10^{-3} S/cm at room temperature. However, their soft morphology, poor mechanical properties, and considerable viscosity may lead to internal short-circuits, give rise to safety concerns, and make polymer gel electrolytes unsuitable for high-speed manufacturing processes [98].

Gels can be obtained as a result of either a chemical or a physical cross-linking process. Chemical cross-linking, or covalent cross-linking, is a process associated with the covalent bonding of polymer chains by means of a chemical reaction to form a certain number of tie or junction points, as presented in Figure 2.6. Covalent cross-linking leads to the formation of irreversible gels. In such gels, the number of tie-points does not essentially change upon variation of external conditions such as temperature, concentration, or stress. By contrast, the gel network formed via physical cross-linking is called an entanglement network.

One promising gel electrolyte is based on poly(vinylidene fluoride) (PVDF). In 1983, Tsuchida and his coworkers [100, 101] found that the physically cross-linked gelled PVDF had a conductivity of 1×10^{-3} S/cm at 25°C.

Another gel system that has been extensively studied is the polyacrylonitrile (PAN) system. It displays higher conductivities than that of PEO [102]. The PAN-lithium salt system also has better thermal stability than PEO [103]. Dong's group [104] prepared a PAN polymer electrolyte with LiClO_4 salt and found that it was a poor ion conductor (1.51×10^{-8} S/cm at room temperature). However, when PC was

added, the conductivity of this gel hybrid film increased to 4.16×10^{-4} S/cm at ambient temperature.

2.4 PEO-based polymer electrolytes

Basic atomic structure

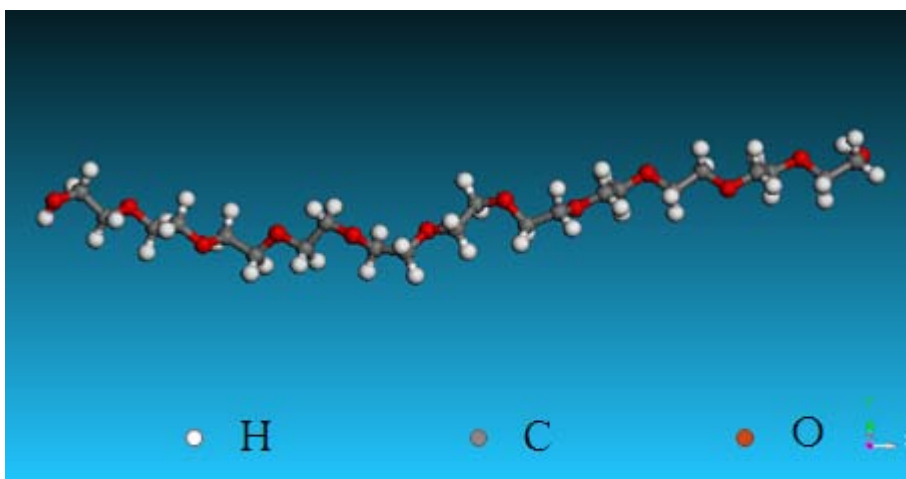


Figure 2. 7 A segment of a polyethylene oxide chain

So far, PEO based polymeric electrolytes have been the most suitable and extensively studied polymer ionic conductors because of the beneficial structure of PEO in supporting fast ion transport and their good compatibility, easy accessibility, and manufacturability. A segment of a PEO polymer chain is shown in Figure 2.7. The polymeric chain of PEO is capable of wrapping around lithium cations, creating coordination bonds and promoting dissolution and ionization of a lithium salt [105]. PEO has very good solvating properties for a wide variety of

salts, due to the interaction of its ether oxygen with cations. However, its performance as an electrolyte is strongly limited by crystallization of either pure polymer or complexes of PEO with salt [31].

Physical property

The melting point (T_m) of PEO is a function of the average molecular weight and the molecular weight distribution of the sample. Usually, it varies from 60°C for lower molecular weights (~4000 g/mol) to 66°C for higher molecular weights (~100,000 g/mol) [106]. The glass transition temperature (T_g) is also closely related to molecular weight. It increases from -65°C for a sample with a molecular weight of ~100,000 g/mol [104] to -17°C by decreasing the molecular weight to 6000 g/mol [107]. PEO is completely soluble in water at room temperature and is also soluble in a wide range of common organic solvents [103]. The thermal stability of PEO could be improved by adding inorganic fillers in order to increase T_m and decrease T_g .

Dry PEO electrolytes commonly exhibit conductivities at a level of 10^{-8} S/cm, which excludes practical applications at ambient temperature [55]. The conductivity can be increased to the level of 10^{-4} S cm^{-1} at room temperature by

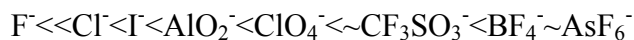
using various conductivity promotion methods. However, this conductivity level still does not quite satisfy the basic requirements for the electrolyte in a solid-state supercapacitor. The conductivity of PEO increases with increasing temperature. The temperature dependence of polymer electrolytes conductivity indicates that it is an activated process.

Mechanism of solvation of salt in PEO

For most polymer/salt complexes, cations should bind to the polymer chain instead of other ions. Also, to freely move in the polymer matrix, anions should have minimal interactions with polymers and cations [108]. A salt with a small univalent cation and a large anion is needed to satisfy all these requirements, e.g., weak anion-cation interaction and strong cation-polymer bonding.

The solubility and ionization of a salt in the PEO is determined by cation–polymer interactions, which can be predicted by the hard/soft acid base (HSAB) principle [106, 108]. The HSAB principle was formulated by Pearson as a means to explain and predict the solubility of complexes between Lewis acids and bases. A “hard” acid consists of smaller and non-polarizable cations, e.g. alkali ions, while a “soft ” acid has larger and easily distorted cations, e.g. Hg^{2+} . A “hard” base has non-

polarizable ligands with high electronegativity, e.g. ether oxygen, while a “soft” base has ligands with more polarizable groups, e.g. the thio group in thioether. The HSAB principle states that matching hard acids with hard bases or soft acids with soft bases yields the strongest interactions, or the strongest solvation. Therefore, for PEO polymers with hard bases, the best candidates for cations are non-polarizable small cations, e.g. Li^+ or Na^+ . A large anion with delocalized charge is required to dissolve ions in less polar solvents, such as polyether. The following order predicts the most appropriate anions for polyether-based polymer electrolytes [106, 108, and 109]:



Large and polarizable monatomic anions are very easily dissolved in polyether-based polymer electrolytes. The conductivity of commonly used PEO/LiX ($\text{X}=\text{AlO}_2^-$, ClO_4^- , TFS $^-$) polymer electrolytes are summarized in Table 2.5.

Table 2. 5 Summary of PEO/LiX ($\text{X}=\text{AlO}_2^-$, ClO_4^- , TFS $^-$) polymer electrolyte.

Electrolyte	Filler	$\sigma(\text{S/cm})$	$E_a(\text{eV})$	Ref.
PEO	$\text{SiO}_2+\text{PO}_4^-$	10^{-4} (160°C)		[110]
PEO	SBA15	10^{-5}		[111]
PEO	ZnO:Ga	10^{-7}		[112]
PEO	SiO_2	$10^{-6} \sim 10^{-4}$		[113]
PEO, LiI/I $_2$	TiO_2	1.6×10^{-6}		[114]
PEO+NaI		1.1×10^{-7}	1.5	[65]
PEO+NaI	$\beta\text{-Al}_2\text{O}_3$	2.5×10^{-6}	0.83	[65]
PEO+NaI	NASICON	1.5×10^{-5}	0.66	[65]

PEO+PMMA+LiI+EC	Composite	5.0×10^{-4}	0.55	[65]
PEO+PMMA+LiI+EC	MgO	2×10^{-4}	0.833	[65]
PEO+PMMA+LiI+EC	SiO ₂	0.1×10^{-4}	0.756	[65]
PEO+ LiClO ₄		10^{-6}	0.046	[65]
PEO+ LiClO ₄	α -Al ₂ O ₃	2.5×10^{-8}	0.048	[65]
PEO+ LiClO ₄		6.1×10^{-7}	1.26	[65]
PEO+ LiClO ₄	ionic glass	5×10^{-6}	0.82	[65]
PEO+ LiClO ₄	Ionite	2.2×10^{-6}	0.99	[65]
PEO+LiClO ₄	ZnAl ₂ O ₄	2.23×10^{-6}		[115]
PEO+LiClO ₄	LiAlO ₂	5.0×10^{-7}		[116]
PEO+ LiCF ₃ SO ₃ PEO	Li ₂ S,LiI,B ₂ S ₃ ZnO:Ga	$3.5 \times 10^{-5} \sim 10^{-7}$	3	[65]
PEO+ LiCF ₃ SO ₃ PEO	LiN ₃ SiO ₂	$10^{-6} \sim 10^{-4}$	0.17	[65]
PEO+LiClO ₄	ZnAl ₂ O ₄	2.23×10^{-6}		[25]
PEO+LiCF ₃ SO ₃	ZrO ₂		0.42	[26]

Mechanism of ionic conduction

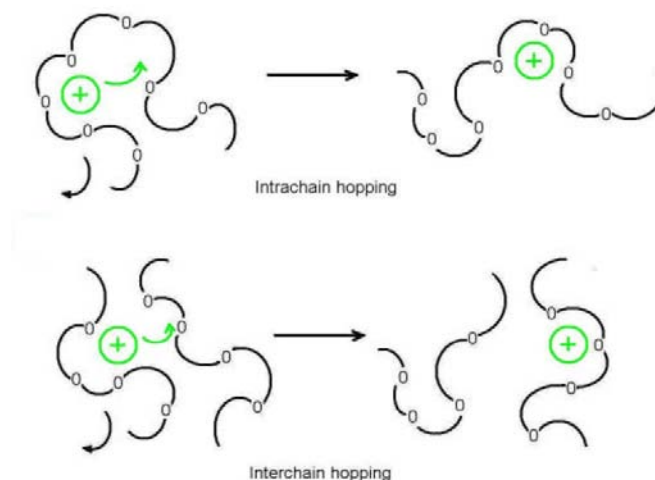


Figure 2. 8 Cation motion in a polymer electrolyte assisted by polymer chains only [98].

As a result of the motion of polymer chains, cations are able to move between coordination sites, either on one chain or between neighboring chains, called intrachain hopping and interchain hopping, respectively, shown in Figure 2.8 [106].

Moreover, considering ion association from the ion-ion interactions between ions,

there are other types of hopping mechanisms involving ion clusters, as shown in Figure 2.9. The extent of these movements is dependent on the concentration of ions in the polymer host. It is assumed that interchain hopping brings about high ionic conductivity [106].

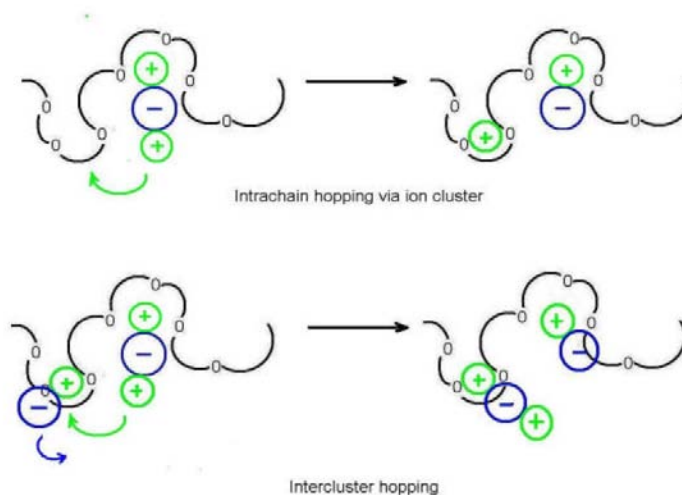


Figure 2. 9 Cations motion in a polymer electrolyte facilitated by the ionic cluster [98]

The amorphous phase is responsible for ionic conductivity [106, 108]. The electrolyte performance is strongly limited by the crystallization of pure polymer, or PEO/salt complexes [31]. PEO and most PEO/salt mixtures exhibit co-existence between crystalline and amorphous phases; in fact only 15-30% of PEO is in the amorphous phase at room temperature [117]. The unit structure of crystalline PEO could be established by X-rays and neutron scattering experiments [90, 117, 118].

For example, the phase diagram of PEO/LiTFS as illustrated in Figure 2.10 provides information about the various phases present in the system PEO-LiCF₃SO₃ in thermodynamic condition at each temperature [119-122]. The usual description of PEO-LiTFS composite structure consist of three-component, crystals of (PEO)₃LiTFS, crystals of PEO, and an amorphous PEO. At temperatures lower than 60°C, PEO polymer exists in its crystalline form together with the crystalline compound PEO₃LiCF₃SO₃. Above the melting temperature of the PEO matrix, the crystalline compound with an EO/Li molar ratio of 3: 1 is still present in the mixture with molten PEO in any sample with n ranging from 3 to 30. Above the PEO₃LiTFS compound melting temperature, the whole system is a a liquid (amorphous) state.

2.5 Methods for improving PEO-based electrolytes

There are five methods reported in the literature for improving the properties, especially conductivity, of PEO-base polymer electrolytes:

- 1) A significant improvement of ionic conductivity of polymer electrolytes can be achieved by choosing an anion to reduce the fraction of the crystalline phase in electrolytes, which would disturb regular alignment of polymer chains during

crystallization and act as a plasticizer in the polymer matrix.

A widely known example is the trifluoromethanesulfone (TFS) anion, which can form special PEO_3LiTFS crystalline structures at high concentration or become dissociated at low salt concentration [119, 120]. An additional advantage of the TFS anion is its low lattice energy, which improves solubility and allows for achieving high values of ionic conductivity and minimizing ion-ion interactions [123]. The glass transition temperature T_g of electrolytes with LiTFS salts are usually lower than that of electrolytes with other types of salts e.g. LiI or LiAlO_2 [123]. However, those plasticizing properties of LiTFS are limited to electrolytes with low amounts of salt content.

2) The addition of ceramic fillers into electrolytes is an effective strategy to further improve conductivity and mechanical properties of PEO electrolytes. Researchers have hypothesized that the interaction between surface groups on the polymer chains and charge carriers can improve the ionic conductivity. Thus, the electrolyte crystallinity can be decreased by introducing ceramic fillers [124]. However, sedimentation of the ceramic fillers, leading to inhomogeneity of the electrolyte and nucleation of crystalline phase on the filler grains, has to be

avoided. The ceramic fillers used in previous works include three families: 1) nano-sized oxide particles, e.g., SiO₂, Al₂O₃, TiO₂, ZnO; 2) layered clays, e.g., montmorillonite; and 3) mesoporous materials, e.g. SiO₂ and TiO₂.

Wang et al. report that the silane modified SiO₂ could further improve the compatibility of SiO₂ with the PEO/LiClO₄ matrix and effectively reduce the crystallinity of PEO/LiClO₄/SiO₂ composite electrolytes. XRD results show that the crystallinity of PEO decreases with an increases in the content of SiO₂. Thus, the conductivity of the PEO based electrolytes is gradually enhanced [111]. Zoppi et al. also found that the addition of SiO₂ could improve the ion conductivity of a PEO/LiClO₄/ SiO₂ electrolytes from 10⁻⁶ to 10⁻⁴ S/cm at room temperature [113].

Due to its particular structure, ordered-mesoporous silica could provide a great deal of “inner surface”, which facilitates the entrapment of liquid electrolytes into the mesoporous [125]. The conductivity increase upon adding SiO₂ is usually attributed to inert fillers, which could enhance the formation of an amorphous phase in semi-crystalline electrolytes [126]. Because ionic conduction takes place primarily through the amorphous phase of the polymer, high crystallinity leads to low conductivity. However, some research shows that T_m increases when the SiO₂

particles are added. This means that the volume fraction of crystalline phase increases. This is the opposite from former suggestions [126]. But it is in accordance with recent assertions by Choi et al. [127, 128], who reported that the formation of the crystalline phase is possible if the filler particle acts as a nucleation center of the crystalline polymer phase. Comparing the reported results can be ambiguous since the conductivity is sensitive to many factors such as the salt species and its concentration, particle size, temperature, thermal history, and preparative methods.

3) Incorporating suitable plasticizer into the polymer electrolyte is one of the most successful approaches in increasing the amorphous nature (i.e., reduction of polymer crystallinity) and hence ionic conductivity. The essence of plasticization is to enhance the conductivity of solid polymer electrolytes using low molecular weight and high dielectric constant additives, such as propylene carbonate (PC), ethylene carbonate (EC), polyethylene glycol (PEG), etc. [129-131]. These additives increase the amorphous content of the polymer matrix and tend to dissociate ion-pairs into free cations and anions, thereby leading to an overall enhancement in conductivity. Introducing side-chain structures provides another

effective method for improving the ion conduction by preventing regular alignment of the polymeric chains into lamellae during crystallization [131-133].

The approaches above rely on the preparation of polymer blends and composites. These additives inhibit the crystallization of PEO based electrolytes and often increase the polyether chain flexibility, causing an increase in ambient and subambient temperature conductivity.

4) A stretching process is used to stiffen the polymer chains and cause the alignment of the PEO helices in the force direction. As a result, very few helices remain oriented in the perpendicular direction. This process forms additional thermally stable phases [134-138]. One of the explanations for the conductivity increase is the creation of ion migration channels within the helical chains. Despite the conventional wisdom that ion transport in polymer electrolytes is mediated primarily by polymer segmental motion, Golodnitsky et. al have measured semicrystalline PEO complexes with LiI, which suggests that transport occurs preferentially along the PEO helical axis, at least in the crystalline phase. The principal basis for this claim is an observed enhancement by a factor of 5–20 in electrical conductivity in stretched polymer electrolyte films. Stretching results in

partial alignment of the PEO helices and also induces small but observable changes in the Li^+ solvation sheath. These results are correlated with the ionic conductivity enhancement in the stretched polymer [135].

2.6 Electrode materials

2.6.1 Carbon electrode

Carbon is the most frequently used electrode material for supercapacitors. Reasons for using carbon are manifold, and include (i) low cost, (ii) high surface area, (iii) accessibility, (iv) different forms attainable (powder, fibers, foams, fabrics, composites) and adaptable porosity with various surface functionality, (v) environmentally friendly, and (vi) easy processability [139-142]. Different carbon material electrodes have been intensively studied [142-144].

2.6.2 Polymer electrode

Conducting polymers such as p- and n-dopable poly(3-arylthiophene), p-doped poly(pyrrole), polyaniline, polythiophenes, poly(1,5-diaminoanthraquinone), poly-3-(3,4-difluorophenyl) thiophene, poly-3-(4-cyanophenyl) thiophene, poly-(3-para-fluorophenyl)thiophene and poly[bis(phenylamino)disulfide] have been suggested by

several authors as electrodes for supercapacitors [145-147].

The typical cyclic voltammogram of a polymer is not rectangular shape, as is expected for a typical capacitor, but exhibits a current peak at the respective redox potential of the polymer. In order to be able to use the same electrode material on both capacitor electrodes, polymers with a cathodic and an anodic redox process were recently utilized [147].

2.6.3 Metal oxides

Trasatti et al. first used RuO_2 as supercapacitor electrodes [148]. The RuO_2 -aqueous system has been extensively studied, and the specific capacitance was reported to be as high as 750 F/g with the H_2SO_4 electrolyte at low temperature [149-151]. Conducting metal oxides as RuO_2 or IrO_2 were the favored electrode materials in early SCs used for space or military applications [152]. The cyclic voltammogram of RuO_2 (and also IrO_2) electrodes have an almost rectangular shape and exhibit good capacitor behavior [150, 151]. However, the shape of the cyclic voltammetry is not a consequence of pure double layer charging, but of a sequence of redox reactions occurring in the metallic oxide. The valence state of

Ru may change from III to VI within a potential window of slightly >1 V. High specific capacitance in combination with low resistance resulted in very high specific powers. These capacitors, however, turned out to be too expensive. In addition, these capacitor materials are only suitable for aqueous electrolytes, thus limiting the nominal cell voltage to 1 V.

Several attempts were undertaken to keep the advantage of the material properties of such metal oxides at reduced cost. Other forms of metal compounds such as MnO_2 , [153, 154] NiO , [155] SnO_2 , [156] Fe_3O_4 , [157] were investigated. However, these materials are impractical for commercial use in SCs. As discussed above, different electrode materials have different benefits and drawbacks. In order to take full advantage of different electrode materials, composite supercapacitor electrodes made from metal oxide, conducting polymer, carbon nanotube or activated carbon have been studied.

2.7 Characterization methods

The common characterization methods for SC include electrochemical characterization and instrumental analyses.

2.7.1 Electrochemical characterizations

2.7.1.1 Galvanostatic method and cyclic voltammetry (CV)

The electrochemical performance of a supercapacitor can be characterized by galvanostatic and cyclic voltammetry methods. When using the galvanostatic method (constant current charge/discharge, CC), the supercapacitor is charged and discharged at a constant current within a potential range of 0 to V_{max} (V_{max} is the decomposition voltage of the electrolyte), and the voltage (V) is recorded as a function of time (t). When using the cyclic voltammetry (CV) method, the voltage (V) is swept between two voltages at a constant scan rate (s). The resulting current (I) is recorded as a function of time (t). For an ideal double layer capacitor, the current is independent of potential and shows a rectangular plot. However, if redox reactions occur, the rectangular shape is distorted, showing reduction and oxidation peaks.

2.7.1.2 Electrochemical Impedance Spectroscopy (EIS)

EIS has been embraced by corrosion specialists and electrochemical device researchers. The EIS data is usually used to build a nonlinear least-squares fitting routine model to extract physically meaningful properties of the electrochemical

system and analyze the mechanism of its behavior. EIS data may be obtained by using Nyquist plots or Bode plots. The real and imaginary components of the impedance can also be plotted against frequency on a log-log scale; this type of plot is known as a Bode plot. To fit the EIS data in the frequency domain, an equivalent circuit model is required [10].

Because of the difference in the mechanisms of storing charges between double-layer and conventional capacitors, traditional capacitor models are inadequate for supercapacitors. A number of models currently exist that apply to the operation of double-layer capacitors. The diagrams in Figure 2.10 represent a hierarchy of equivalent circuit, from those for a simple capacitor to those involving simple combinations of capacitor elements with either one or two resistors or capacitor, to more complex equivalent circuits involving distributed capacitance with ohmic elements in series or parallel coupling with capacitive elements and resistances in parallel with the capacitive elements. Figure 2.10(a) represents ideally polarizable interfacial capacitance by a capacitance (C_{dl}). Figure 2.10(b) represents interfacial capacitance in series with ohmic resistance. A simple model for a double-layer capacitor can be represented by a capacitance (C_{dl}) with an equivalent series

resistance (ESR) and an equivalent parallel resistance (EPR) or pore resistance (R_p) as shown in Figure 2.10(c). The ESR models power losses that may result from internal heating, which is important during charging and discharging. By determining these three parameters, one is able to develop a first order approximation of electrical double-layer capacitor behavior. If an EPR element changes into faradic leakage resistances, it indicates the contribution from pseudocapacitance associated with surface redox functionalities. Figure 2.10(d) is also called a Randle circuit with a constant phase element (CPE) replacing the double layer capacity (Cdl). The difference to Figure 2.10(c) is diffusion impedance $-W-$. While the simple model provides a first approximation of a double layer capacitor's behavior, it is observed that there is a large error when compared with experimental results. In this way, more complicated equivalent circuit modes are provided as shown in Figure 2.10(e) and (f).

ESR reduction of supercapacitors is very important in order to compete with other storage devices. There are at least four different contributions to the ESR originating from the (i) electrolyte including separator, (ii) current collector, (iii) porous layer including contact to current collector, and (iv) other contact

resistances. In order to prevent short circuits between neighboring capacitor electrodes, a porous separator has to be used as a spacer. Independent of the choice of electrolyte, the spacer has to be thin and highly porous in order to keep the resulting resistance low.

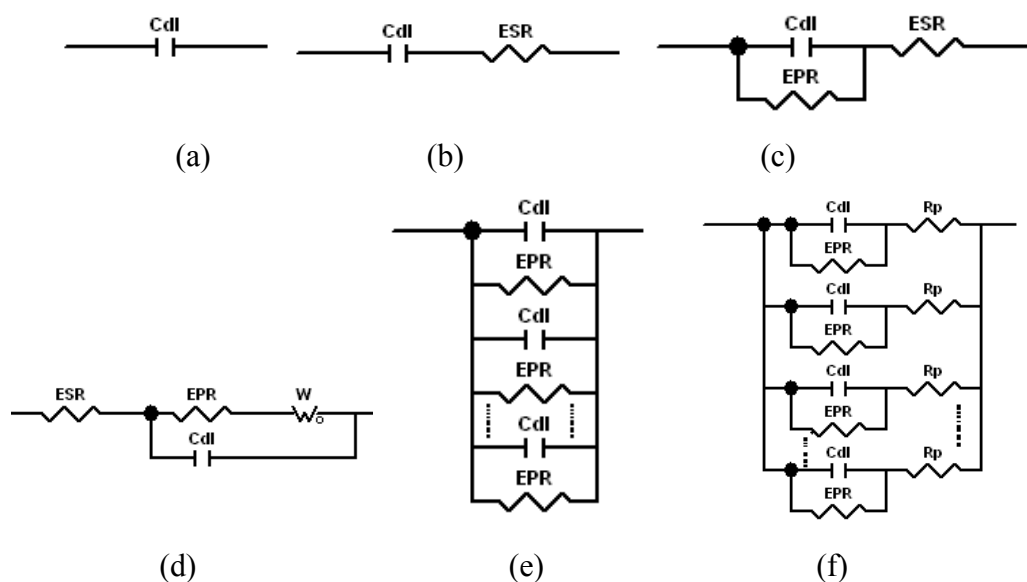


Figure 2. 10 Hierarchy of equivalent circuit (a) Simple capacitor (b) Capacitor with equivalent series resistance (ESR) (c) Capacitor with equivalent series resistance and equivalent parallel resistance (EPR) (d) Capacitor with equivalent series resistance and equivalent parallel resistance (EPR) in series with a Warburg element (e) Parallel combination of n C and EPR (f) parallel C, EPR elements connected with pore-resistance elements, R_p [19].

2.7.2 Instrumental analysis

Since the membrane electrolyte and electrode materials were prepared to assemble the electrochemical cell, scanning electron microscopy (SEM),

differential scanning calorimetry (DSC), fourier transform infrared spectroscopy (FTIR), nuclear magnetic resonance (NMR), X-ray diffractometry (XRD), X-ray Absorption Spectroscopy (XAS), and energy dispersive X-ray spectroscopy (EDS) have been applied to characterize the SC material.

2.7.2.1 SEM

The scanning electron microscope (SEM) is an electron microscope that images the sample surface by scanning it with a high-energy beam of electrons in a raster scan pattern. The electrons interact with the atoms that make up the sample producing signals that contain information about the sample's surface topography, and composition. Magnification in a SEM can be controlled over a range of up to 6 orders of magnitude from about 10 to 500,000 times. The specimens for an SEM testing must be electrically conductive, at least at the surface, and electrically grounded to prevent the accumulation of electrostatic charge at the surface. Nonconductive specimens tend to charge when scanned by the electron beam; therefore, they are usually coated with an ultrathin coating of electrically conducting material, commonly gold, deposited on the sample either by low vacuum sputter coating or by high vacuum evaporation. Coating prevents the

accumulation of static electric charge on the specimen during electron irradiation and increases the signal and surface resolution, especially with samples of low atomic number (Z).

2.7.2.2 EDAX

Since each element has a unique atomic structure, energy dispersive X-ray spectroscopy (EDAX or EDS) could be used for the elemental analysis through interactions between electromagnetic radiation and matter, analyzing X-rays emitted by the matter in response to being hit with charged particles. The energy of the X-rays is characteristic of the difference in energy between the two shells, and of the atomic structure of the element from which they were emitted. This allows the elemental composition of the specimen to be measured. EDAX systems are most commonly found on scanning electron microscopes (SEM-EDAX) and electron microprobes. A detector is used to convert X-ray energy into voltage signal and send to a pulse processor, which measures the signals and passes them onto an analyzer for data display and analysis. According to P. Staiti [201], EDX analyses were performed on different regions, which are chosen from the SEM figure of each sample to determine representative values of potassium contents.

Thus an atomic ratio calculated from EDAX will be considered representative for all samples.

2.7.2.3 DSC

Differential scanning calorimetry (DSC) is a thermoanalytical technique in which the difference in the amount of heat required to increase the temperature of a sample and reference are measured as a function of temperature. The DSC is mainly applied to study phase transitions, such as melting, glass transitions, or exothermic decompositions. These transitions involve energy changes or heat capacity changes that can be detected by DSC with great sensitivity. The result of a DSC experiment is a curve of heat flux versus temperature or versus time as shown in Figure 2.11. The exothermic reaction of the sample appears as a positive peak in Figure 2.11. Glass transitions (T_g) may occur as the temperature of an amorphous solid is increased. These transitions appear as a step in the baseline of the recorded DSC signal. This is due to the sample undergoing a change in heat capacity [159]. As the temperature increases, an amorphous solid will become less viscous. At one point the molecules may obtain enough freedom of motion to

spontaneously arrange themselves into a crystalline form. This is known as the crystallization temperature (T_c). This transition from amorphous solid to crystalline solid is an exothermic process, and results in a peak in the DSC signal. As the temperature increases the sample eventually reaches its melting temperature (T_m). The melting process results in an endothermic peak in the DSC curve. The ability to determine transition temperatures and enthalpies makes DSC an invaluable tool in producing phase diagrams for various chemical systems [159].

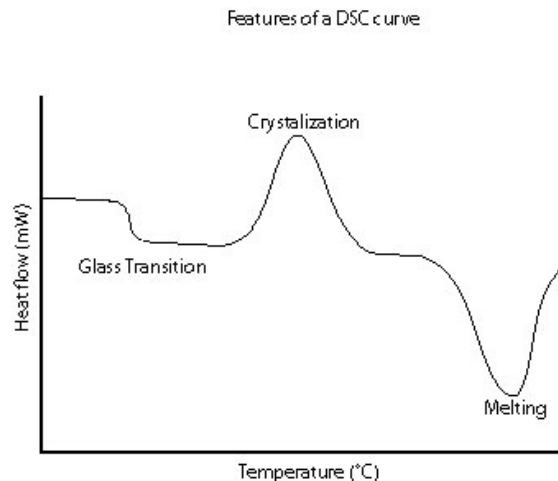


Figure 2. 11 Schematic DSC curve demonstrating the appearance of several common features

The morphology of a semicrystalline polymer, including PEO crystallized

isothermally, consists of primary crystals in a lamella stack. The closer the temperature of isothermal crystallization to the melting point, the larger the crystals grow as larger nuclei are formed that have to survive the thermal disorder. Upon cooling, smaller crystals or secondary crystals form, which leave the polymer amorphous chains in a metastable or nonequilibrium order. As the same polymer chain enters both amorphous and crystalline regions upon reheating, the smaller crystals melt out to free the amorphous chains and reform onto the larger crystals. Thus melting and recrystallization occur simultaneously. In a typical thermal scan from the glass transition to above the melting point, there are three melting endothermic regions. A jump in the specific heat first occurs at the T_g and long range motion of the polymer chains ensues. This is followed by a low temperature melting endothermic that occurs in the smaller secondary crystals. This again is followed by a melting endotherm of the primary crystals that is associated with the isothermal crystallization and then a large peak of recrystallized polymer melts at a higher temperature.

2.7.2.4 FTIR

Fourier transform infrared (FTIR) spectroscopy is a powerful tool for identifying types of chemical bonds in a molecule by producing an infrared absorption spectrum as a molecular "fingerprint". The principle of this technique is that molecular bonds vibrate at various frequencies depending on the elements and the type of bonds. There are several specific frequencies at which any given bonds can vibrate. According to quantum mechanics, these frequencies correspond to the ground state (lowest frequency) and several excited states (higher frequencies). One way to cause the frequency of a molecular vibration to increase is to excite the bond by having it absorb light energy. Molecular bonds vibrate at various frequencies depending on the elements and the type of bonds. Since FTIR provides information about the chemical bonding or molecular structure of materials without causing destruction, it could be used to identify unknown materials, detect the organic and some inorganic additives in the level of few percent, and characterize the chemical structure change and solvent residue. The FTIR peaks that appear in PEO based polymer electrolytes are listed in Table 2.6[160-164].

The appearance of the new peaks in FTIR spectrum indicates the formation of new

chemical bond, while the small position shift of the certain peak reflects the chemical environment change. The weakening or broadening of a peak means the materials with this chemical bond are being consumed or undergoing degradation [165]. In-situ FTIR is a really useful tool for monitoring the reaction process. Disappearance of reactant peaks may indicate that the reactant was fully consumed.

Table 2. 6 FTIR peak for PEO based polymer electrolyte.

Peak Position	peak assignment
650 to 600 cm^{-1}	peak of $\text{t}(\text{ClO}_4^-)$ band
636 cm^{-1}	cis C-H wagging mode
772 cm^{-1}	CF_3 stretching
787–790 cm^{-1}	the combination of C-S and S -N stretching
842 cm^{-1}	CH_2 wagging
918 cm^{-1}	stretching of C---N of acetonitrile
959 cm^{-1}	trans C-H wagging mode
962 cm^{-1}	the stretching of ether bond (C-O) of PEO
991 cm^{-1}	CH_2 twisting
1033 cm^{-1}	symmetric SO_3 vibrations of LiCF_3SO_3
1040 cm^{-1}	stretching of C---N of acetonitrile
1062 cm^{-1}	the C-O-C stretching vibrations
1100 cm^{-1}	the stretching of ether bond (C-O) of PEO
1107 cm^{-1}	the C-O-C stretching vibrations
1144 cm^{-1}	the C-O-C stretching vibrations
950-1250 cm^{-1}	the C-O-C stretching vibrations
1207 cm^{-1}	CF_3 stretching
1266 cm^{-1}	asymmetric SO_3
1267–1164 cm^{-1}	-C-F and - CF_2 - stretching
1282 cm^{-1}	CH_2 twisting vibration from PEO
1350 cm^{-1}	the CH_2 wagging mode
1355 cm^{-1}	asymmetric SO_2 stretching mode
1408 cm^{-1}	-C-F stretching
1450 cm^{-1}	Asymmetric bending

1465-1485 cm^{-1}	CH_2 scissoring
1602 cm^{-1}	C-C bonds stretching vibration in aromatic ring, the C=C bonds of benzene rings
1630 cm^{-1}	the bending mode of water molecules
1688 cm^{-1}	-CH = CF- skeletal bending
1693 cm^{-1}	overoxidation of the polymers in the mixed electrolytes, resulting in the formation of carboxyl groups on the polymer chains
1950-1970 cm^{-1}	Asymmetric stretching
2700 cm^{-1}	C-H stretching mode
2800-2935 cm^{-1}	C-H stretching mode
2982 cm^{-1}	C-H stretching mode
3000 cm^{-1}	C-H stretching mode
3300-3500 cm^{-1}	N-H stretch
3200-3600 cm^{-1}	OH stretch from alcohol or phenol

2.7.2.5 XRD

The atomic planes of a crystal cause an incident beam of X-rays to interfere with one another as they leave the crystal. This phenomenon is called X-ray diffraction. X-ray crystallography is a method of determining the atom arrangement within a crystal or the crystalline structure of materials, including the size of atoms, the lengths and types of chemical bonds, and the atomic-scale differences. XRD can be used to measure the average distance between layers or rows of atoms, determine the orientation of a single crystal or grain, find the crystal structure of an unknown material, and measure the size, shape and internal stress of small crystalline regions [166].

For polymer electrolytes, the information about molecule structure and atom arrangement could be evaluated from XRD so as to build atom models for those polymer electrolytes [167]. For polymer electrolytes, XRD can be used to examine the influence on the crystallinity caused by adding filler [168]. In this way, the optimal amount of filler can be determined according to the lowest PEO peak intensity observed from XRD patterns. For electrode materials, XRD not only confirms the crystal structure of the electrode, but also detects whether there is residue or side reaction during the preparation [169, 170].

2.8 Summary

All-solid-state supercapacitors promise a non-leaking, non-corrosion, environmentally benign, and high life cycle power source. However, up to now, the specific energy and specific power of supercapacitors are limited.

As mentioned, the key challenges for the all-solid-state supercapacitors are 1) to increase the conductivity of the electrolyte in porous electrodes, and 2) to mitigate the contractor or accessibility problem. The previous optimization of supercapacitor electrodes usually focused on electrode parameters, e.g. pore size distribution, particle size, binder and thickness.

This thesis presents two approaches to improve the all-solid-state supercapacitors. First, we will tailor and improve the conductivity of PEO polymer electrolytes using a hot pressing method, adding select lithium salt with different anions and SiO₂/TiO₂ inorganic fillers. Secondly, the I₃⁻/I⁻ mediators will be added to PEO electrolytes to provide the pseudocapacitance for the composite supercapacitor. This approach also promises to solve or mitigate the accessibility problem, and to increase the conductivity.

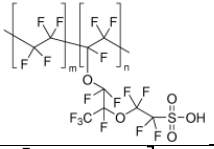
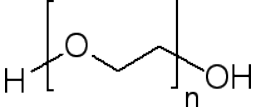
Electrochemical measurements including cyclic voltammetry, electrochemical impedance spectroscopy, and charging/discharging will be performed to assess the performance of supercapacitors. A number of analytical tools such as DSC, XRD, FTIR, and SEM will be used to examine the stability, phase purity, morphology, porosity, chemical properties of various components used in constructing the supercapacitors.

CHAPTER 3 EXPERIMENTAL

3.1 Materials

The trade names, chemical names, molecular weights, molecular structures, concentration/purity, and sources for the materials used in this dissertation are listed in Table 3.1. Nafion 117 and PEO are used as polymer matrices. LiAlO_2 , LiClO_4 , and LiTFS are added to PEO as Lithium sources, EC and PC are added as plasticizers in the electrolyte materials. NaI and I_2 are the mediator materials. Active carbon (AC) is the electrode material. AN, ethanol and DI water are the solvents.

Table 3. 1 Materials used in the experiment.

	molecule	Molecular weight	Structure	Concentration /state/ Grade	Source
Nafion 117				~5% in lower aliphatic alcohols and water/purum	Aldrich
PEO	Poly(ethylene oxide)	~400,000		powder	Aldrich
LiAlO_2	Aluminum lithium oxide	65.92	LiAlO_2	powder and chunks/ 97%	Aldrich
LiClO_4	Lithium perchlorate	106.39	LiClO_4	trace metals basis/98%	Fluka

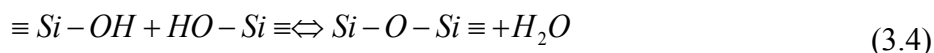
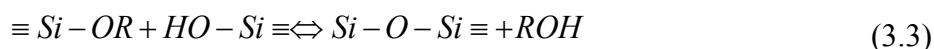
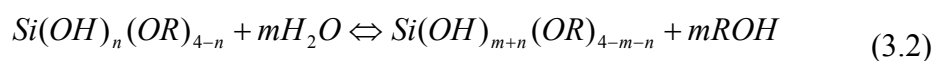
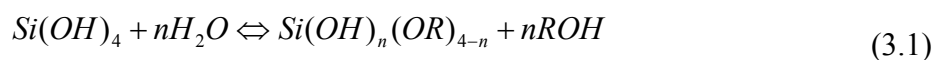
LiTFS	Lithium trifluoromethanesulfonate	156.01		powder/Purum	Fluka
AC	Active Carbon	12.	C	Black powder VULCAN XC72R	Cabot
TEOS	Tetraethyl orthosilicate	208.33		trace metals basis/99.999%	Aldrich
Ti source	titanium(IV) isopropoxide	284.22		Purum/ 97%	
EC	Ethylene carbonate	88.06		anhydrous/99%	Aldrich
PC	propylene carbonate	102.09		Selectophore/ ≥99.0% (GC)	Fluka
NaI	Sodium iodide	149.89	NaI	anhydrous, trace metals basis powder/99.55%	Alfa Aesar
I ₂	iodine	253.81	I ₂	ACS reagent, Powder/99.8%	Alfa Aesar
HCl	Hydrochloric acid	36.46	HCl	0.5N volumetric solution/analyzed	J.T.Baker
H ₂ O	Distilled water	18.02	H ₂ O		FIU
P123	Phencyclidine hydrochloride	279.85		C ₁₇ H ₂₅ N · HCl	Sigma
EtOH	Ethanol	46.07	CH ₃ CH ₂ OH	200 proof, anhydrous/99.5%	Aldrich
AN	Acetonitrile	41.05	CH ₃ CN	anhydrous/99.8%	Aldrich

3.2 Fabrication of PEO/LiX (X=AlO₂⁻, ClO₄⁻, TFS⁻) base SCs

3.2.1 Preparation mesoporous SiO₂ and TiO₂ with sol-gel method

i) SiO₂ sol-gel preparation

The SiO₂ sol was prepared by diluting tetraethyl orthosilicate (TEOS) (C₈H₂₀O₄Si, Fluka, >98%, 10.4g) in absolute ethanol (23 g), deionized water (9 g), and hydrochloric acid (0.5N, 9 ml) in a beaker. The solution is constantly stirred using a magnetic stirrer. The pH of the solution is monitored using a pH meter. The formation of silica networks from tetraethoxysilane as a silica source can be described as follows.



The final concentration of the SiO₂ sol-gel is 6.75 mmol/g.

ii) TiO₂ sol-gel preparation

The TiO₂ sol was prepared by diluting titanium (IV) isopropoxide (TiOCH(CH₃)₂)₄ Sigma-Aldrich, 97%, 14.2g) in absolute ethanol (23 g), deionized

water (9 g), and hydrochloric acid (0.5N, 9 ml) and then constantly stirring using a magnetic stirrer. The pH of the solution is monitored using a pH meter. The procedure for preparation of TiO₂ sol-gel is similar to that for preparing SiO₂ sol-gel.

3.2.2 Preparation of PEO/LiX(X=AlO₂⁻, ClO₄⁻, TFS⁻) polymer electrolyte

The PEO/Lithium salt (LiX) (X=AlO₂⁻, ClO₄⁻, TFS⁻) composite polymer electrolytes were fabricated with high-molecular-weight (MW=4×10⁶ g/mol) PEO and lithium salt in the molar ratio of 8:1 by a solvent-casting technique. The lithium salt includes lithium aluminate (LiAlO₂) powder, lithium trifluoromethanesulfonate (LiTFS) powder and lithium perchlorate (LiClO₄) powder.

PEO/LiAlO₂ based polymer electrolytes were prepared by dissolving the PEO and LiAlO₂ in an acetonitrile (AN) solution and then stirring at 60°C for about three hours until the suspensions turned into a homogeneous translucent gel. Then SiO₂ or TiO₂ prepared in 3.3.1 was added in PEO/LiAlO₂ (PA) gel and stirred at 60°C for another hour to make the homogeneous translucent PEO/LiAlO₂/SiO₂

(PAS) or PEO/LiAlO₂/TiO₂ (PAT) electrolytes gel. The mass ratio of acetonitrile solution to the total mass of the mixture of solid components was usually 10:1.

The PEO/LiTFS/EC (PLE) or PEO/LiTFS (PL) polymer electrolytes were prepared by dissolving PEO, LiTFS, and ethylene carbonate(EC) in acetonitrile (AN) with a mole ratio of PEO/LiTFS/Eth=8:1:1. LiTFS is dispersed in acetonitrile under strong ultrasonic first. Then, it was added into PEO/LiTFS composite solution. The mixture was stirred for three hours at 60°C with a magnetic bar to until slurry become homogeneous gel.

The PEO/LiClO₄ (PLC) polymer electrolytes were prepared using the same method. PEO was mixed with LiClO₄ powder and dissolved in acetonitrile solution to prepare the PEO/LiClO₄ composite polymer electrolyte. The mix was stirred at 60°C for about four hours until the suspensions turned into a homogeneous translucent gel.

The composite polymer electrolyte gel were weighed and poured in a template made from a Teflon dish. The solvent evaporated gradually at room temperature in dry air for 24 hrs. Thin foil was obtained after drying the solvent in a vacuum chamber overnight. Finally the homogeneous and mechanically stable films with a

thickness range from 8mm to 16mm were obtained. The preparation procedure of the PEO/LiX ($X=\text{AlO}_2^-$, ClO_4^- , TFS^-) based polymer electrolytes composite with SiO_2 is shown in Figure 3.1.

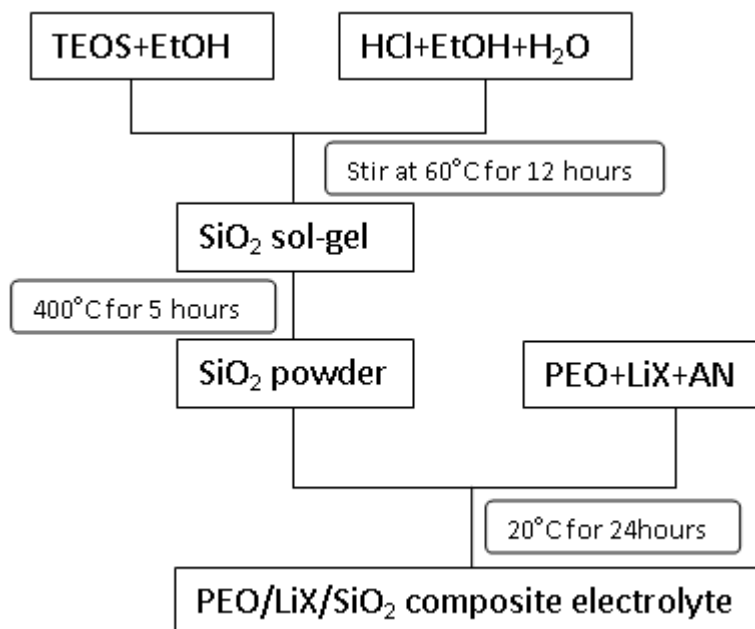


Figure 3. 1 Preparation procedure for PEO/LiX/SiO₂ ($X=\text{AlO}_2^-$, ClO_4^- , TFS^-) electrolyte.

3.2.3 Add iodide/iodine/ (I^-/I_2) mediators into PEO/LiX gel

Sodium iodide (NaI) powder and iodine (I_2) crystals were mixed in the molar ratio of 2:1, then dissolved in H_2O solution with 20% ethanol. The NaI/ I_2 solution was added into the PEO gel that was prepared using the procedure stated above. The mass ratio of the mediators to PEO/LiX ($X=\text{AlO}_2^-$, ClO_4^- , TFS^-) was around

1. Activated carbon (VULCAN XC72R) powder (Carbot) (AC) was added for the PEO/LiX ($X=\text{AlO}_2^-$, ClO_4^- , TFS^-) gel. The solid content mass ratio of PEO/LiX ($X=\text{AlO}_2^-$, ClO_4^- , TFS^-) gel to NaI/I₂ solution to carbon powder is 1:1:1. The gel was sonicated for at least one hour before use.

3.2.4 Preparation of electrode and electrode assembly

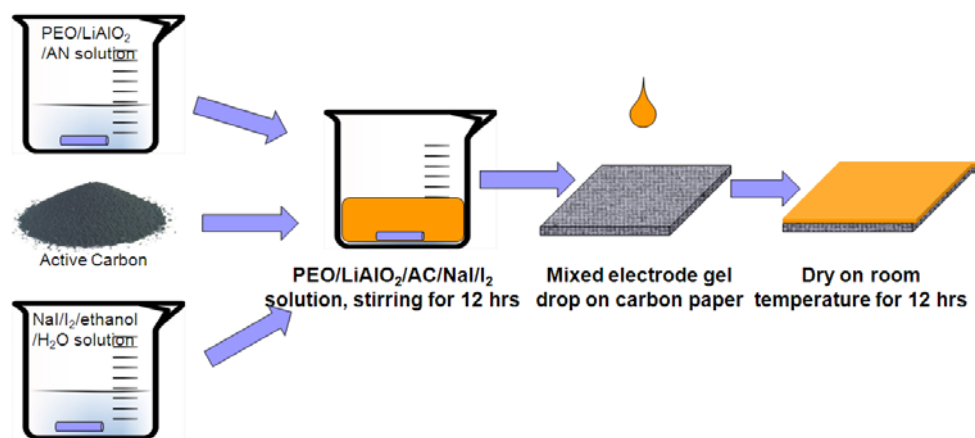


Figure 3. 2 Preparation procedure for Mediator enhanced PEO/LiX/AC ($X=\text{AlO}_2^-$, ClO_4^- , TFS^-) based electrode.

A nanofoam carbon paper was acquired from Marketch International Inc. The specification of the carbon paper is as follows: density, 0.25 - 1.0 g/cm³, surface area, BET 400 m²/g, average pore size 0.7 nm, electrical resistivity, 0.010-0.040 ohm/cm, and specific capacitance 30 F/g. The prepared PEO/LiX/AC ($X=\text{AlO}_2^-$, ClO_4^- , TFS^-) gel was dropped on a piece of nanofoam carbon paper. After loading

with the PEO/LiX/AC ($X=AlO_2^-$, ClO_4^- , TFS^-) gels, the electrodes were dried naturally in air for about twelve hours and then were sealed in a plastic bag. To make a supercapacitor assembly, a piece of Nafion 117 membrane was immersed in 0.5 M sulfuric acid at room temperature for two hours before application. The sandwich of two carbon electrodes ($1.0-2.5\text{ cm}^2$) either loaded or not loaded with mediator and a Nafion membrane was pressed at about 4500 psi for one minute. The supercapacitor assembly is schematically illustrated in Figure 3.3. One piece of gold frame was applied as current collector on each side. In order to remove the effect of nanofoam carbon paper, PEO/LiX/AC ($X=AlO_2^-$, ClO_4^- , TFS^-) gel was painted on each side of the Nafion 117 membrane with a cosmetic brush as an electrode for part of the samples.

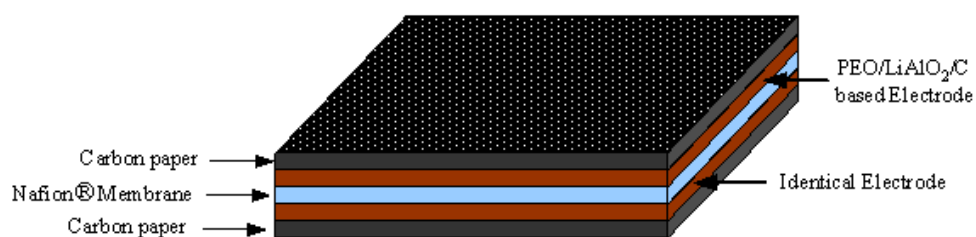


Figure 3. 3 Schematic of supercapacitors for electrochemical tests.

3.3 Characterization and evaluation of PEO electrolyte-based supercapacitors

3.3.1 Phys-chemical property Characterization

SEM has been the most commonly used tool to characterize the morphology and topology of different samples. The surface morphologies of the composite electrolyte and electrode were investigated using scanning electron microscopy (JEOL JSM 5900LV) and Table-top SEM (Phenom). All the samples were covered by gold film using a gold sputtering device before testing. An Olympus BX60 light microscope with polarized light function was also used to observe the surface state of the membrane.

X-ray diffraction (XRD, Seifert diffractometer) was used for examination of morphology and structure of the hybrids and silica gel obtained in this work. XRD experimentation was conducted on the membranes with an automated X-ray diffraction system configured with a theta/two-theta goniometry, fitted with a Peltier-type solid-state detector at a scan rate of $0.02^{\circ}\text{C}/\text{min}$ and a step of 0.04°C . Data was recorded before and after heating the film. The XRD beam penetrated the sample to a depth of 10–15Å, which ensured that only the bulk polymer on top of the pores was being examined.

Fourier transform infrared spectroscopy (Bio-Rad FTS-60VM FTIR spectrometer) was used for examination of the complexity of the composite membranes obtained in this work. This method facilitates characterization of vibrations in molecules by measuring the absorption of light of certain energies that correspond to the vibration excitation of the molecules from lower to higher states.

Differential Scanning Calorimetry (DSC) was carried out under nitrogen atmosphere with Dupont TA 2910 modulated DSC. The sample weight and the weight of the crimped pan and sample were taken before and after each thermal scan. The relevant regions of temperature that we are interested in are the glass transition temperature (T_g) and melting temperature (T_m). Thermal scans were made at 10°C/min between -120 °C to 120 °C and extended to 220 °C if deviation in value occurred at a specific heat for the first thermal cycle. The sample was air quenched in the DSC TA 2920 and then scanned for a second thermal cycle; thus a common thermal history was given to the samples. The thickness was measured for each sample.

3.3.2 Electrochemical performance evaluation

A GAMRY potentiostat/Gavanotat/ZRA analyser was used to run all the electrochemical tests. Both electrochemical impedance spectroscopy (EIS) and cyclic voltammetry (CV) measurements were taken at ambient temperature using solid-state electrochemical cells assemblies by sandwich electrolyte membrane between two planar electrodes.

3.3.2.1 In-plane conductivity measurement

A four-point In-plane conductivity measurement was also applied to get In-plane conductivity of polymer electrolyte. The frequency range for the impedance test was 1 Hz–100 KHz. The schematic of a four-point fixture for the conductivity measurement of a polymer electrolyte membrane is shown in Figure 3.4. The two Pt wires are used as working sense and reference electrodes while the wires in connection with the stainless sheets are used as working and counter electrodes. While a small AC current is passed through the membrane, the working sense and reference electrodes detect the potential drop along the distance between the two Pt wires. The resistance between the two Pt wires is then used to evaluate the conductivity, σ , by,

$$\sigma = \frac{l}{RS} \quad (3.5)$$

where R is the resistance, l is the distance between the two Pt wires, and S is the cross section area of the membrane. The four electrode method is not strongly related to the interfacial state of the cell and can provide reliable In-plane conduction information.

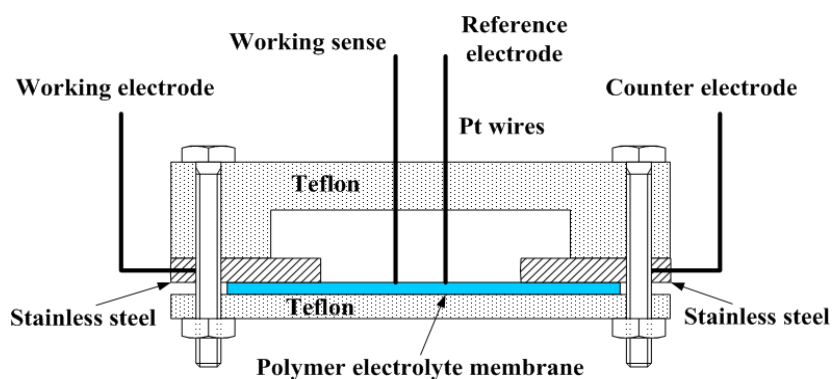


Figure 3. 4 Schematic of the fixture for a standard four-point conductivity measurements.

3.3.2.2 Through-plane conductivity measurement

The through-plane conductivity of the membrane was carried out using electrochemical cells formed by sandwiching the given electrolyte membrane sample between two blocking graphite electrodes as shown in Figure 3.5. This was also named the two electrode conductivity measurement method. The membrane was sealed in a cell and heated in vacuum oven where AC Impedance was conducted over a temperature range of 30–80°C. The through-plane resistance was

read by the intercept point of the Nyquist curve of the high frequency part with the axis of the real impedance. The EIS result for PEO based electrolyte is usually a semi-circle followed by a straight line. However, sometimes the semicircle is not fully exhibited in Nyquist plot due to the limit of maximum measurement frequency. On the one hand, the interpretation of EIS results relies on nonlinear equivalent circuit models, which will cause simulation error, the influence of interface resistance will also cause measurement error. On the other hand, the In-plane resistance is the sum of the bulk and surface resistances, while the Through-plane resistance is mainly bulk resistance. Therefore, thinner membranes may appear to have higher conductivity if the surface conductivity is much greater than the bulk conductivity. Even if the conductivity from the two-electrode method is not as reliable as that of the four-electrode method, it is a good confirmation for the four-electrode method and it is closer to practical application of measurement methods.

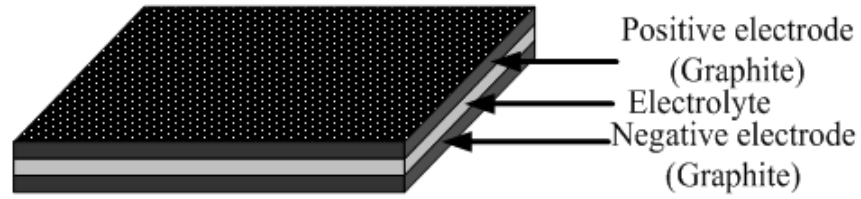


Figure 3. 5 Schematic of the Two-electrode Through-plane conductivity measurements.

3.3.2.3 Cyclic voltammetry measurements

Cyclic voltammetry (CV) tests a supercapacitors response to a changing voltage, and can be used to calculate capacitance. CV testing involves applying a voltage which increases constantly with time (referred to as a voltage sweep).

Electrochemical cells (ECs) were formed by sandwiching the given electrolyte membrane sample between two composite electrodes loaded on the carbon paper.

The membrane was placed between two gold nets held at a constant force. The responsive current to the voltage sweep is recorded. The average specific capacitance is evaluated by

$$C = \left(\int_0^{V_r} \frac{dq}{dV} dV / \int_0^{V_r} dV \right) \frac{1}{m} = \left(\int_0^{V_r} \frac{idt}{dV} dV / \int_0^{V_r} dV \right) \frac{1}{m} = \frac{Q}{V_r} \frac{1}{m} \quad (3.6)$$

where V_r is the potential range, Q is the total charge in a half cycle, i is the current, and m is the mass. The specific power is evaluated by

$$P = \text{Max}(i \times V) / m \quad (3.7)$$

The ECs were tested at various scan rates. The results of the CV testing were plotted as a voltammogram, which gives insight into the capacitive and pseudocapacitive behavior of the EC.

In this chapter, the effects of anions, adding inorganic ceramic fillers, increasing temperature, hot pressing, and the dispersing of mediators on conductivity of polymer electrolytes will be evaluated. Mechanisms for improvement will be discussed.

4.1 Effect of different anions

4.1.1 Conductivity measurement results

Table 4.1 shows that both in-plane and through-plane conductivities of PEO/LiX (X=AlO₂⁻, ClO₄⁻, TFS⁻) electrolytes follow the order of PEO/LiAlO₂ < PEO/LiClO₄ < PEO/LiTFS. Since all the other parameters except the type of anion are the same in the polymer electrolytes, the cause for conductivity difference must be related to anion type. Ionic conductivity is primarily controlled by the number of free ions and the mobility of the ions. Because the molar ratios of salts in the PEO polymer electrolyte are the same, the difference in conductivity is primarily controlled by the number of free carrier ions or the dissociation degree or solubility of the salts in PEO.

Table 4. 1 In-plane conductivity and through-plane conductivity of PEO/LiX (X=AlO₂⁻, ClO₄⁻, TFS⁻) polymer electrolytes ($\sigma_{\text{in-plane}}$ is the in-plane conductivity and $\sigma_{\text{through-plane}}$ is the through-plane conductivity)

	Thickness (cm)	Density (g/cm ³)	$\sigma_{\text{in-plane}}$ (S/cm)	$\bar{\sigma}_{\text{in-plane}}$ (S/cm)	$\sigma_{\text{through-plane}}$ (S/cm)	$\bar{\sigma}_{\text{through-plane}}$ (S/cm)
PEO ₈ /LiAlO ₂	0.025	1.23	3.55×10 ⁻⁵	4.45×10 ⁻⁵	2.61×10 ⁻⁷	3.77×10 ⁻⁷
			4.13×10 ⁻⁵		3.48×10 ⁻⁷	
			5.67×10 ⁻⁵		5.22×10 ⁻⁷	
PEO ₈ /LiClO ₄	0.020	1.30	1.14×10 ⁻⁴	1.01×10 ⁻⁴	1.02×10 ⁻⁶	1.12×10 ⁻⁶
			1.75×10 ⁻⁴		0.98×10 ⁻⁶	
			1.42×10 ⁻³		1.36×10 ⁻⁶	
PEO ₈ /LiTFS	0.015	1.07	1.84×10 ⁻⁴	1.22×10 ⁻⁴	1.38×10 ⁻⁶	5.29×10 ⁻⁶
			0.82×10 ⁻⁴		1.11×10 ⁻⁵	
			1.00×10 ⁻⁴		3.42×10 ⁻⁶	

The addition of a salt that is highly dissociable in PEO is one convenient method to increase the number of free carrier ions. A lithium salt of low lattice energy usually results in more amorphous phases in PEO/LiX (X=AlO₂⁻, ClO₄⁻, TFS⁻) electrolytes [171, 172]. Under the same mobility, the ionic conductivity is proportional to the lattice energy, which can be calculated from the differential scanning calorimeter (DSC) cycle [123, 173, 174]. The lattice energy of the salt is proportional to the logarithm of the dissociation degree. Since the number of carrier ions is determined by the dissociation degree of the salt, the logarithm of normalized ionic conductivity should be inversely proportional to the lattice energy of the salt,

or the lower the lattice energy, the greater the solubility. The crystal structures of LiAlO_2 [175], LiClO_4 [176], and LiCF_3SO_3 [177] are shown in Figure 4.1. Figure 4.1(a) shows the crystal structure of LiAlO_2 , in which oxygen ions are shown in grey, lithium ions in black, and aluminum in white. Four ions of oxygen forming tetrahedral coordination around an Al ion are shown in the upper left part of the figure. LiAlO_2 crystallizes in three different structures, and the tetragonal γ -phase is stable. Perspective view of the crystal structure of LiClO_4 along [001] is shown in Figure 4.1 (b). The chains of edge connected $[\text{LiO}_6]$ octahedral run along [010]. LiClO_4 has orthorhombic symmetry. In the crystal structure of LiClO_4 the Li^+ ion is surrounded octahedrally by six oxygen atoms that belong to six ClO_4^- ions. Each perchlorate ion is coordinated by six Li^+ ions and exhibits nearly perfect tetrahedral symmetry. A view of the molecular packing of LiTFS within the unit cell is shown in Figure 4.1(c). It has been reported that the lattice energy of LiTFS and LiClO_4 is lower than LiAlO_2 but whether the lattice energy of LiTFS is greater than that of LiClO_4 is not yet known [123]. According to HSAB principle stated in Chapter 2.4, polymers with hard bases, the best candidates for cations are non-polarizable small cations. To dissolve ions in less polar solvents, such as PEO, a large anion and

polarizable monatomic anions are very easily dissolved [106, 108, 109]. In addition to the relationship between the conductivity and solubility, Boldyrev also proposed that larger and more polarizable monatomic anions are more easily and readily dissolved in polyether-based polymer electrolytes [109]. The size of these three different anions follows the order of $\text{LiAlO}_2 < \text{LiClO}_4 < \text{LiTFS}$. Thus, the LiTFS is highest solubility in the PEO and PEO/LiTFS has the greatest conductivity is in line with the previous evidence.

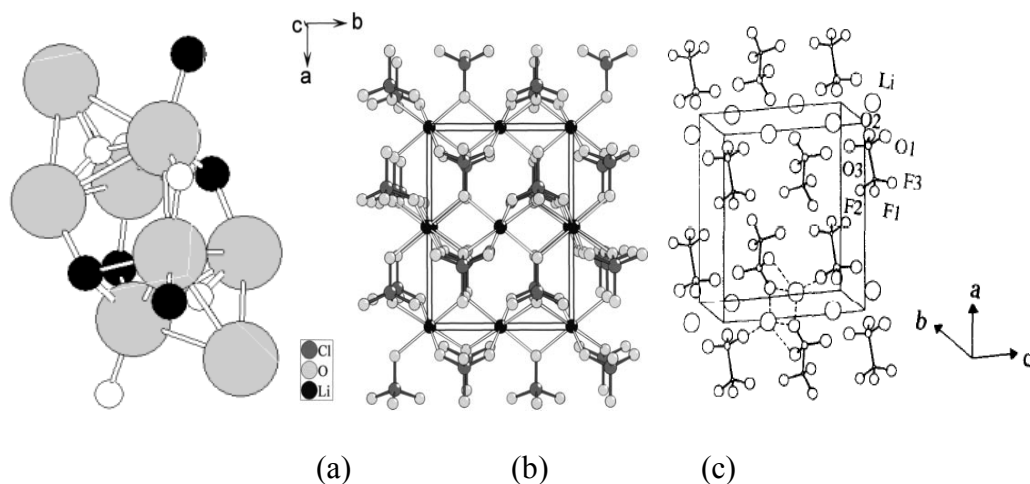


Figure 4. 1 The crystal structure of Lithium salt (a) LiAlO_2 , (b) LiClO_4 , and (c) LiTFS .

4.1.2 XRD analysis

The XRD spectra for PEO/ LiAlO_2 and PEO/ LiTFS are illustrated in Figures 4.2-4.3, respectively. The spectra indicate that the PEO membranes are primarily

composed of low molecular weight PEO or polyethylene glycol (PEG). The major difference between the spectra for PEO/LiAlO₂ and PEO/LiTFS is that in the spectrum for PEO/LiAlO₂ there are obvious peaks for LiAlO₂ whereas there is no obvious peak for LiTFS in the spectrum for PEO/LiTFS. This means that in PEO/LiTFS polymer electrolytes, either the LiTFS salt is completely dissolved or dissociated, or the LiTFS salt is in an amorphous state. The former case is more possible because no amorphous characteristic is presented in the spectrum. These results strongly support the conclusion that LiTFS is much more soluble in PEO than LiAlO₂ in PEO.

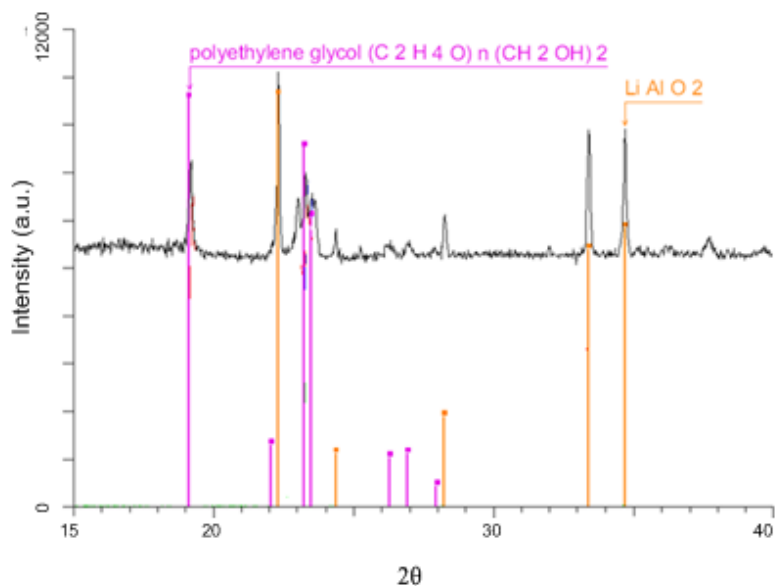


Figure 4. 2 XRD spectrum of a PEO/LiAlO₂.

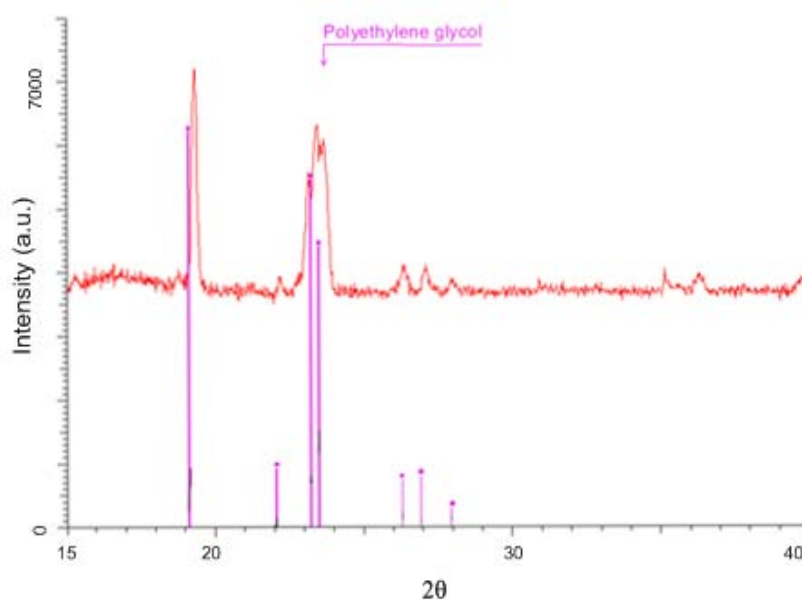


Figure 4. 3 XRD spectrum of a PEO/LiTFS.

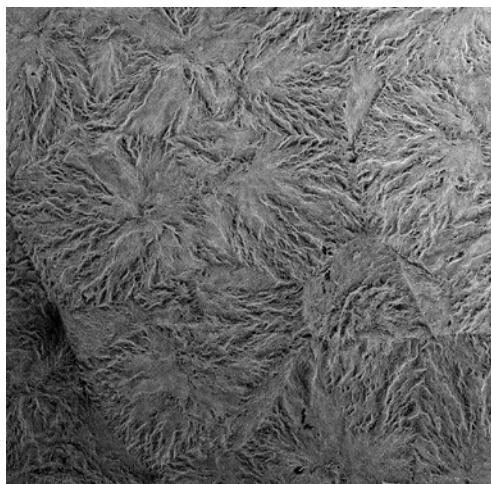
SEM analysis

PEO/LiX ($X=\text{AlO}_2^-$, ClO_4^- , TFS^-) polymer electrolyte membranes with different anionic groups were examined using a SEM and shown in Figures 4.4 (a), (c), and (e). Both PEO/LiAlO₂ and PEO/LiTFS samples show crystalline structures whereas the PEO/LiClO₄ does not. In the case of PEO/LiTFS, the crystalline regions, which are often called spherulites, are circular or spherical (in term of a 3-D description). PEO/LiTFS electrolytes show one sphere and part of other spheres with spherulites growing outward from a center or a nucleus of crystallization. The diameter of each spherulite (shown as circles in Figure 4.4(e)) is around 50 μm . In

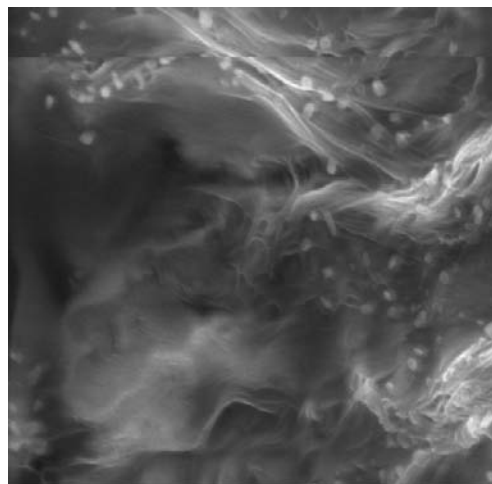
each spherulite, the fibrous bands start from the center of the sphere showing the details of the crystallization. There are clear boundaries between these crystalline regions.

In the case of PEO/LiAlO₂, a close examination may help identify the individual spherulites. However, there are many dendrites and voids (100 nm < pore size < 200 nm) in the spherulites. The boundaries between the spherulites are not clear. As can be seen from Figure 4.4 (b) and (f), micro-voids appear in both PEO/LiAlO₂ and PEO/LiTFS electrolytes.

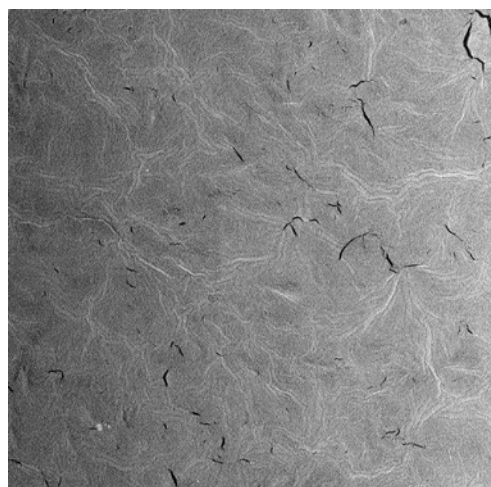
In the case of the PEO/LiClO₄ sample, it is difficult to identify the crystalline regions from the micrograph. This is because the hygroscopicity of LiClO₄ makes them absorb the moisture from the environment if preserved in the outside for a period of time. The moisture in the PEO/LiClO₄ electrolyte turns it into more of a gel electrolyte than a solid electrolyte.



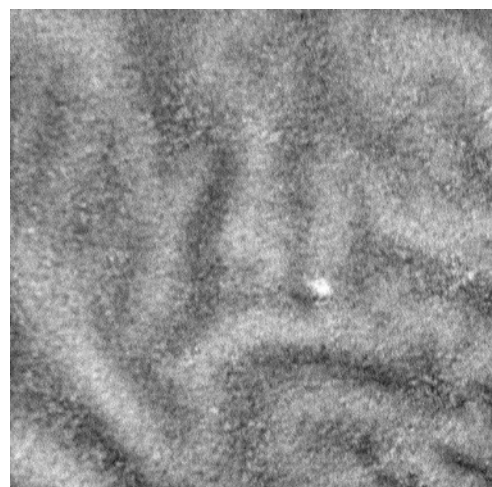
(a)



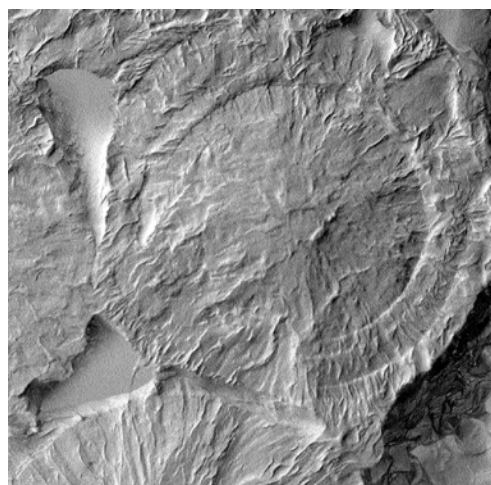
(b)



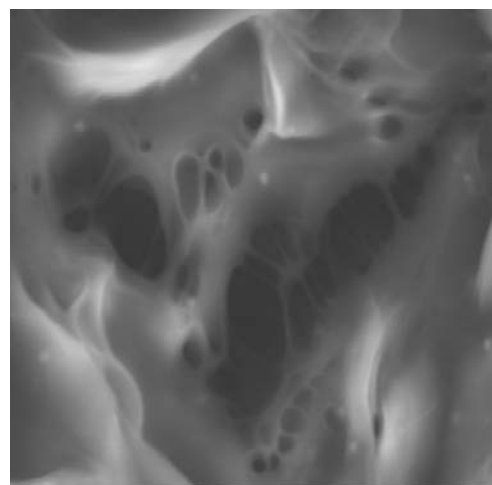
(c)



(d)



(e)



(f)

Figure 4. 4 The morphology of PEO/LiX polymer electrolytes X= (a) LiAlO₂(×1300); (b) LiAlO₂(×10,000); (c) LiClO₄ (×1180), (b) LiClO₄ (×240000)and (c) LiTFS (×1180). (f) LiTFS (×5000).

4.2 Effect of fillers

4.2.1 Conductivity measurement results

To determine the effect of filler on conductivity of PEO/LiAlO₂ composite electrolytes, the four-electrode method was used to carry out the test. The filler concentration, sample density, and in-plane conductivity of PEO/LiAlO₂ composite electrolytes are listed in Table 4.2. According to Table 4.2, the in-plane conductivity of PEO/LiAlO₂/TiO₂ electrolytes is 8 to 16 fold greater than that of pristine PEO/LiAlO₂ electrolytes. The conductivity of PEO/LiAlO₂/TiO₂ composite electrolytes increases with increasing the concentration of TiO₂. The in-plane conductivity of PEO/LiAlO₂/SiO₂ electrolytes is 5 to 7 fold greater than that of pristine PEO/LiAlO₂ electrolytes. The conductivity is a constant with respect to the concentration of SiO₂ filler between 1.0 and 10 wt%.

Table 4. 2 In-plane conductivity of PEO/LiAlO₂ based composite electrolytes

Sample	SiO ₂ Content (wt%)	TiO ₂ Content (wt%)	Density (g/cm ³)	$\sigma_{\text{in-plane}}$ (S/cm)
PA			1.23	4.45×10^{-5}
PAS1	1		1.20	3.11×10^{-4}
PAS3	3		1.17	2.58×10^{-4}
PAS5	5		1.18	3.00×10^{-4}
PAS7	7		1.15	2.02×10^{-4}
PAS10	10		1.05	3.00×10^{-4}
PAT1		1	1.28	2.60×10^{-4}
PAT3		3	1.13	3.00×10^{-4}

PAT5		5	1.20	3.02×10^{-4}
PAT7		7	1.35	4.03×10^{-4}
PAT10		10	1.38	7.24×10^{-4}

4.2.2 FTIR analysis

FTIR spectra were taken of three poly(ethylene oxide) based films using attenuated total reflectance (ATR) as the sampling technique. An expanded view of PA, PAS, PAT and PEO in the region ranging from $1800\text{--}600\text{ cm}^{-1}$ is provided in Figure 4.5. The first film is PEO with the addition of the ion-conducting filler LiAlO_2 (PA). The second and third films further comprise inert ceramic fillers, SiO_2 and TiO_2 (PAS and PAT, respectively). The films were pressed against a ZnSe crystal with mirrored faces at 45° . To aid comparing the spectra, the spectra were baseline corrected (with selected absorbance minima brought to zero and the rest of the spectrum adjusted in relation) and rescaled based at the peak at 1538 cm^{-1} .

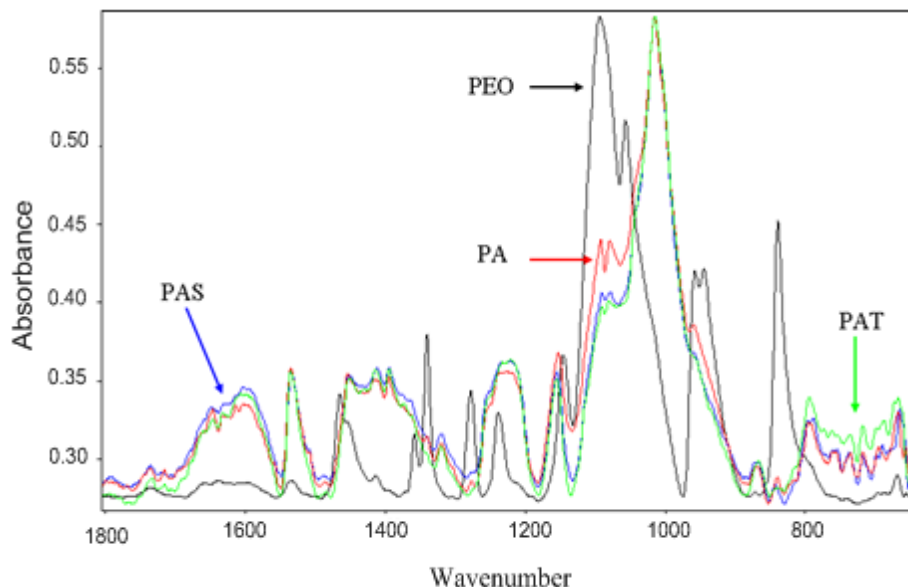


Figure 4. 5 Baseline corrected spectra comparing pure PEO (black) and PEO/LiAlO₂ (blue) electrolytes. The C-O-C stretching (1100 cm⁻¹) is indicated by the red arrows and the downshift (1020 cm⁻¹) due to the polyether-salt interactions is indicated with the green arrows.

As can be seen, the general structures of PEO and PA samples in the spectra are similar, but the relative intensities of the peaks have changed for the PA spectrum. The most notable absorbance band in the PEO spectrum is the band at around 1100 cm⁻¹, which is typically assigned to the asymmetric C-O-C stretching [178-182]. The broad peak around 3400 cm⁻¹ and 1660 cm⁻¹ suggests terminal hydroxyl and ester groups. The strong bands around 2900 cm⁻¹ are generally assigned to the symmetric and antisymmetric C-H stretching modes of the methylene (CH₂) unit. The similarly shaped, but less intense, bands at about 1460 cm⁻¹ and 870 cm⁻¹ are

also assigned to the methylene unit, but are due to the asymmetric CH₂ bending and CH₂ rocking, respectively.

The presence of a crystalline PEO phase is confirmed by the presence of the triplet peak of the C–O–C stretching vibrations with maxima at ~1140, 1100, and 1050 cm⁻¹. The CH₂ wagging mode observed at ~1350 cm⁻¹ is also split with two peaks at ~1343 and 1360 cm⁻¹; this is also evidence for the presence of a crystalline PEO phase. The downshift of the maximum from the value of 1116 cm⁻¹ of the C–O–C mode recorded for the amorphous pure polyether phase confirms interactions between PEO and salts leading to the formation of transient cross-links which weaken the C–O–C polyether bonds. The aliphatic CH stretching vibrational band (ca. 2900 cm⁻¹) shows a decrease in intensity and width caused by the addition of lithium salt [179].

The IR C–O–C stretching region could be used to analyze polyether–salt interactions with the maxima of the C–O–C stretching occurring around 1110 cm⁻¹. The maximum shifts down and splits into 1100 and 1090 cm⁻¹ with the addition of lithium salt [180]. The positions of the maximum of the C–O–C band are similar for all electrolytes studied with the same lithium salt. If the cations were

coordinated with the ether oxygen of PEO, changes in the ether oxygen vibrational modes, such as C-O-C asymmetric and symmetric stretching modes, and deformation modes in the range of 900–1200 cm^{-1} are expected. The asymmetric stretching band of pure PEO at 1050 cm^{-1} is shifted to 1020 cm^{-1} with the addition of lithium salt, as shown in Figure 4.5. It is apparent that broad C-O-C symmetric and asymmetric stretching mode width around 1100 cm^{-1} is severely decreased in the composite of lithium salt [179]. Not only is there a decrease in the C-O-C mode width but also its maximum shifts to a lower wave-number when compared to pure PEO and pure PEO:LiX (X=AlO₂⁻, ClO₄⁻, TFS⁻) complex films. This downshift is most likely due to polyether-LiAlO₂ interactions, and corresponds to a weaker ion-polymer interaction that provides more free Li⁺ for improved ionic transport [181].

It is worth emphasizing that the addition of SiO₂ or TiO₂ filler in PEO could further decrease C-O-C stretching modes around 1100 cm^{-1} in the composite of lithium salt, which indicates a further promotion of multiple interactions through cross-linking within the composite electrolyte [180]. This downshift in the C-O-C

stretching suggests that the filler may influence the interaction of the polymer chain and lithium ion by forming new chemical bonding between surface groups of SiO₂ or TiO₂ filler and lithium ion.

4.2.3 XRD analysis

The XRD spectra for PEO/LiAlO₂, PEO/LiAlO₂/SiO₂, and PEO/LiAlO₂/TiO₂ are illustrated in Figures 4.6. The spectra indicate that the PEO membranes are mainly composed of low molecular weight PEO or polyethylene glycol (PEG). The major difference between the spectra for PEO/LiAlO₂ and PEO/LiAlO₂/TiO₂ is that in the spectrum for PEO/LiAlO₂ there are obvious peaks for crystalline LiAlO₂ whereas there is no obvious peak for LiAlO₂ in the spectrum for PEO/LiAlO₂/TiO₂. This means that in PEO/LiAlO₂/TiO₂ polymer electrolyte, the LiAlO₂ salt is completely dissolved or dissociated due to the addition of TiO₂. Since a higher dissociation of lithium salt leads to higher electrolyte conductivity, addition of TiO₂ filler can result in an increase in conductivity. In the XRD spectrum of PEO/LiAlO₂/SiO₂ electrolytes, the peaks for crystalline LiAlO₂ are still present. This could explain the observation that a PEO/LiAlO₂/TiO₂

electrolyte has greater conductivity than a PEO/LiAlO₂/SiO₂ electrolyte with the same filler content.

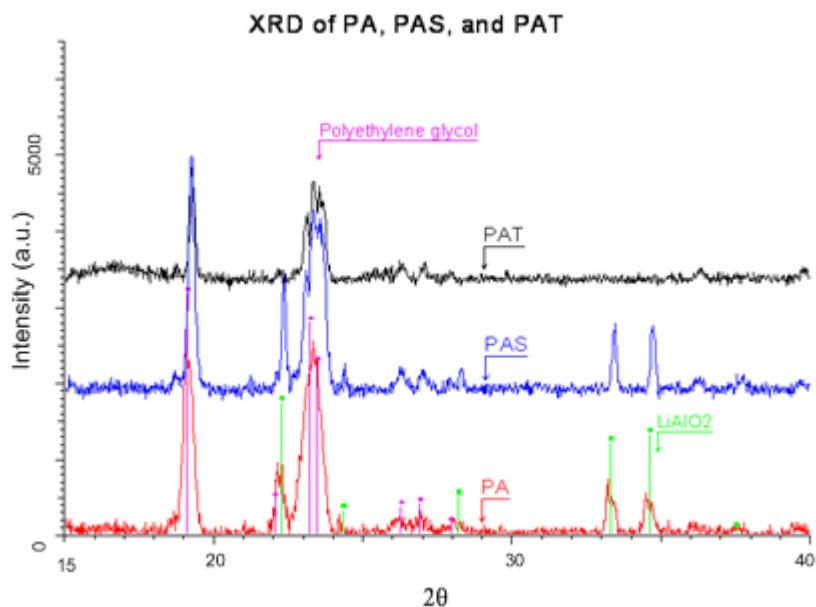


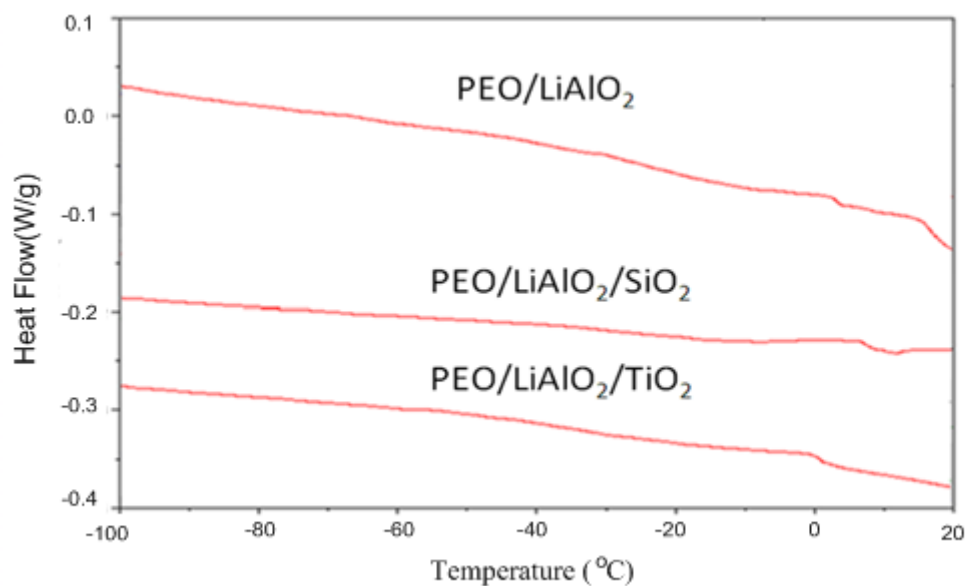
Figure 4. 6 XRD spectrum of a PEO/LiAlO₂, PEO/LiAlO₂/SiO₂ and PEO/LiAlO₂/TiO₂ electrolytes.

4.2.4 DSC analysis

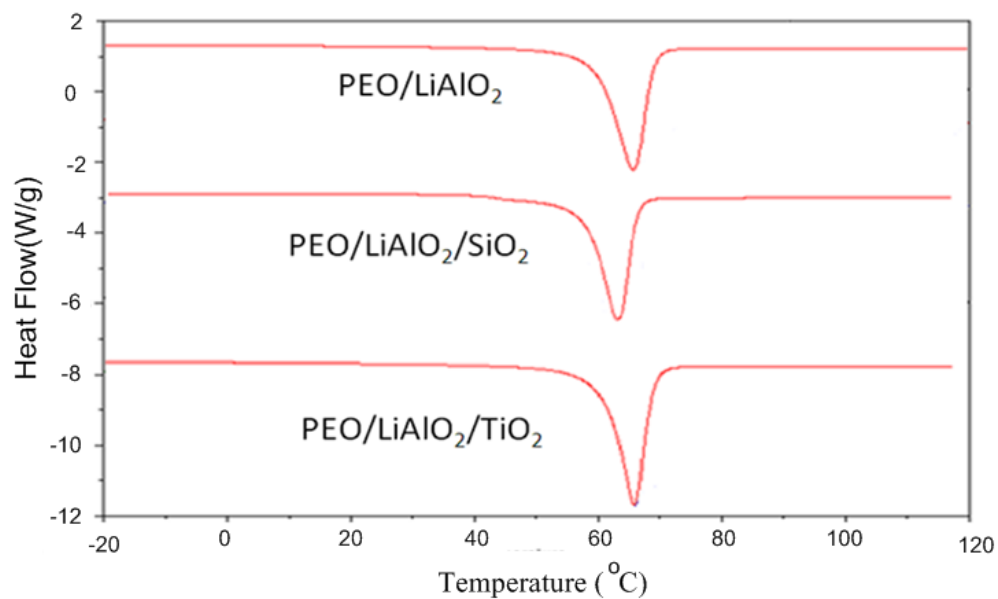
The DSC results for PEO/LiAlO₂, PEO/LiAlO₂/SiO₂ and PEO/LiAlO₂/TiO₂ sample are shown in Figures 4.7 (a) for the scan in the T_g region and (b) for the scan in the T_m region. Values of these transition temperatures are listed in Table 4.3. There is no noticeable sign of glass transition for the pristine PEO/LiAlO₂, PEO/LiAlO₂/SiO₂ and PEO/LiAlO₂/TiO₂ samples in the first heating cycle.

However, for the second heating cycle, T_g can be determined. PEO/LiAlO₂/SiO₂ has a lower T_g (-28°C) than PEO/LiAlO₂ ($T_g = -44^\circ\text{C}$), which indicates the enhancement of polymer chain mobility [183, 184].

T_m of pure PEO is 68 °C [185]. Normally, the introduction of Li salt into PEO decreases T_m due to the dissolution of the lithium salt. T_m depends on the molecular weight of the polymer. A lower molecular weight polymer usually has a lower melting point. As can be seen from Table 4.3, T_m of the PEO/LiAlO₂ sample (65°C) is slightly lower than that of pure PEO due to the dissolution of the LiAlO₂ salt. Pristine PEO/LiAlO₂/SiO₂ also shows T_m (63°C) slightly lower than that of PEO/LiAlO₂ (65°C), which indicates that the crystals in PEO/LiAlO₂/SiO₂ can melt to amorphous structure under lower temperature. The addition of TiO₂ filler does not decrease T_m . The similar T_m of three compositions indicates that the addition of SiO₂ or TiO₂ will not cause a significant molecular weight variation of the polymer.



(a)



(b)

Figure 4. 7 DSC curves of PEO/LiAlO₂, PEO/LiAlO₂/SiO₂ and PEO/LiAlO₂/TiO₂ electrolytes at cycle 1 (a) T_g curves; (b) T_m curve

Table 4. 3 Thermal transitions parameter of the sample for DSC measurements

Sample	Cycle	T _g (°C)	T _m (°C)	ΔH (J/g)	χ _c
PEO/LiAlO ₂	Run 1	N/A	65.66	140.5	73%
	Run 2	-44.04	60.39	115.3	60%
PEO/LiAlO ₂ /SiO ₂	Run 1	N/A	63.46	115.3	60%
	Run 2	-28.02	59.23	96.48	50%
PEO/LiAlO ₂ /TiO ₂	Run 1	N/A	65.58	133.2	69%
	Run 2	-52.49	61.78	114.1	59%

The percentage of crystalline phase (χ_c) in a PEO/LiX (X=AlO₂⁻, ClO₄⁻, TFS⁻)

sample can be calculated from equation [186]:

$$\chi_c = \left(\frac{\Delta H_m}{\Delta H_m^0} \right) \times 100\% \quad (4.1)$$

where ΔH_m^0 is the melting heat of pure PEO crystalline, 193 J/g (100% crystalline)

and ΔH_m the fusion heat of PEO/LiX (X=AlO₂⁻, ClO₄⁻, TFS⁻). ΔH_m can be

calculated from the integral area of the DSC curves. The values of ΔH_m and χ_c

are summarized in Table 4.3. The values of fusion heat are 140 and 115 J/g for

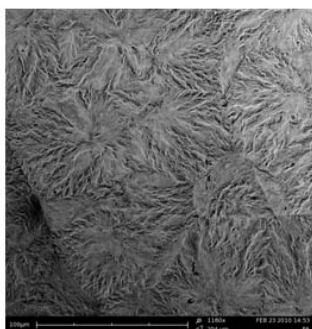
PEO/LiAlO₂ and PEO/LiAlO₂/SiO₂ respectively. Those indicate that the addition

of filler could reduce the amount of crystalline phase and polymer chain mobility

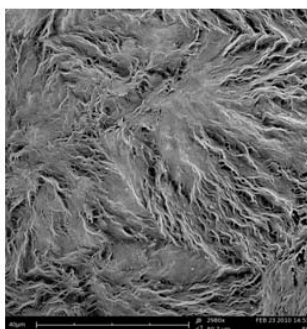
[187]. The SiO₂ filler is more effective in suppressing crystallization.

4.2.5 SEM analysis

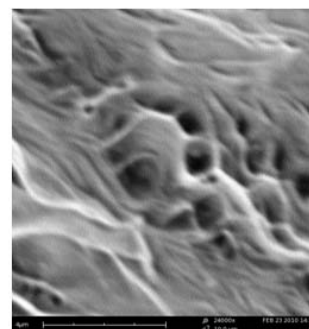
Pristine PEO/LiAlO₂



(X1180)



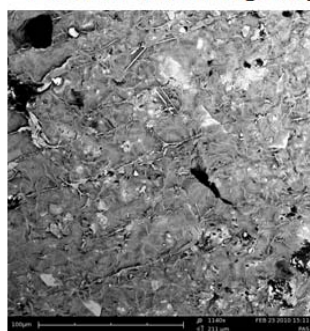
(X2980)



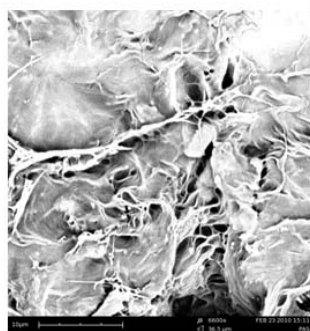
(X24000)

(a)

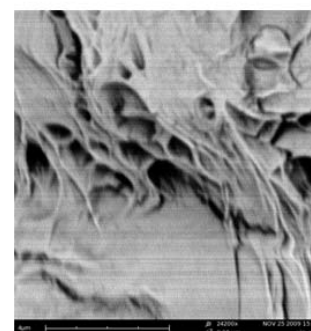
Pristine PEO/LiAlO₂/SiO₂



(X1140)



(X6600)



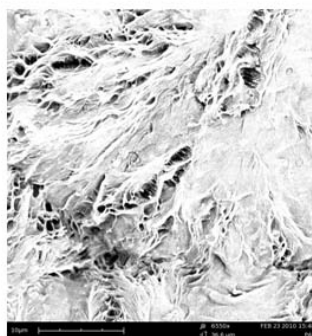
(X24200)

(b)

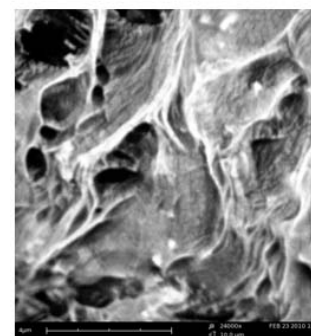
Pristine PEO/LiAlO₂/TiO₂



(X1240)



(X6600)



(X24000)

(c)

Figure 4. 8 Table-top SEM images of pristine and hot pressed PEO/LiAlO₂ composite electrolytes: (a) without filler; (b) with SiO₂ filler; (c) with TiO₂ filler.

Pristine PEO/LiAlO₂, PEO/LiAlO₂/SiO₂, PEO/LiAlO₂/TiO₂ membranes were examined using an SEM (Figure 4.8). All samples show spherulites and dendrites under lower magnifications ($\times 1180$ and $\times 2980$) and fibrous bands under the higher magnification ($\times 24000$). The dendrites are believed to be the crystalline part of the PEO/LiAlO₂ electrolyte. In Figure 4.8(a), very clear spherulites and dendrites can be observed for the pristine PEO/LiAlO₂ electrolyte whereas the filler are hard to identify in the samples with SiO₂ or TiO₂ fillers. The amount of the spherulites and fibrous bands decreased after the addition of TiO₂ fillers and particularly SiO₂ fillers. This confirms the crystalline ratio we get from DSC result; SiO₂ filler is more effective in converting the crystalline phase of PEO electrolyte into amorphous phase.

The apparent conductivity of a PEO electrolyte is a weighted average of the conductivity of the amorphous phase and that of the crystalline phase [187]. It is commonly accepted that the conductivity of crystalline PEO electrolytes is much lower than that of the amorphous PEO electrolytes because in crystalline PEO, the conduction paths or channels are blocked and the segmental mobility of the backbone is minimum [187]. Addition of filler could inhibit the PEO chain

crystallization so as to increase amount of the amorphous phase in the PEO polymer electrolyte [187], thereby increasing the conductivity of the PEO polymer electrolyte.

Another mechanism for increasing conductivity is that the interaction between chemical groups on the filler surface and the lithium salt could improve the dissociation of the salt in PEO electrolyte [35] thereby increasing the concentration of free charge carriers or ions. This mechanism can explain why TiO₂ fillers are less effective than SiO₂ in increasing amorphism but more effective than SiO₂ in promoting conductivity. Formation of new chemical bonds between the ceramic filler with PEO polymer or with lithium salt may also cause the conductivity to increase [191]. However, there is no evidence of this in current research.

4.3 Effect of hot pressing

4.3.1 Conductivity results of PEO/LiTFS electrolytes

Hot pressing treatment was conducted at 110°C and 5000 lb. The pressure was about 2500 psi. After the hot pressing treatment, the surface also became very smooth. More importantly, the PEO/LiTFS/EC membranes that were initially

opaque or translucent became transparent and the transparency remained for months. This is believed to be an indication of amorphism of the PEO polymer.

Table 4.4 lists results of conductivity and density measurements for PEO/LiTFS/EC electrolyte membranes. The values are averages of five measurements. From the results, it is clear that hot pressing yields much greater increase in conductivity for the three variations of composition. The maximum increase in conductivity due to hot pressing is 15 fold from 1.22×10^{-4} to 1.71×10^{-3} S/cm. Probably because of minor variations of the preparation history including mixing, casting, drying, and hot pressing, for each specific sample the density varies from 1.00 to 1.23 g cm^{-3} while a density value of 1.13 g/cm^3 was labeled for the pristine PEO powder that was used for preparing the membranes. The thickness varies from 0.0076 to 0.0229 cm. Increasing the EC plasticizer from 20% to 33.3% in the PEO/LiTFS/EC can increase the conductivity more than 100%, which is expected according to the previous study. However, hot pressing seems to be less effective for higher EC concentrations than for lower concentrations. The increase in conductivity due to hot pressing is 4.68 times. These above conductivity measurements were conducted up to 12 hours after hot

pressing treatment. In order to confirm that this conductivity change is not temporary, the conductivity of a hot pressed sample was measured several times.

The conductivity versus the storage time is exhibited in Figure 4.9. These results show that the conductivity increased by 9 times after hot pressing treatment and the conductivity in fact increase slightly in the following days.

Table 4. 4 In-plane conductivity measurement result for PEO/LiTFS/EC electrolytes under hot pressing treatment

Sample Code	Thickness (cm)	Hot pressing time (min)	Composition			Density (g/cm ³)	σ (S/cm)
			PEO (wt%)	LiTF S (wt%)	EC (wt%)		
PLE	0.0152	Pristine	40	40	20	1.15	1.22×10^{-4}
	0.0177	5				1.20	4.64×10^{-4}
	0.0102	15				1.10	1.15×10^{-3}
	0.0076	35				1.16	1.71×10^{-3}
PLEE	0.0127	Pristine	33	33	34	1.08	2.82×10^{-4}
	0.0152	5				1.01	1.07×10^{-3}
	0.0076	15				1.00	4.39×10^{-4}
	0.0127	35				1.15	1.32×10^{-3}

In order to distinguish the effects of high temperature and high pressure, PLE samples were subjected to high temperature under atmospheric pressure. All four pieces of PLE were cut from the same PLE membrane: one piece was used as the benchmark, the second piece was kept at 110°C in an oven for 5 min, the second piece was kept for 15 min, and the fourth one was kept for 35 min. The thickness,

density, and in-plane conductivity are listed in Table 4.5. After the high temperature treatment, the membranes became transparent with some tiny air bubbles. The surface showed some crazes or irregular marks. As we observe from Table 4.5, the in-plane conductivity also increases with duration of the high temperature treatment. The in-plane conductivity increased 7 fold after 35 min of hot treatment. These results indicate that high temperature is the main reason for conductivity increase in the hot pressing treatment and high pressure results in a more uniform membrane and improvement of the integrity of the PEO membrane.

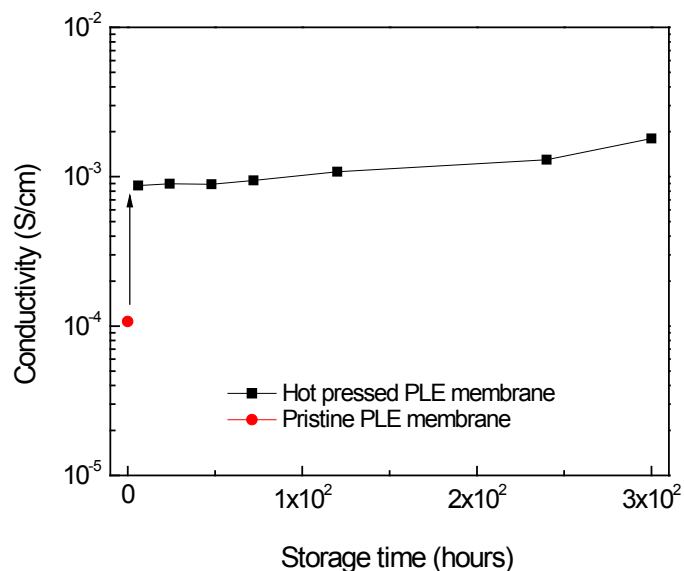


Figure 4. 9 Conductivity of pristine and hot pressed PEO/LiTFS/EC electrolytes vesus storage time

Table 4. 5 In-plane conductivity measurement result for PEO/LiTFS electrolytes under the high temperature treatment

Sample Code	Thickness (cm)	Hot treatment time (min)	Composition			Density (g/cm ³)	σ (S/cm)
			PEO (wt%)	LiTFS (wt%)	EC (wt%)		
PLE	0.025	Pristine	40	40	20	0.96	3.45×10^{-4}
	0.035	5				1.10	6.44×10^{-4}
	0.028	15				1.03	1.07×10^{-3}
	0.025	35				1.13	2.09×10^{-3}

In order to identify the true reason for the effect of hot pressing, a few possible reasons are evaluated one by one. Possible reasons so far are as follows:

1) Hot pressing can increase the density of the PEO membrane and hence the density of the charge carriers in a unit volume.

2) Hot pressing results in a thinner membrane. If the surface conductivity is greater than the bulk conductivity, a thinner membrane can show a greater conductivity.

3) Hot pressing may cause chemical reactions, break-down of chemical bonds, or formation of new bonds that may promote conductivity.

4) Hot pressing increases amorphism and this increment can be maintained when the membrane is cooled.

Analyses of these possibilities are presented in the following sections.

Effect of density

From the data shown in Table 4.4 and 4.5, no definite correlation can be found between conductivity and density. The density values are actually randomly distributed around the density value for the pure PEO polymer (1.13 g/cm^3) within a 15% variable. The difference of the density can be considered as the experimental error of density measurements.

Effect of membrane thickness

Secondly, there is no definite correlation between thickness and conductivity. In order to confirm that surface conductivity does not play an important role in ionic conduction, a series of through-plane conductivity measurements were conducted. Table 4.6 lists the through-plane conductivity of three PLE electrolyte samples. One large piece of membrane was cut into three pieces. One of them was not hot pressed. The second one was hot pressed for 20 minutes. The third one was hot pressed for 1 hour. The thickness of the samples decreases with the duration of hot pressing from 0.0254 to 0.0089 cm whereas the through-plane conductivity increases from 5.29×10^{-6} to 2.22×10^{-3} S/cm. The two-electrode through-plane measurement was usually considered less reliable than the four-electrode method

because the interpretation of the EIS actually relies on an equivalent circuit model and the use of different models may give different values of internal or series resistance and hence different conductivity values. Nevertheless, the trend and magnitude are similar to that of the in-plane four-electrode measurement results. In summary, because in the through-plane conductivity measurement, surface conduction cannot contribute to total conductivity, the same order of magnitude of conductivity values obtained from both in-plane and through-plane measurements confirms that the increase of conductivity is not likely due to decrease of the thickness.

Table 4. 6 Through-plane conductivity measurement result for PEO/LiTFS electrolytes

Sample label	Hot pressing time (min)	Thickness (cm)	Density (g cm^{-3})	Conductivity (S cm^{-3})
PLE	Pristine	0.025	1.07	5.29×10^{-6}
PLE-20	20	0.018	1.14	4.45×10^{-4}
PLE-60	60	0.009	1.13	2.22×10^{-3}

FTIR analysis

In order to identify the reason for the effect of hot pressing, a poly(ethylene oxide) membrane saturated with LiCF_3SO_3 and ethylene carbonate (EC) to form a solid state electrolyte membrane. This piece of film was cut into three samples.

One of these was kept in its pristine form. The second and third ones were hot pressed at 110°C and 5000 lb for 20 minutes and 60 minutes respectively. These samples were labeled PLE, PLE-20, and PLE-60 and were investigated using a FTIR. The samples' thicknesses and conductivities are listed in Table 4.6. Hot pressing resulted in thinner films and increased the degree of smoothness in addition to the decrease in the resistivity of the membranes. FTIR spectra were obtained for three poly(ethylene oxide) based samples using attenuated total reflectance (ATR) as the sampling technique. Samples were slightly pressed against a ZnSe crystal with mirrored faces at 45°.

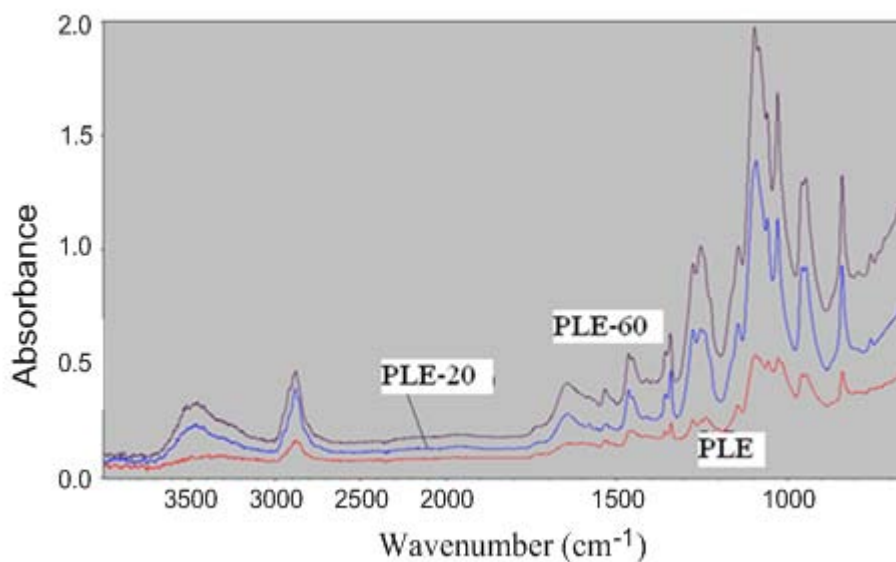


Figure 4. 10 Unaltered FTIR spectra of PLE, PLE-20 and PLE-60.

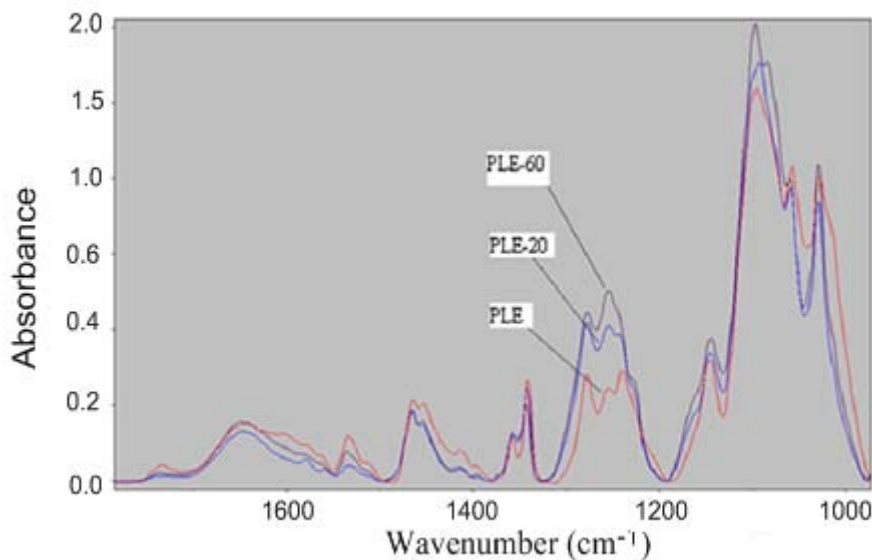


Figure 4. 11 Baseline corrected and rescaled FTIR spectra of PLE, PLE-20, and PLE-60.

Figure 4.10 shows a representative spectrum of each sample. These are “as is” spectra that have not been rescaled or offset. The peaks of PLE-20 are nominally four times greater in magnitude than those of PLE. To make a comparison of the spectra easier, the spectra were baseline corrected (the selected absorbance minima brought to zero and the rest of the spectra moved accordingly) and rescaled to a common magnitude. From the FTIR spectra, no peak around 2500 cm^{-1} (related to the $\text{-C}\equiv\text{N}$ stretching) or 1778 cm^{-1} (belong to EC component) can be identified, which rules out that the conductivity enhancement in the PEO composite electrolyte could relate to the excess solvent adsorbed residue and the PLE membrane we get is dry solvent-free solid state polymer electrolyte. The peak at

840 cm^{-1} was used to scale the spectra. The rescaled spectra are shown in Figures 4.11. From low to high wave numbers, the peaks appear at 639, 842, 962, 1031, 1062, 1100 (Tallest), 1149, 1242, 1280, 1342, 1360, 1467, 2883 cm^{-1} and could be assigned to vibration modes as shown in Table 2.6. All of the samples exhibit fairly strong hydroxyl bands in the 3400 cm^{-1} region as well as fairly strong bands in the 1640 cm^{-1} region. These features are indicative of low molecular weight poly(ethylene oxides) (order of 1000 Mw or less) where the terminal hydroxyl or esterified hydroxyl functionality is reasonably predominant. These substances are generally referred to as polyethylene glycols with lower molecular weight than the PEO powder. High molecular weight poly(ethylene oxides) of several thousand and greater have bands in these regions that are very small or nonexistent. Thus, the three samples appear to be poly(ethylene oxide) of fairly low molecular weight (polyethylene glycols). Because no additional band can be observed in the spectra, the presence of the LiCF_3SO_3 or ethylene carbonate additives cannot be directly confirmed by FTIR in this case, which is probably an indication that the lithium salt is completely dissolved and dispersed in the membrane. The region of the spectrum between approximately 1800 cm^{-1} and 1000 cm^{-1} exhibits the greatest

differences in the peak intensity and is shown in Figure 4.11.

Possible reasons for these differences in the peak intensity are 1) that hot pressing alters the relative numbers of bonds in the samples or the population of the vibration modes and 2) that the differences are simply due to differences in surface smoothness, because coarser surfaces resulted in spectra with lower absorbance while the smoother surfaces resulted in spectra with significantly greater absorbencies. However, the peak intensity near 1260, 1530, 1730, and 1600 cm^{-1} do not appear to be in the same order. Thus, this observation suggests a rejection of the second possibility that the differences in the peak intensity are due to the differences in the surface smoothness of the sample because if this were the case, a uniform order in peak intensity would be obtained.

Table 4. 7 Assignment of the FTIR peaks to the vibration modes of molecules.

Peak Position	peak assignment
636 cm^{-1}	cis C-H wagging mode
842 cm^{-1}	CH ₂ wagging
962 cm^{-1}	stretching of ether bond (C-O) of PEO
1033 cm^{-1}	symmetric SO ₃ vibrations of LiCF ₃ SO ₃
1062 cm^{-1}	C-O-C stretching vibrations
1100 cm^{-1}	stretching of ether bond (C-O) of PEO
1242 cm^{-1}	C-O-C stretching vibrations or -C-F and -CF ₂ - stretching
1282 cm^{-1}	CH ₂ twisting vibration from PEO
1350 cm^{-1}	CH ₂ wagging mode
1467 cm^{-1}	CH ₂ scissoring
2800-2935 cm^{-1}	C-H stretching mode

XRD analysis

The XRD of the PLE (PEO/LiTFS) electrolytes for in-plane and through-plane conductivity measurement are shown in Figures 4.12 and 4.13. The samples used for generating the XRDs in Figure 4.12 are the cut from the samples of in-plane conductivity measurements presented in Table 4.4. For all samples, polyethylene glycol ((C₂H₄O)_n(CH₂OH)₂) matches most closely the polymer component of these samples. Also in all samples, the measured diffraction pattern is slightly shifted to the right of where the “sticks” in the reference pattern predict. This shift is related to a height error in mounting the samples for diffraction. However, the shift could be related to the polymer, but would require powder diffraction for confirmation. Generally speaking, the peaks in the four XRDs match very well and no new peak appears as the duration of hot pressing prolongs. Two variations can be observed from the XRDs as a function of hot pressing duration. First, the peaks “smear” and become short for longer durations and, secondly, for the longer durations the XRD shows a “hump” in smaller diffraction angles between 15° and 19°. These phenomena suggest that PEO electrolytes lose their crystallinity.

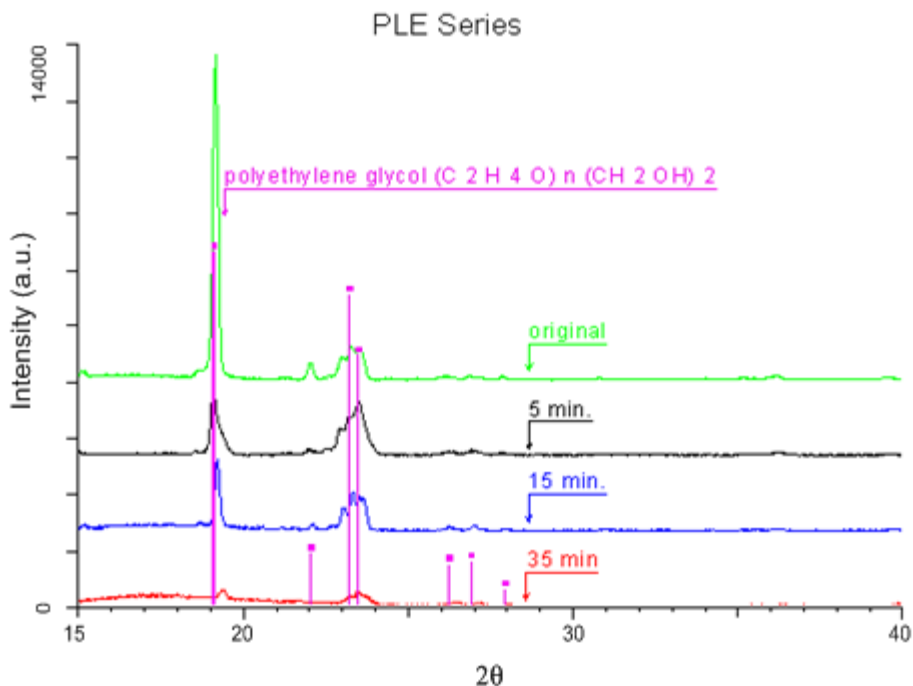


Figure 4. 12 XRD spectra for PEO/LiTFS electrolytes (The upper spectra is for a pristine sample, others are for hot pressed samples).

In order to verify what was found with the data shown in Figure 4.12, the samples that were cut from the same cast of membrane and analyzed using FTIR were examined using XRD. The XRDs in Figure 4.13 also show the same trend. However, the change for the 20 minute duration was not as significant as that shown in Figure 4.12 and that of 60 minute duration. Two XRDs are shown for two PLE samples in Figure 4.13. The trend of the variation due to prolonged duration is similar to those manifested in Figures 4.12 and 4.13.

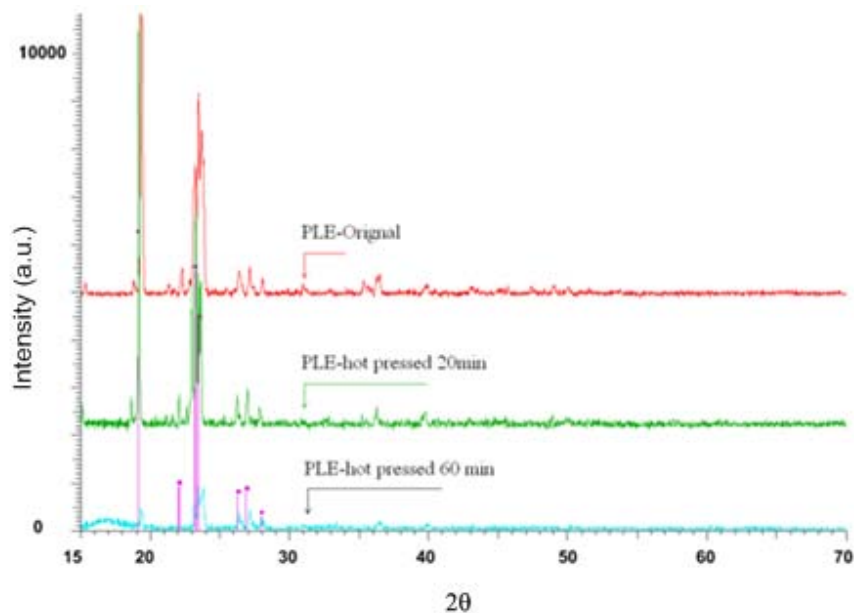


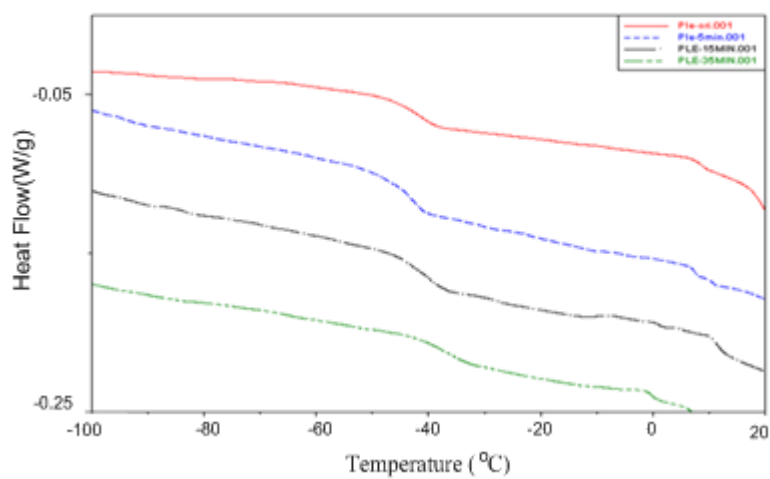
Figure 4. 13 XRD spectra for PEO/LiTFS electrolytes (The upper spectra is for a pristine PLE sample, the middle one is for a sample that was hot pressed for 20 min, and the bottom one is for a sample that was hot pressed for 60 min).

DSC analysis

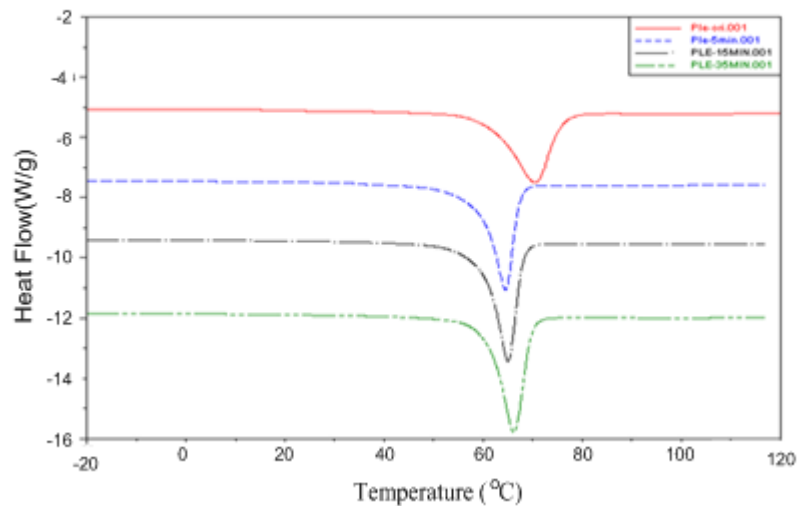
The thermograms for PEO/LiTFS electrolytes are shown in Figure 4.14 in the region of T_g and T_m with the hot pressing times of 0, 5, 10, 15 and 35 minutes at 110 °C. Values of these transition temperatures are listed in Table 4.8. While the variation of T_g does not show a definite trend, hot pressing does decrease T_m of the PEO/LiTFS membranes. By applying a high temperature treatment at 110°C, a temperature well above the melting temperature may give rise to disintegration and shortening of the polymer chains and hence a decrease of melting temperature [192].

Table 4. 8 Thermal Transitions Parameter of the PEO/LiTFS electrolytes for DSC Measurements

Sample	Hot pressing time (min)	Weight before DSC (mg)	Weight after DSC (mg)	Cycle	T_g ($^{\circ}\text{C}$)	T_m ($^{\circ}\text{C}$)	Heat (J/g)
PLE	Pristine	38.6	38.3	Run 1	-41.41	70.47	148.9
				Run 2	-34.72	67.20	122.7
	5	28.3	28.2	Run 1	-43.66	64.46	140.6
				Run 2	-42.71	63.59	127.2
	15	28.4	28.7	Run 1	-39.75	68.12	150.5
				Run 2	-31.71	62.56	130.0
	35	29.3	29.1	Run 1	-37.68	66.12	150.5
				Run 2	-40.16	62.68	137.2



(a)



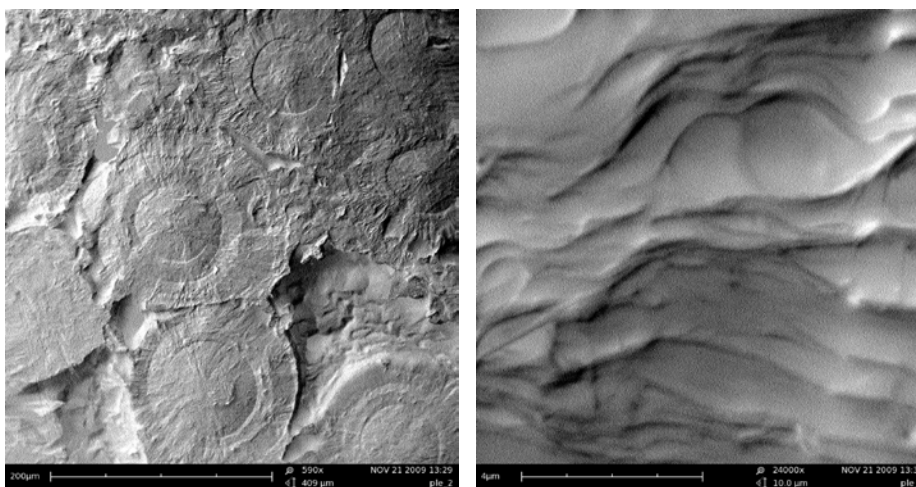
(b)

Figure 4. 14 DSC curves of PEO/LiTFS electrolyte (a) T_g curve; (b) T_m curve (solid red line is the pristine sample, blue dash line is hot pressed 5 min sample, black dash dot line is hot pressed 15 min sample, green dash dot dot line is hot pressed 35 min sample)

SEM analysis

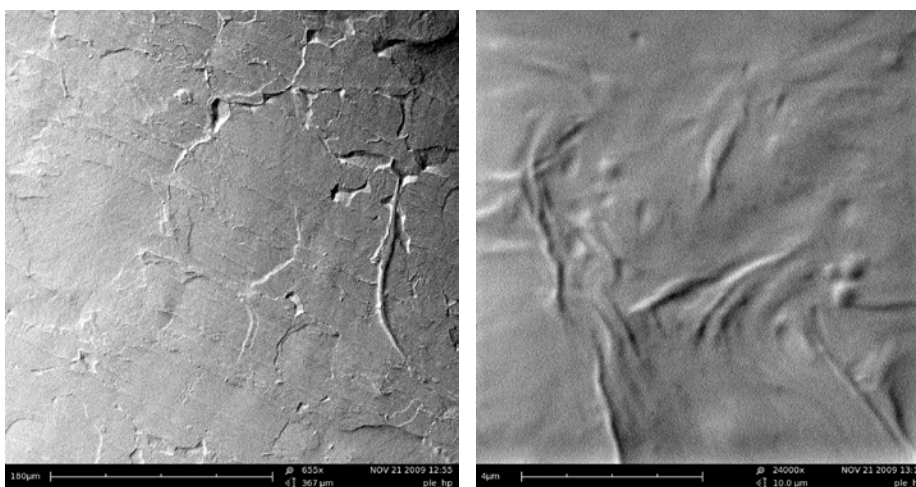
Pristine PEO/LiTFS and hot pressed PEO/LiTFS electrolytes were examined using an SEM. Pristine PEO/LiTFS (Figures 4.15 (a) and (b)) shows spherulite structure or spherical crystalline region with some dendrites inside each spherulite under SEM. The diameter of each spherulite is around 50 μ m. In each spherulite, the dendrites, or fiber-like bands, start from the center of the sphere showing a characteristic of crystallization. However, after the hot pressing process (Figures

4.15 (c) and (d)), most of the spherulites disappeared while a little trace of at the edge of the former spherulites remained.



(a) PLE x650

(b) PLE x24000



(c) PLE-hot pressed (60min) x650 (d) PLE-hot pressed (60min) x24000

Figure 4. 15 Scanning electrical microscopy (SEM) images of the PEO/LiTFS electrolytes (a) pristine PLE (x650); (b) pristine PLE (x24000); (c) hot pressed PLE (x650); (d) hot pressed PLE (x24000).

Spherulites in PEO have a Maltese cross-extinction pattern and a very fine texture [127, 128, 191]. The present PEO samples exhibit a typical compact

spherulitic morphology and its cross-extinction pattern can be observed clearly. During the hot pressing process, the semicrystalline phase of PEO melted into the amorphous phase above the glass transition temperature ($\sim 60^{\circ}\text{C}$). The small remaining trace of the spherulitic texture in the hot pressed samples may be the result of recrystallization. During cooling after the hot pressing process, the amorphous part of the PEO will re-crystallizes. However, according to the present SEM examinations, only a small part of PEO re-crystallizes.

4.3.2 Conductivity results of PEO/LiAlO₂ electrolytes

Similar effects of hot pressing were also observed for PEO/LiAlO₂ electrolytes with filler and without filler as shown in Table 4.9. These data reveal that hot pressing treatment can increase the conductivity of PEO/LiAlO₂ membranes by 2-9 times, as in the results for the PEO/LiTFS membranes. For the membranes with TiO₂ fillers, the increase is 2-3 times whereas for the membranes with SiO₂ fillers the increase is 3-9 times. A careful examination of the data reveal that this is because of a synergetic effect of filler and hot pressing. It is because the conductivity of the pristine membranes with TiO₂ is higher than that for the pristine

membranes with SiO₂. Nevertheless, these results reveal that the hot pressing treatment can increase the ambient temperature conductivity of different PEO polymer electrolytes.

Table 4. 9 Conductivity data for PEO/ LiAlO₂ electrolytes

Sample	Condition	Composition (wt%)				σ (S/cm)
		PEO	LiAlO ₂	TiO ₂	SiO ₂	
PA	Pristine	84.5	15.5			4.45×10^{-5}
	5 min, 110°C					1.19×10^{-3}
	10 min, 110°C					6.77×10^{-4}
	20 min, 110°C					1.25×10^{-3}
PAT1	Pristine	83.6	15.4	1		2.60×10^{-4}
	5 min, 110°C					8.16×10^{-4}
	10 min, 110°C					7.90×10^{-4}
	20 min, 110°C					7.77×10^{-4}
PAT3	Pristine	82.0	15.0	3		7.41×10^{-4}
	5 min, 110°C					1.08×10^{-3}
	10 min, 110°C					1.48×10^{-3}
	20 min, 110°C					2.63×10^{-3}
PAT5	Pristine	80.3	14.7	5		3.02×10^{-4}
	5 min, 110°C					5.50×10^{-4}
	10 min, 110°C					5.50×10^{-4}
	20 min, 110°C					8.84×10^{-4}
PAT7	Pristine	78.6	14.4	7		4.03×10^{-4}
	5 min, 110°C					1.02×10^{-3}
	10 min, 110°C					8.64×10^{-4}
	20 min, 110°C					1.40×10^{-3}
PAT10	Pristine	76.1	13.9	10		7.24×10^{-4}
	5 min, 110°C					5.77×10^{-4}
	10 min, 110°C					8.62×10^{-4}
	20 min, 110°C					1.98×10^{-3}
PAS1	Pristine	83.6	15.4		1	3.11×10^{-4}
	5 min, 110°C					5.41×10^{-4}
	10 min, 110°C					4.07×10^{-4}
	20 min, 110°C					8.93×10^{-4}
PAS3	Pristine	82.0	15.0		3	2.58×10^{-4}
	5 min, 110°C					1.00×10^{-3}
	10 min, 110°C					5.89×10^{-4}

	20 min, 110°C					2.25×10^{-3}
PAS5	Pristine	80.3	14.7		5	3.00×10^{-4}
	5 min, 110°C					1.01×10^{-3}
	10 min, 110°C					1.22×10^{-3}
	20 min, 110°C					1.89×10^{-3}
PAS7	Pristine	78.6	14.4		7	2.02×10^{-4}
	5 min, 110°C					8.67×10^{-4}
	10 min, 110°C					1.79×10^{-3}
	20 min, 110°C					1.48×10^{-3}
PAS10	Pristine	76.1	13.9		10	3.00×10^{-4}
	5 min, 110°C					7.51×10^{-4}
	10 min, 110°C					1.20×10^{-3}
	20 min, 110°C					1.38×10^{-3}

4.4 Effect of mediator concentration

PEO/LiTFS, PEO/LiClO₄, and PEO/LiAlO₂ polymers were doped with NaI/I₂ mediator and the membrane samples are denoted as IPLE, IPLC, and IPA, respectively. The data of in-plane conductivity measurements is listed in Table 4.10 and plotted as Figure 4.16. The highest conductivity that was reached was 0.109 S/cm for PEO/LiTFS membranes doped with 50% mediator. XRD spectra for a PEO/LiTFS and PEO/LiAlO₂ samples are shown in Figures 4.18 and 4.19, respectively. Although the weight percentage for the mediator in the polymer electrolyte is 50%, the volumetric concentration is 0.00101 mol cm⁻³. In the XRD spectra, no sign for NaI and I₂ is identified, suggesting that the mediator is dissolved in the PEO polymer electrolytes. If C_A is the concentration of I₂,

substituting Eq. (1.4) into Eq. (1.5), the relationship between the apparent conductivity and the concentration of Γ can be given by

$$\sigma = \left(\frac{F^2}{RT} D_{AX} \right) C_A + \left(\frac{F^2 \delta_{AX}^2 k_{AX}}{6RT} \right) C_A^2 = aC_A + bC_A^2 \quad (4.2)$$

The experimental data of conductivity is also shown as a function of concentration of mediator and type of PEO polymer. The dependence is certainly non-linear. The data is also fitted into a polynomial equation with a power of 2. The results of regression parameters are shown in Table 4.11. According to Ref. [192], the diffusivity of iodine species in an ionic liquid is $6.35 \times 10^{-7} \text{ cm}^2 \text{ s}^{-1}$. The diffusivity obtained by the curve fitting Eqs. (4.2) ranges from 0.66×10^{-5} to $1.35 \times 10^{-5} \text{ cm}^2 \text{ s}^{-1}$, which is a descent matching given that the error of the curve fitting at low iodine concentrations is high. The evaluation for the reaction rate of electron transfer reaction gives a value ranging between 0.67 and $2.67 \times 10^8 \text{ M}^{-1} \text{ s}^{-1}$. The fastest reaction rate may be that for the electron transfer between $\text{K}_3\text{Fe}(\text{CN})_6$ and $\text{K}_4\text{Fe}(\text{CN})_6$ and is $\sim 10^9 \text{ M}^{-1} \text{ s}^{-1}$. Thus, the values evaluated for iodine species are acceptable.

Table 4. 10 Composition and in-plane conductivity of PEO/LiX (X=AlO₂⁻, ClO₄⁻, TFS⁻) electrolytes doped with NaI/I₂ mediator.

Sample	PLE (%)	PLC (%)	PA (%)	SiO ₂ (%)	TiO ₂ (%)	I ₂ /NaI (%)	Conductivity (S/cm)
IPLE5	95.0					5.0	0.0009
IPLE10	90.0					10.0	0.00572
IPLE20	80.0					20.0	0.00753
IPLE30	70.0					30.0	0.0272
IPLE50	50.0					50.0	0.109
IPLC5		95.0				5.0	0.00374
IPLC10		90.0				10.0	0.00535
IPLC20		80.0				20.0	0.00787
IPLC30		70.0				30.0	0.0481
IPA5			95.0			5.0	0.00102
IPA10			90.0			10.0	0.00431
IPA20			80.0			20.0	0.00582
IPA30			70.0			30.0	0.0387
IPAS5			92.1	2.9		5.0	0.00133
IPAS10			87.3	2.7		10.0	0.00466
IPAS20			77.5	2.5		20.0	0.00509
IPAS30			67.9	2.1		30.0	0.0376
IPAS50			48.5	1.5		50.0	0.128
IPAT5			92.1		2.9	5.0	0.00114
IPAT10			87.3		2.7	10.0	0.00421
IPAT20			77.5		2.5	20.0	0.0084
IPAT30			67.9		2.1	30.0	0.0475
IPAT50			48.5		1.5	50.0	0.196

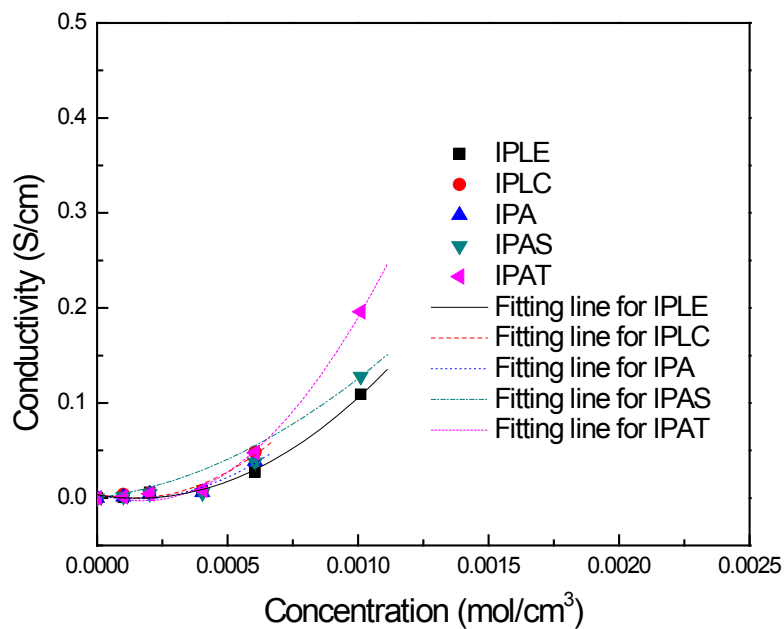


Figure 4. 16 Conductivity of PEO/LiX ($X=\text{TFS}^-$, AlO_2^-) electrolytes with filler and NaI/I_2 mediator

Table 4. 11 Regression parameters for Eq. 4.2.

Parameter	IPLE	IPLC	IPA	IPAS	IPAT
a	50.94	28.56	38.40	37.18	24.75
b	0.56×10^5	0.84×10^5	0.42×10^5	0.88×10^5	1.67×10^5
$D_{AX}, 10^{-5} \text{ cm}^2 \text{ s}^{-1}$	1.35	0.76	1.02	0.99	0.66
$k_{AX} (10^8 \text{ M}^{-1} \text{ s}^{-1})$ if $\delta_{AX} = 1 \text{ nm}$	0.89	1.34	0.67	1.41	2.67

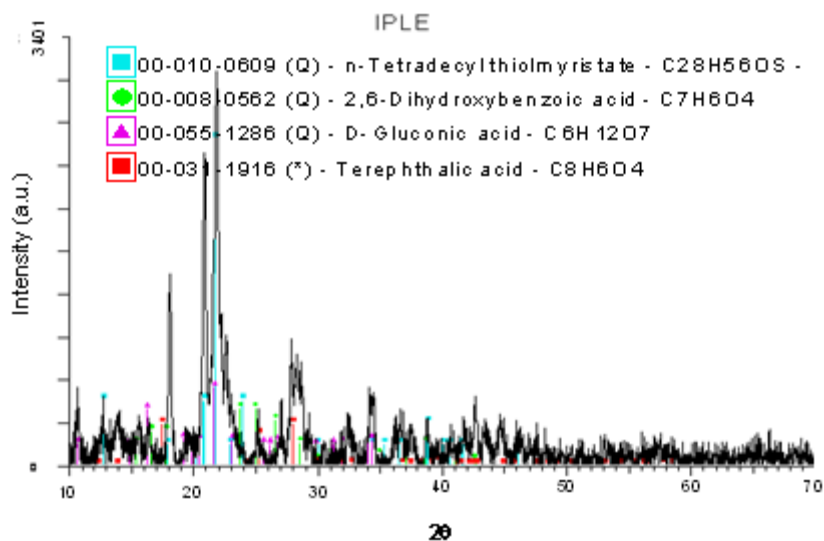


Figure 4. 17 XRD spectrum for PEO/LiTFS doped with 50% NaI/I₂.

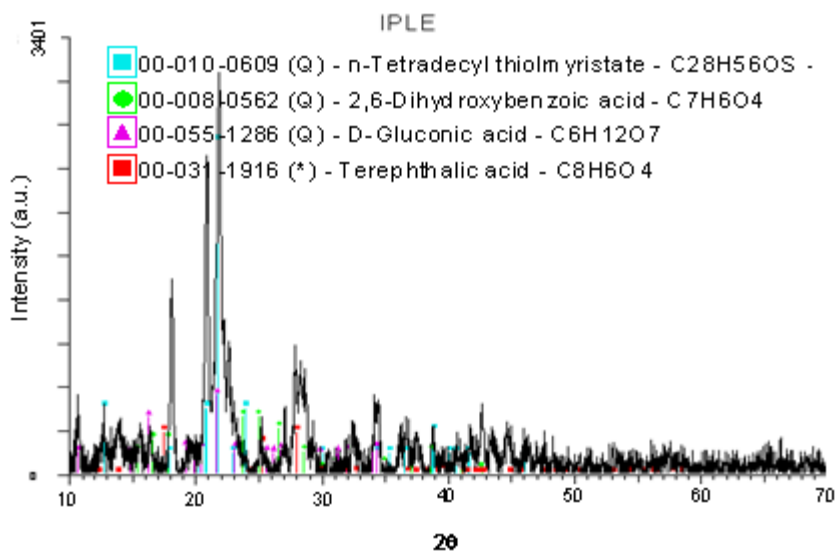


Figure 4. 18 XRD spectrum for PEO/LiAlO₂ doped with 50% NaI/I₂.

4.5 Discussions

A detailed description of the formation of the two-phase structure has been presented in *Fundamental Principles of Polymer Materials* by S. Rosen [193].

First of all, two crystalline structures may exist: 1) fringed micelle, where individual chains pass from one crystallite of 10 nm to 200nm zone with sections of chains aligned on one direction, to another crystallite through a disordered zone or amorphous zone (Figure 4.19); and 2) lamellar crystals, where the direction of the chains is perpendicular to the large face of a plate-shaped crystal of 1 to 100 micrometers (Figure 4.20). Not only are polymer chains arranged to form crystallites but these crystallites often aggregate into supermolecular structures known as spherulites. They start from a point of nucleation until other spherulites are encountered. In a spherulite, branched lamellar grow from the center to form root-like or dendrite-like patterns. The micro fibrous structure observed in Figure 4.15(a) and (b) belongs to lamellar crystals. Since size of the fringed micelle crystalline phase is smaller than the wavelength of visible light ($\sim 550\text{nm}$), the polymer membrane with pure fringed micelle crystals and amorphous phase should be transparency. The transparency improvement of PEO complex membrane after hot pressing treatment could be explained as that the spherulite crystalline phase converted into fringed micelle crystalline phase or amorphous phase. The X-ray diffraction pattern of fringe micelle crystals consists of a lot of

short 'crystal-like' reflections, which usually considered as diffuse background for high molecular polymer. However, no individual crystal peak could be assigned to fringed micelle crystals [194]. Since the fringed micelle cannot be detected by XRD, the crystalline peak dwindle after hot pressing treatment in Figure 4.12 and Figure 4.13 could be also explained as that the spherulite crystals converted into either fringe micelle crystals or amorphous phase. Because DSC results indicate that the mass ratio of crystalline phases in PEO complex membrane does not change significant, it is more possible that the spherulite crystalline phase was converted into fringed micelle crystalline phase. Because the fringed micelles disperse among the amorphous phases, there are more conduction paths than in the case with co-existence of amorphous and spherulite crystalline phases.

The phases that may exist in the PEO/LiX ($X=AlO_2^-$, ClO_4^- , TFS^-) polymer and the equilibrium phase composition have been a research topic for a long period of time. A detailed phase diagram was provided by Sorensen and Jacobsen [195] (Figure 4.21). They also claimed that the crystalline phase had a stoichiometry of $R=4$. However, the conductivity of the crystalline phase is almost negligible and the total conductivity is controlled by the conductivity of the amorphous phase.

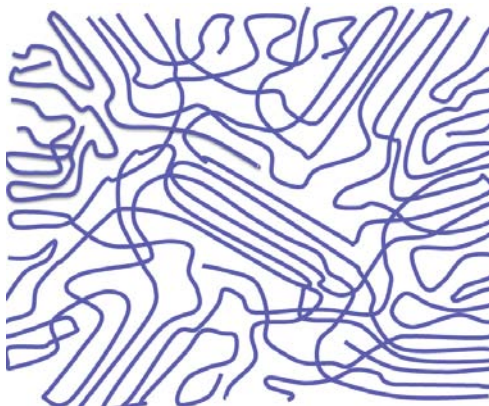


Figure 4.19 The fringed micelle model of the two phase structure of polymer.

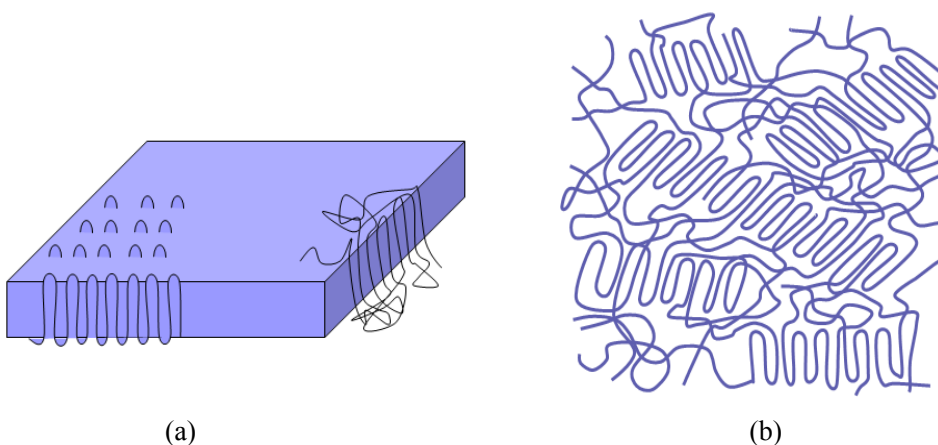


Figure 4.20 (a) Plate-like re-entry model of lamellar crystal; (b) folded chain lamellae tied together by inter-lamellar amorphous chains.

In fact, according to the DSC measurement data (Tables 4.3 and 4.8), there is 30-40% amorphous phase in the pristine PEO/LiAlO₂ and PEO/LiTFS electrolytes at room temperature. It is probably a universal case for all polymer materials that a complete crystallinity is never reached. In comparison to metals and alloys, the amount of crystalline defects in the periodic structures is only in the ppm level. This difference is due to the size of the molecules and the nature of the intermolecular forces. In addition to these general trends, salts with large anions

are easier to dissociate and more potent to promote amorphism in the electrolyte than salts with small anions. This is clearly reflected in the experimental results for pristine PEO/LiAlO₂ (small anion) and PEO/LiTFS (large anion) polymer electrolytes.

With addition of fillers, the amount of amorphous phase increases (according to XRD, SEM, and DSC data) leading to a significant increase in conductivity. However, the experimental data also reveals that although the final effect is a conductivity increase, the mechanisms for the addition of SiO₂ and addition TiO₂ are different. SiO₂ promotes amorphous whereas TiO₂ promote dissolution and dissociation of salts.

The major finding of this research involves the hot pressing treatment. XRD, FTIR, and SEM data indicate that the acquisition of a high conductivity in the level of 0.001 S/cm is because the hot pressing process results in a decrease in crystallinity or an increase in amorphism. However, the data of the melting heat from DSC analyses suggest that in fact the amount of crystalline phase does not vary significantly with respect to the duration of hot pressing. A possible explanation of this paradox is that at elevated temperature (110°C), all crystallites

are converted into amorphous phase and during the natural cooling process small crystallites (e.g. 10 nm) rather than large (10 micrometers) lamellae form. This assumption clearly explain the lowering of the peak height and appearance of the “hump” in the XRD, the disappearance of the spherulites and lamellae or dendrites in SEM, and a slight change of crystalline phase. When the crystallites are very small due to the size of fringed micelles, there may be more interconnecting amorphous paths than in the case where there are many large obstacles (lamellae and spherulites) from one side to the other side of a membrane. In fact, the effect of high temperature on the conductivity has been recorded in a previous study by Marzantowicz et al. [6]. However, the authors did not realize that the high temperature changed the structure of the polymer electrolyte, resulting in a significant increase of conductivity. They conducted in-situ and online conductivity measurements in an oven. They first raised the temperature from 25°C to 110°C and then reduced the temperature back to 25°C. They found that at temperature above 25°C the conductivity in the reverse half cycle was 500 times greater than that in the temperature rising half cycle. At 25°C they monitored a continuous reduction of conductivity. However, the conductivity did not return

back to the original value at the beginning of the heating cycle. The difference was in consistent with the present finding about one order of magnitude.

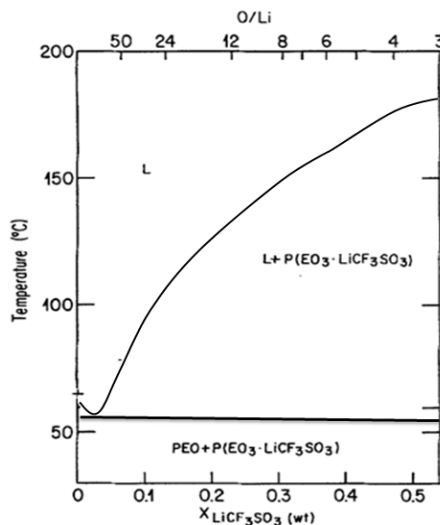


Figure 4. 21 Schematic phase diagram of PEO/LiTFS polymer electrolytes. There are crystalline, amorphous (L), pure salt, and pure polymer phases.

This assumption can also explain why the membranes became transparent after hot pressing. It is well known that a single phase polymer membrane (e.g. amorphous polymer at elevated temperature) is transparent [193]. If there are particles of a second phase (e.g. crystallites), scattering of visible light at the interface will result in a translucent membrane. If the particle size is smaller than the wavelength of the visible light (0.4-0.7 micrometers), the scattering of light decreases. Thus, both amorphous phase polymers and dual phase polymers with small crystallites can be transparent.

4.6. Conclusions

PEO/LiX ($X=\text{AlO}_2^-$, ClO_4^- , TFS^-) composite polymer electrolyte membranes were obtained by a solution casting method and further addition of appropriate lithium salt, SiO_2 or TiO_2 inorganic filler, hot pressing, and increased temperatures were applied to improve the conductivity and morphology of composite membranes. The characteristic properties of PEO-based polymer electrolytes were studied by FTIR, XRD, DSC and SEM. The in-plane and through-plane ionic conductivities of alkaline PLE composite polymer electrolyte films were evaluated via four-electrode and two-electrode methods, respectively. It was found that the in-plane ionic conductivity of PEO/LiTFS electrolyte at room temperature can be increased by 10 times to 1.71×10^{-3} S/cm and the increment is a function of duration of the hot pressing process. Similar tendencies can be obtained for the through-plane ionic conductivity at room temperature. The SEM, FTIR and XRD characterization results suggest that the crystalline phase in PEO/LiTFS composite polymer electrolytes was converted from spherulite crystalline phase into fringed micelle crystalline phase or amorphous phase after hot pressing, correlating to the increase of conductivity. Similar phenomena are observed for PEO/LiAlO₂ electrolytes.

The ionic conductivity of high molecular weight PEO composites with LiX (X= AlO_2^- , ClO_4^- and TFS $^-$) have been discussed in 4.1. The addition of lithium salts, especially those with large anions and low lattice energies, could improve the in-plane conductivity up to 9 fold and the through-plane conductivity up to 90 fold. Both ClO_4^- and TFS $^-$ anions have larger anion size and lower lattice energy than AlO_2^- anions, which leads to a higher degree of dissociation and better anion mobility. Since the number of carrier ions is larger and carrier mobility is better, the corresponding ionic conductivity of PEO/LiX (X= AlO_2^- , ClO_4^- , TFS $^-$) electrolyte is higher. With better ionic conductivity of the electrolyte, the higher effective capacitance could be obtained for the same Carbon paper-PEO electrolyte- Carbon paper electrochemical cell. However, the hygroscopic property of LiClO_4 prohibits the corresponding polymer electrolyte from becoming a fully solvent-free solid electrolyte. Its weak mechanical property limits its further study.

The addition of SiO_2 or TiO_2 inorganic filler to the PEO/ LiAlO_2 inhibits the growth of PEO crystalline domain so as to reduce the size of each crystalline phase. Also, the addition of those fillers to PEO/ LiAlO_2 shows increased ion conductivity. The addition of inorganic filler could also increase the ionic

conductivity of PEO/LiClO₄ and PEO/LiTFS electrolytes.

The addition of mediators into PEO electrolytes is very effective in enhancing their conductivity. In fact, the addition of mediators overwhelms the effect of all other methods, including hot-pressing, adding fillers, and using salts with large anions. The maximum conductivity reaches 0.2 S/cm with a concentration of 50 wt% NaI/I₂ in PEO electrolytes. However, the volumetric concentration of the mediators in the PEO electrolyte is not particularly high (1.0 mol/L).

Although more detailed study may be necessary, the results suggest that the enhancement of conductivity is due to the charge transfer between mediators because conductivity is usually a linear function of concentration. However, it is worth noticing that this conductivity is not a pure ionic conductivity. The conductivity is a combination of ionic conductivity and electronic conductivity. Thus, the PEO electrolyte cannot be used as a separator to insulate the transport of electrons, but can be used in the porous electrodes of the supercapacitors.

Chapter 5 PEO/LiX/AC BASED SUPERCAPACITOR

In this chapter, PEO/LiX/AC ($X=\text{AlO}_2^-$, ClO_4^- , TFS^-) composite materials were applied to prepare the electrode for supercapacitors. All-solid-state supercapacitors were fabricated using the prepared composite electrodes and a Nafion 117 membrane as a separator. The method that was used to fabricate the electrochemical cell was to impregnate the suspension with electrode materials (PEO/LiX/activated carbon and acetonitrile) on a piece of carbon nanofoam and then to press the carbon nanofoam on the both sides of a Nafion 117 membranes. In some cases, SiO_2 or TiO_2 was added into the suspension of PEO/LiX/activated carbon ($X=\text{AlO}_2^-$, ClO_4^- , TFS^-) as inorganic filler. In some other cases, a NaI/I_2 mediator was also added into the suspension of PEO/LiX/activated carbon ($X=\text{AlO}_2^-$, ClO_4^- , TFS^-). CV and EIS measurements were conducted to evaluate the electrochemical properties of the composite electrodes. Long-term charge/discharge cycle tests were conducted to evaluate the stability, durability, and cycle life of the systems. The morphology of the composite electrodes was characterized using optical microscopes and SEM.

Effects of concentrations of inorganic filler, mediator, and CV scan rate on the

performance of the supercapacitors are discussed below.

5.1 Effect of different lithium salts

Figure 5.1 is the cyclic voltammetry results of a supercapacitor with PEO/LiX/AC (X=AlO₂⁻, ClO₄⁻, TFS⁻) composite electrodes containing different lithium salts. The composition of each sample is listed in Table 5.1. The specific capacitances and specific powers of the supercapacitors with respect to the total mass of the two electrodes and with respect to the mass of the active material (activated carbon and mediator) were calculated using the following equations:

$$C_{electrode} = \frac{Min(q_a, q_c)}{\Delta V \cdot m_{electrode}} \quad \text{or} \quad C_{active} = \frac{Min(q_a, q_c)}{\Delta V \cdot m_{active}} \quad (5.1)$$

$$P_{electrode} = \frac{1}{m_{electrode}} \times Max(i \times V) \quad \text{or} \quad P_{active} = \frac{1}{m_{active}} \times Max(i \times V) \quad (5.2)$$

where q_a and q_c are the sums of charge calculated for the anodic and cathodic polarization half cycles, respectively, ΔV is the potential window of the CV test, $m_{electrode}$ and m_{active} the masses of the supercapacitor and active materials respectively, $Min(q_a, q_c)$ is the minimum value of the q_a and q_c , $Max(i \times V)$ is the maximum value of the product of current (i) and potential (V) or power. The specific capacitance and power values calculated in Eqs. (5.1) and (5.2) are listed

in Table 5.2.

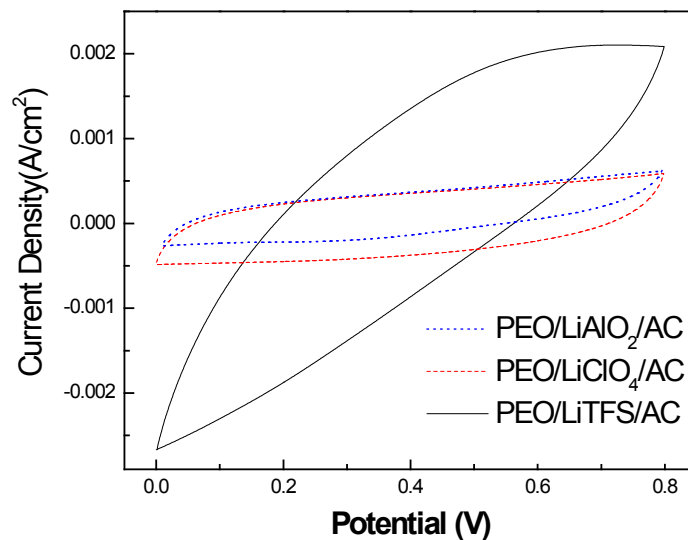


Figure 5. 1 CV results of symmetric PEO/LiX/AC ($X=\text{AlO}_2^-$, ClO_4^- , TFS^-) composite electrode supercapacitor (Potential range: 0~0.8 V, scanning rate: 35 mV/s)

Table 5. 1 Composition of components in the PEO/LiX/AC ($X=\text{AlO}_2^-$, ClO_4^- , TFS^-) composite electrodes. The mass of the Nanofoam carbon paper is not included.

Electrode	PEO (wt%)	LiTFS (wt%)	LiAlO ₂ (wt%)	LiClO ₄ (wt%)	Active Carbon (wt%)
PC: PEO/LiTFS/AC	42	25			33
PAC: PEO/LiAlO ₂ /AC	55		12		33
PLC: PEO/LiClO ₄ /AC	50			17	33

Figure 5.2 shows the Nyquist impedance plots of the supercapacitors with specifications in the figure. The samples used for the EIS study were exactly the

same samples used for the CV study. In Figure 5.2, the Nyquist plots for the supercapacitors with PEO/LiX/AC ($X=\text{AlO}_2^-$, ClO_4^- , TFS^-) composite electrodes show arcs in the high frequency region and straight lines in the low frequency region. The tails at the low frequency range have similar slopes, which are probably due to the transport in porous electrode (Warburg impedance) [189]. The cell resistance, R_s , follows the order of $\text{PEO/LiAlO}_2/\text{C} > \text{PEO/LiClO}_4/\text{C} > \text{PEO/LiTFS}/\text{C}$. The specific capacitance and specific power follows the order of $\text{PEO/LiAlO}_2/\text{C} < \text{PEO/LiClO}_4/\text{C} < \text{PEO/LiTFS}/\text{C}$. These results are consistent with the conductivity measurement results in Chapter 4. For the system with LiTFS with the largest anion size (TFS^-) and lowest lattice energy, the cell resistance, R_s , and charge transfer resistance, R_{ct} , are smaller but the specific capacitance is greater than that for the system with LiAlO_2 that has the smallest anion and greatest lattice energy.

The surface morphology of each PEO/LiX/AC ($X=\text{AlO}_2^-$, ClO_4^- , TFS^-) composite electrode was examined using an SEM. The micrographs are shown in Figure 5.3. These images exhibit similar uniform porous structures that are very different from the surface of PEO/LiX ($X=\text{AlO}_2^-$, ClO_4^- , TFS^-) membranes.

Formation of these porous structures is believed to be closely related to the presence of highly porous activated carbon material.

Table 5. 2 Summary of the electrochemical performance for PEO/LiX/AC (X=AlO₂⁻, ClO₄⁻, TFS⁻) composite electrode supercapacitor (Direct paint sample, with electrode surface area of 1cm²).

Sample Label	Electrode	Separator	R _s (Ω)	Specific Capacitance (F/g)	Specific Power (kW/kg)
PAC-N-PAC	PAC	Nafion 117	92.5	4.56	0.19
PLC-N-PLC	PLC	Nafion 117	39.6	5.19	0.26
PC-N-PC	PC	Nafion 117	29.4	12.9	0.59

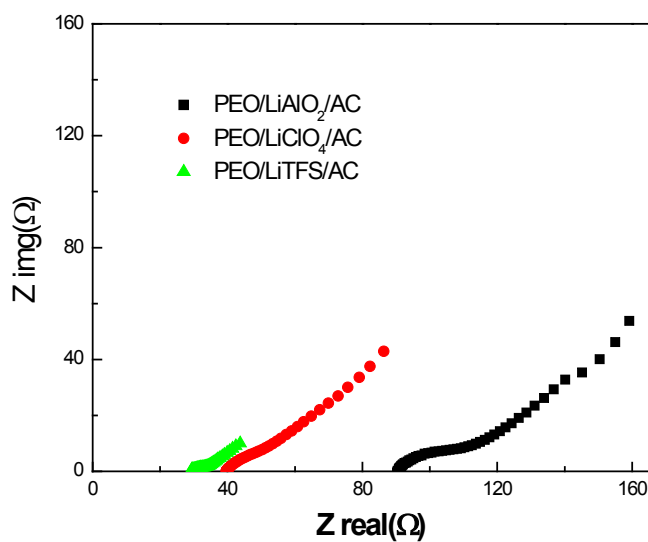


Figure 5. 2 Nyquist plots for symmetric PEO/LiX/AC (X=AlO₂⁻, ClO₄⁻, TFS⁻) composite electrode supercapacitor (1~100,000Hz)

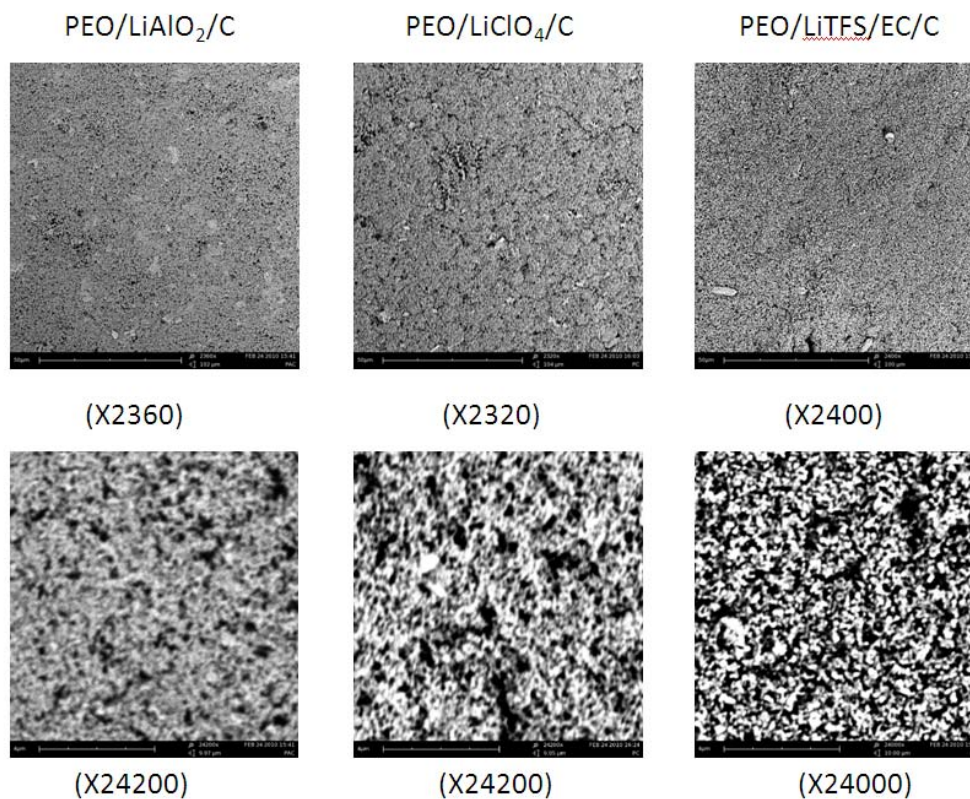


Figure 5. 3 SEM images of the PEO/LiX/AC ($X=\text{AlO}_2^-$, ClO_4^- , TFS^-) composite electrode surfaces.

5.2 Effect of filler and mediator

5.2.1 Effect of filler

The compositions of PEO/LiTFS/AC with or without filler are listed in Table 5.3. Figure 5.4 shows the cyclic voltammetry results of PEO/LiTFS/AC supercapacitors with or without filler. The specific capacitances with respect to the total mass of a composite electrode are calculated using Eqs. (5.1) and (5.2) and are listed in Table 5.4. The specific capacitance of the supercapacitors with PEO/LiTFS/AC composite polymer electrodes increased almost 15% with the

addition of 1wt% SiO₂ inorganic filler. Figure 5.5 show the Nyquist impedance plots of the SCs with specifications indicated in the Figure 5.4. The samples used for the EIS study were exactly the same samples used for the CV study. With the addition of filler, the series resistance of the supercapacitor does not vary significantly because the resistance of the separator, the Nafion membrane, is actually greater than that of the electrodes.

Table 5. 3 Compositions of the PEO/LiTFS/AC electrodes with or without filler.

	PEO (wt%)	LiTFS (wt%)	SiO ₂ (wt%)	TiO ₂ (wt%)	AC (wt%)
PC	42	25			33
PCS	40	24	3		33
PCT	40	24		3	33

Table 5. 4 Summary of the series resistance, specific capacitance, and specific power for supercapacitors with and without filler in the composite electrode

Sample	R(Ω)	Current density (mA/cm ²)	Specific Capacitance (F/g)	Specific Power (kW/kg)
PC	2.4	70	13.0	0.28
PCS	2.3	84	15.3	0.34
PCT	3.0	91	17.5	0.36

More systematic study was conducted for the supercapacitors with PEO/LiAlO₂/AC electrodes. The compositions of the electrodes are listed in Table 5.5. The CV results for supercapacitors with or without filler are exhibited in Figure 5.6. The calculated specific capacitance and power values are presented in

Table 5.6.

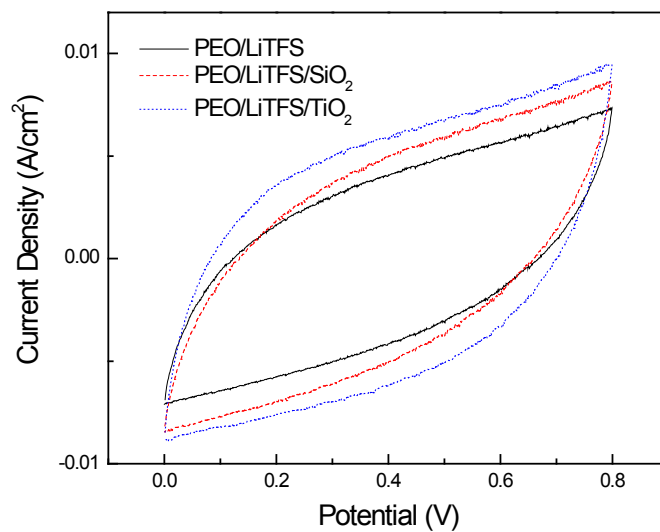


Figure 5. 4 CV results of symmetric PEO/LiTFS/AC, PEO/LiTFS/AC/SiO₂, and PEO/LiTFS/AC/TiO₂ electrode supercapacitor (Potential range: 0~0.8 V, scanning rate: 20 mV/s).

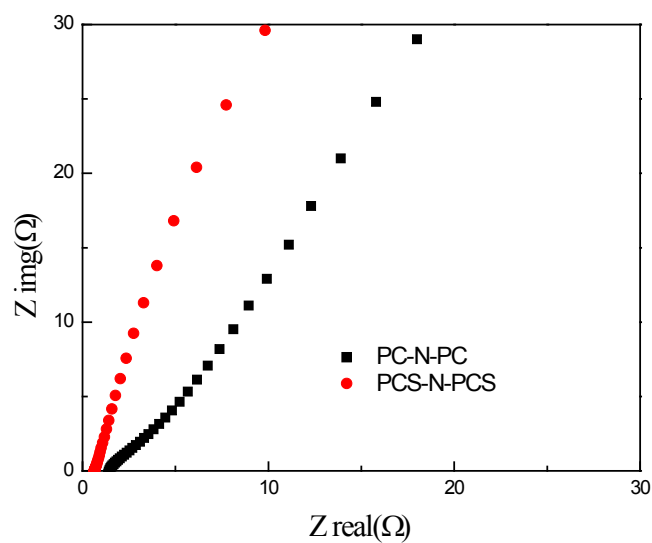


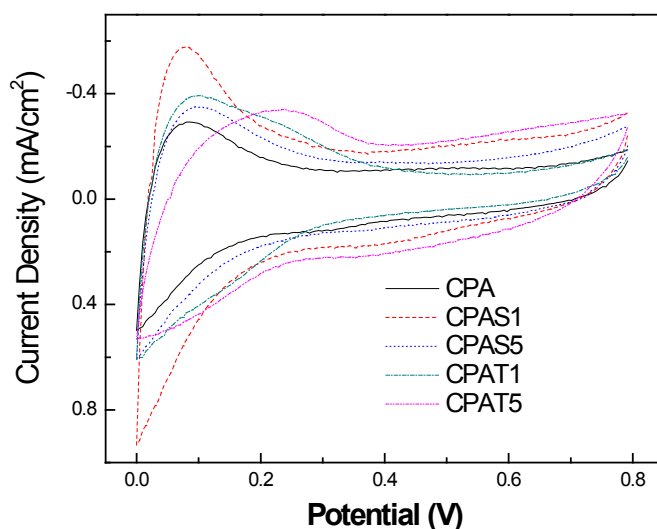
Figure 5. 5 Nyquist plots for PEO/LiTFS/AC polymer electrode supercapacitor and PEO/LiTFS/AC/SiO₂ polymer electrode supercapacitors

Table 5. 5 The compositions of the PEO/LiAlO₂/AC composite electrodes

Sample name	Component of electrode(wt%)				
	PEO	LiAlO ₂	SiO ₂	TiO ₂	AC
CPA	41.7	8.3			50
CPAS1	41.3	8.2	0.5		50
CPAS5	39.6	7.9	2.5		50
CPAT1	41.3	8.2		0.5	50
CPAT5	39.6	7.9		2.5	50

Table 5. 6 Summary of the specific capacitance and specific power for supercapacitors

Sample label	Current density (mA/cm ²)	C _{electrode} (F/g)	P _{electrode} (kW/kg)	C _{active} (F/g)	P _{active} (kW/kg)
CPA	0.497	2.75	0.125	5.50	0.250
CPAS1	0.934	3.75	0.130	11.25	0.39
CPAS5	0.604	2.16	0.129	6.48	0.387
CPAT1	0.608	3.22	0.120	9.66	0.36
CPAT5	0.532	4.31	0.192	12.93	0.576

Figure 5. 6 CV results of symmetric PEO/LiAlO₂/AC electrode based supercapacitors. (Potential range: 0~0.8 V, scanning rate: 35 mV/s).

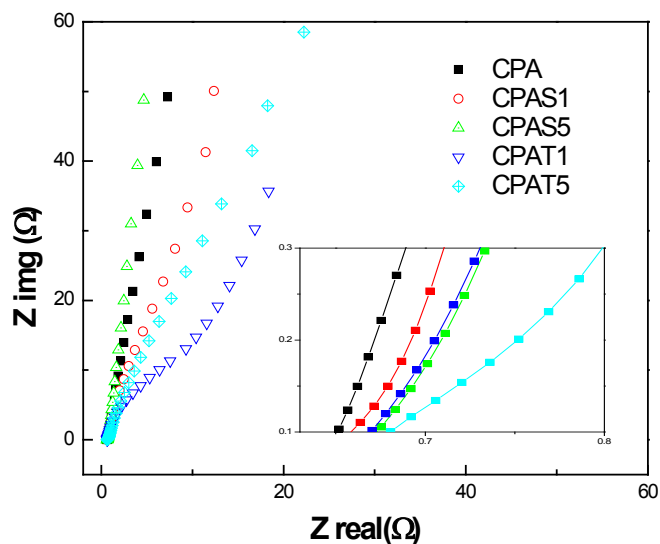


Figure 5. 7 Nyquist plots for symmetric PEO/LiAlO₂/AC electrode based supercapacitor.

In Figure 5.7, the Nyquist plots for the supercapacitor with activated PEO/LiAlO₂/C electrodes are essentially straight lines showing a typical behavior for a dielectric capacitor or an ideal electrical double layer capacitor (EDLC) [19]. The internal cell resistance or series resistance actually increases with the addition of filler. However, it is erroneous to conclude that the addition of filler decreases the conductivity of the PEO polymer electrolyte. This is because the separator is the larger contributor to cell resistance, thus, the difference in series resistance is mostly due to the difference of the separator, the Nafion membrane, which is very sensitive to moisture level and impurity. However, ionic conductivity does play a

major role in the charge/discharge process. A high ionic conductivity can enable a high discharge rate or high power.

5.2.2 Effect of mediator

Table 5. 7 The compositions of the PEO/LiAlO₂/AC/NaI/I₂ composite electrodes

Sample	Label	Composition (wt%)				
		PEO	LiAlO ₂	AC	I ₂	NaI
PEO/LiAlO ₂ /AC/NaI/I ₂	CPAI5	39.6	7.9	47.5	2.75	2.25
PEO/LiAlO ₂ /AC/NaI/I ₂	CPAI10	37.5	7.5	45	5.5	4.5
PEO/LiAlO ₂ /AC/NaI/I ₂	CPAI20	33.3	6.7	40	11.0	9.0
PEO/LiAlO ₂ /AC/NaI/I ₂	CPAI30	28.3	5.7	33	18	15

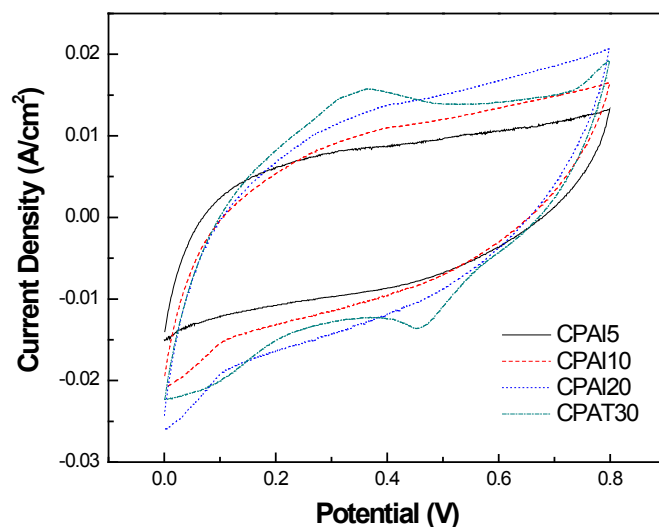


Figure 5. 8 CV results of symmetric polymer electrode supercapacitor with or without mediator. (Potential range: 0~0.8 V, scanning rate: 35 mV/s).

The compositions of the supercapacitor electrode samples with or without mediator are listed in Table 5.7. Figure 5.8 illustrates CV results of a

supercapacitor with nominally identical electrodes that both contain NaI, I₂, and activated carbon (AC). Interestingly, only the CV curve for the supercapacitor with electrodes containing 30% of mediator reveals a symmetric pair of peaks with a mean voltage of about 0.4 V. The iodine and iodide in aqueous solution may undergo two reactions: 1) $I_2(s) + 2e^- = 2I^-$ and 2) $I_3^- + 2e^- = 3I^-$. However, in a gel electrolyte, the onset potential for the reactions with respect to the I₃⁻/I⁻ pair is about 0.4 V [196]. The appearance of the peaks at a high concentration of mediator reveals a transport related limitation. The CV curves for other supercapacitors do not show redox peaks revealing typical behavior for an EDLC. The specific capacitance and power are listed in Table 5.8. These results indicate that addition of mediator can increase the specific capacitance and power by 10-30 times. Nyquist plots for the supercapacitors described in Figure 5.8 are shown in Figure 5.9. The major difference between the Nyquist plots shown in Figures 5.5 and 5.7 and the plots in Figure 5.9 is that there are small semi-circles for the plots in Figure 5.9, whereas there is none for the plots in Figures 5.5 and 5.7. In the cases of Figure 5.5 and 5.7, there is no mediator and the capacitance is originated from EDL. Thus, the shape of these plots is similar to those of a typical dielectric

capacitor or EDLC [19] and the charge transfer resistance at the interface is very high. The semicircles in the plots indicate that the charge transfer resistance in the system is low ($\sim 0.5 \Omega$).

Table 5. 8 Specific capacitance and specific power for supercapacitors with or without mediator.

Sample label	R(Ω)	Current density (mA/cm^2)	Specific Capacitance (F/g)	Specific Power (kW/kg)
CPA	2.5	0.497	5.50	0.250
CPAI5	2.8	13.0	107	3.5
CPAI10	2.4	16.2	120	4.3
CPAI20	3.0	19.0	134	5.0
CPAI30	2.4	19.5	150	5.2

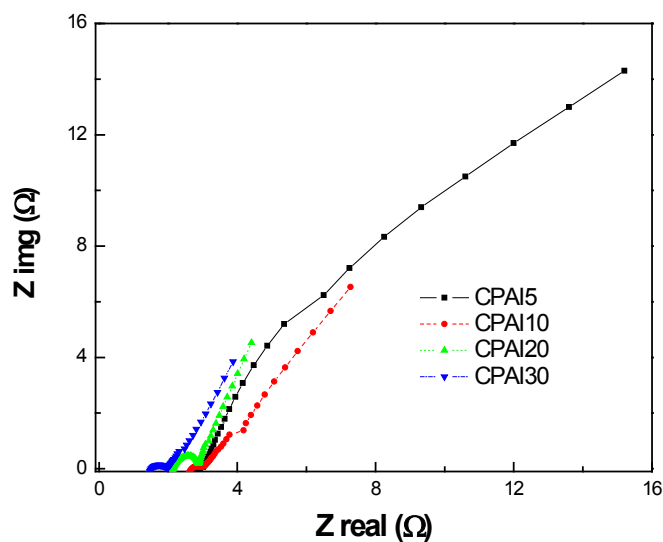


Figure 5. 9 Nyquist plots for PEO/LiAlO₂/AC electrodes with iodine/iodide (I^-/I_2) mediator.

5.2.3 Synergic effect of mediator and filler

The compositions of the supercapacitor electrode samples with or without mediator and filler are listed in Table 5.9. Figure 5.10 illustrates cyclic voltammetry (CV) results of a supercapacitor with nominally identical electrodes that both contain filler, NaI, I₂, and activated carbon (AC). All of these CVs show flat peaks, indicating an insignificant impact of the transport process on the charge/discharge. The specific capacitance and power are listed in Table 5.10. These results indicate that the addition of filler in the electrode with mediator can further increase the specific capacitance and power by two times.

A small semicircle at high frequencies and a nearly straight line at low to intermediate frequencies are observed in Figure 5.11 for the supercapacitors containing NaI/I₂. The appearance of the semicircle indicates that the charge transfer resistance and pseudocapacitance is related to the addition of the mediator. With the addition of 1wt% SiO₂ and TiO₂ filler, shrinking of the semicircle and its shifting to the right reflect a decrease of the series resistance and charge transfer resistance. Further addition of the same filler presents a reverse effect compared to the sample with 1wt% filler.

Table 5. 9 The compositions of PEO/LiAlO₂/AC composite electrodes

Sample	Composition (wt%)						
	PEO	LiAlO ₂	SiO ₂	TiO ₂	AC	I ₂	NaI
PEO/LiAlO ₂ /AC/NaI/I ₂ (CPAI)	28.3	5.7			33	18	15
PEO/LiAlO ₂ /SiO ₂ /AC/NaI/I ₂ (CPAIS1)	28	5.7	0.3		33	18	15
PEO/LiAlO ₂ /SiO ₂ /AC/NaI/I ₂ (CPAIS5)	27.1	5.4	1.5		33	18	15
PEO/LiAlO ₂ /TiO ₂ /AC/NaI/I ₂ (CPAST1)	28	5.7		0.3	33	18	15
PEO/LiAlO ₂ /TiO ₂ /AC/NaI/I ₂ (CPAST5)	27.1	5.4		1.5	33	18	15

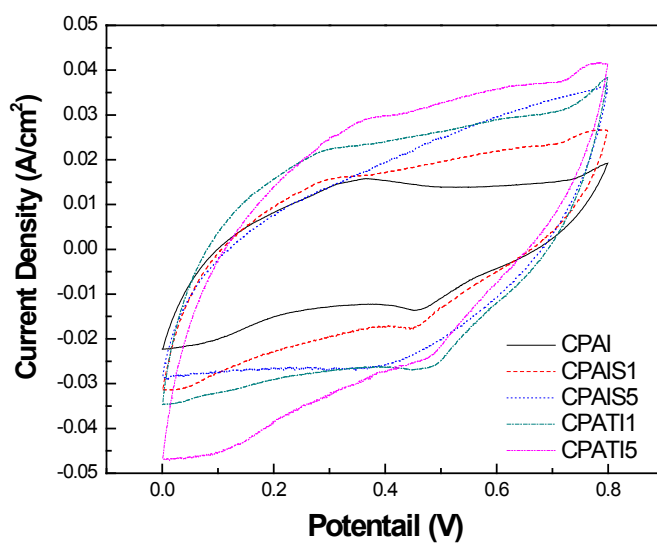


Figure 5. 10 CV results of symmetric PEO/LiAlO₂/AC/NaI/I₂ electrode supercapacitor with or without filler. (Potential range: 0~0.8 V, scanning rate: 35 mV/s)

Table 5. 10 Specific capacitance and specific power for PEO/LiAlO₂/AC/NaI/I₂ electrode supercapacitor

Sample label	R(Ω)	Current density (mA/cm ²)	Specific capacitance (F/g)	Specific power (kW/kg)
CPAI	2.8	19.5	150	5.2
CPAS11	3.1	26.5	207	7.1
CPAS15	2.5	36.4	257	9.7
CPAT11	2.0	38.0	295	10.1
CPAT15	2.8	40.4	333	10.8

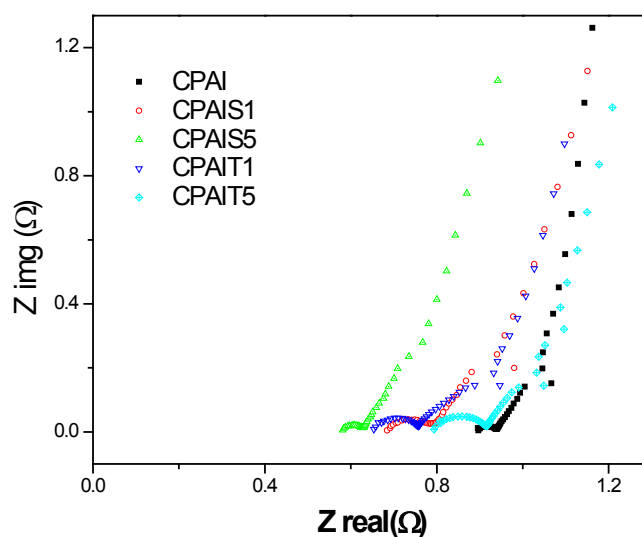


Figure 5. 11 Nyquist plots for polymer electrode supercapacitors with various inorganic filler in the composite electrode. PEO/LiAlO₂/C electrodes were loaded with addition of filler and iodine/iodide (I⁻/ I₂) mediators.

5.3 Effect of scan rate

In order to evaluate the charge/discharge response of the supercapacitors, CV measurements were conducted. Figure 5.12 shows the CV curves obtained with potential scan rates vary from 20 to 200 mV/s for a symmetric PEO/LiAlO₂/AC

electrode supercapacitor. The current level increases as the potential scan rate is increased. This behavior is directly related to the nature of a capacitor and can be explained by

$$I = \frac{dq}{dt} = C \frac{dV}{dt} = C \times (\text{Scan rate}) \quad (5.3)$$

where I is the maximum current density, v is the scan rate, dq , dt , and dV are the variation of charge, time, and potential.

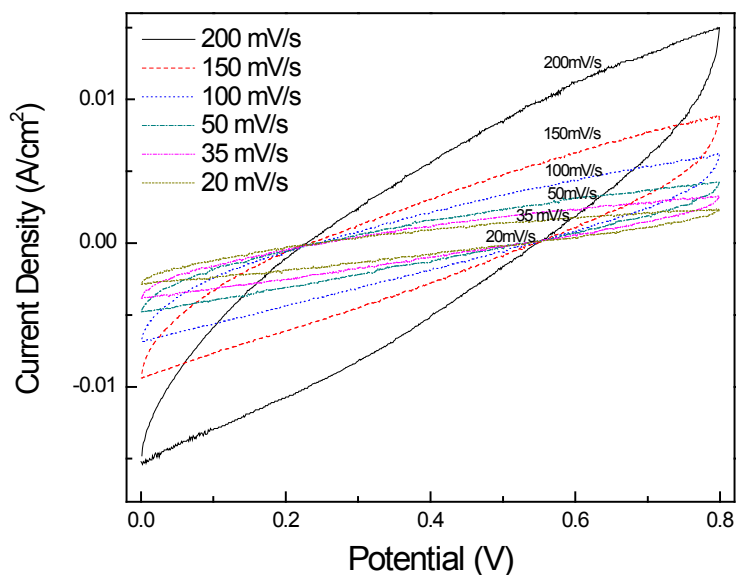


Figure 5. 12 CV results as a function of potential scan rate for PEO/LiAlO₂/AC-Nafion-PEO/LiAlO₂/AC supercapacitors.

However, the slope of the CV curve reveals that the series resistance in the supercapacitor is significant. Addition of NaI/I₂ mediator increases the capacitance and reduces the slope of the CV curve (Figure 5.13). This is expected because the

presence of the mediator can increase the total capacitance with a pseudocapacitance that is much greater than that of EDLC. Figure 5.14 shows the CV curves obtained with potential scan rates from 20 to 200 mV/s for a PLE/AC-Nafion-PLE/AC supercapacitor. Although the capacitance of this supercapacitor is not as high as that of the supercapacitor with mediator (Figure 5.15), the effect of the series resistance is not significant. This is because the PEO/LiTFS is much more conductive than PEO/LiAlO₂. Ragone plots (Figure 5.16) describe the relation between specific power and energy. Indeed, the addition of mediator in the polymer electrolyte increases both the specific power and energy by one order of magnitude.

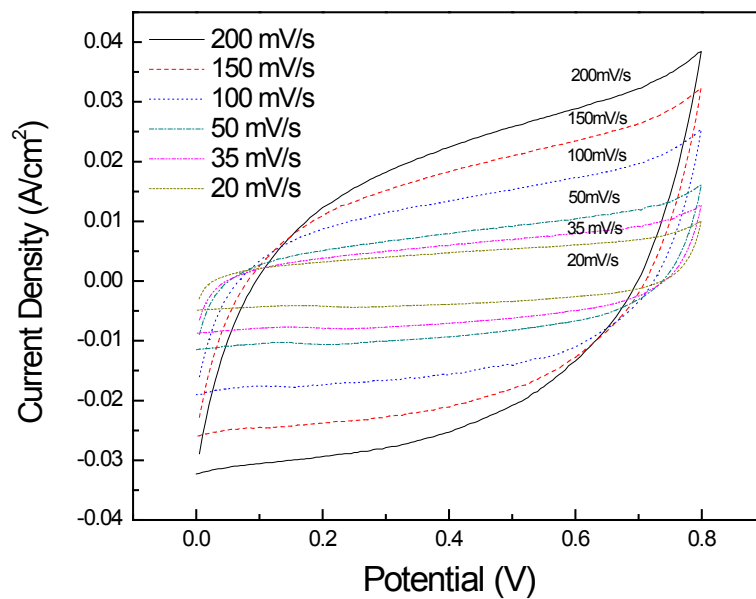


Figure 5. 13 CV results as a function of potential scan rate for PEO/LiAlO₂/AC/NaI/I₂-Nafion-PEO/LiAlO₂/AC/NaI/I₂ supercapacitors.

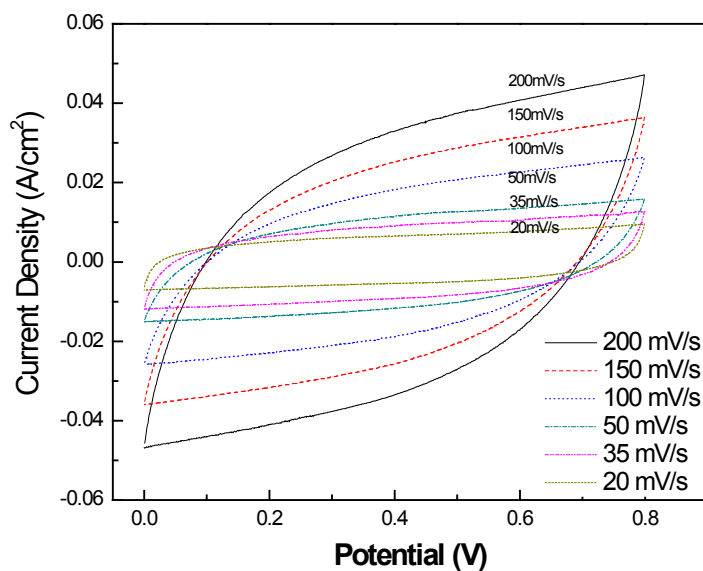


Figure 5. 14 CV results as a function of potential scan rate for PLE/AC-Nafion-PLE/AC supercapacitors.

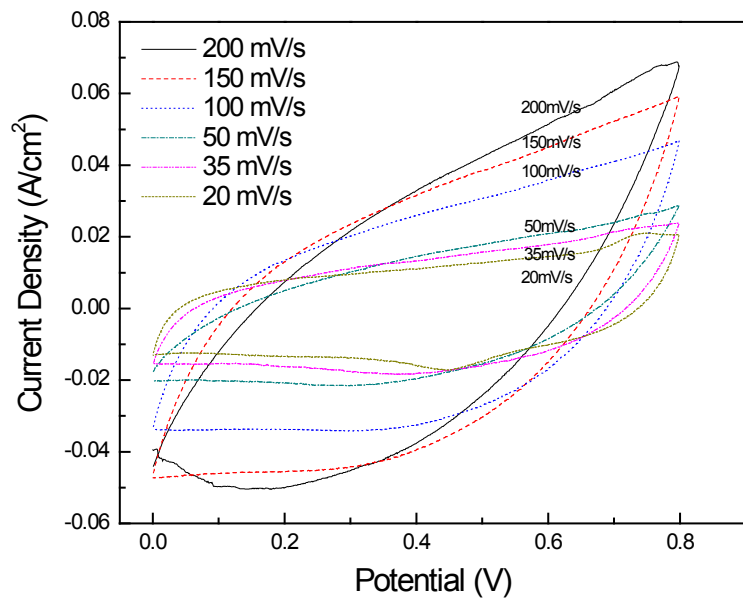


Figure 5.15 CV results as a function of potential scan rate for PLE/AC/NaI/I₂-Nafion-PLE/AC/NaI/I₂ supercapacitors.

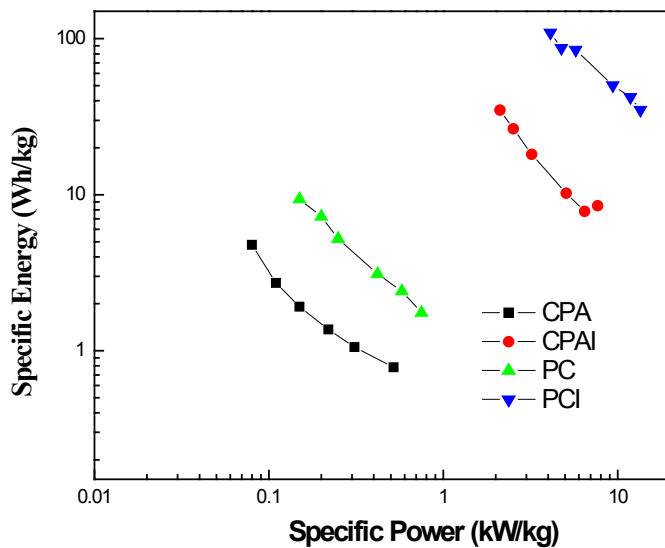


Figure 5.16 Ragone plots (specific power versus specific energy) for supercapacitors with and without mediator.

5.4 Effect of cycle number

The cycle stability and durability of the supercapacitors were evaluated using galvanostatic charge/discharge tests. These tests were conducted by first charging a supercaciotor at a constant current while recording the potential increase and then reversing the current to discharge the supercapacitor at a constant discharge current. For PLE/AC-Nafion-PLE/AC, PLE/AC/NaI/I₂-Nafion-PLE/AC/NaI/I₂, and PEO/LiAlO₂/AC/NaI/I₂-Nafion-PEO/LiAlO₂/AC/NaI/I₂ supercapacitors, the capacitances are almost constant with number of cycles, indicating long cycle stability.

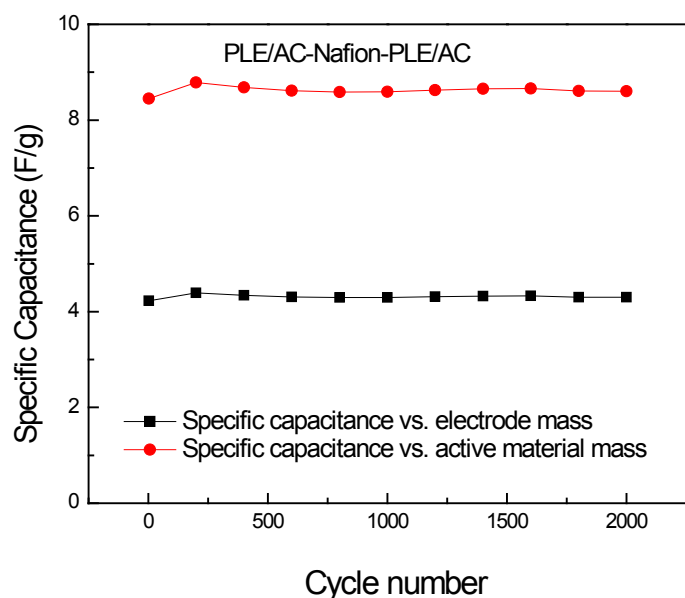


Figure 5. 17 Specific capacitance as a function of charge/discharge cycle numbers for PEO/LiTFS/AC-Nafion-PEO/LiTFS/AC supercapacitor.

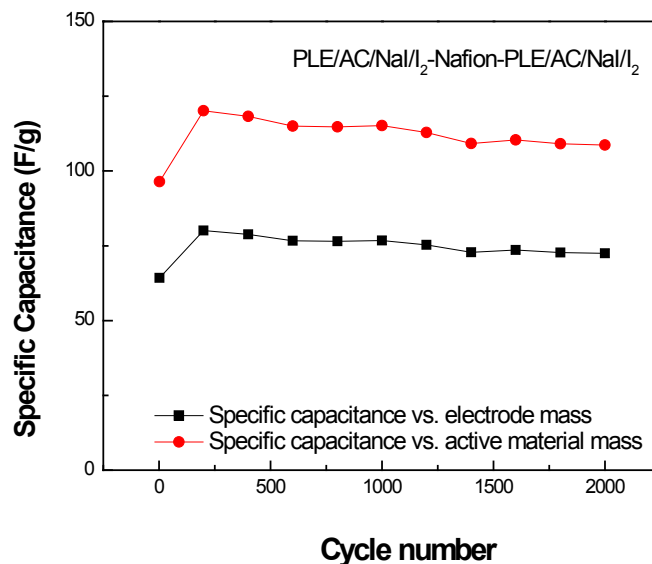


Figure 5. 18 Specific capacitance as a function of charge/discharge cycle numbers for PLE/AC/NaI/I₂-Nafion-PLE/AC/NaI/I₂ supercapacitor.

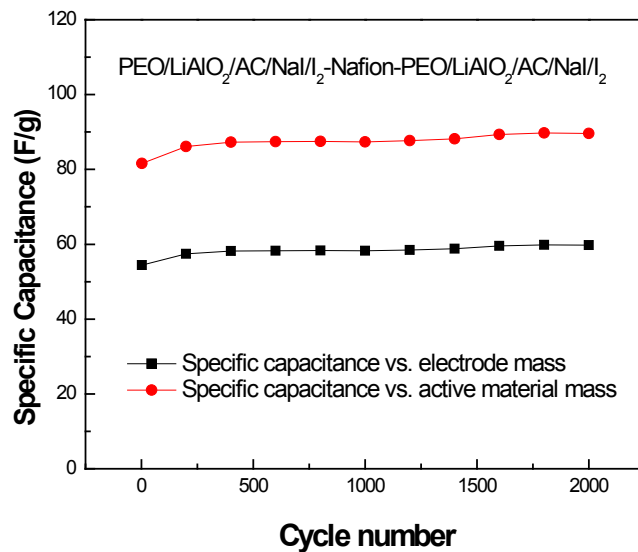


Figure 5. 19 Specific capacitance as a function of charge/discharge cycle numbers for PEO/LiAlO₂/AC/NaI/I₂-Nafion-PEO/LiAlO₂/AC/NaI/I₂ supercapacitor.

Figure 5.17, 5.18, and 5.19 shows the cycling stability of the symmetric PLE

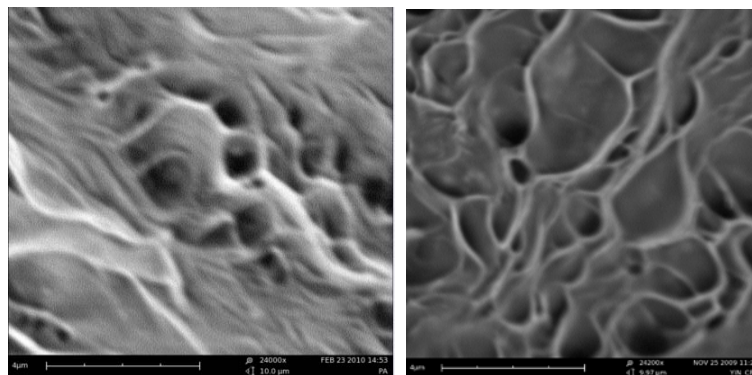
/AC, PLE/AC/NaI/I₂, and PEO/LiAlO₂/AC/NaI/I₂ electrode supercapacitor at room temperature and humidity of 90.

The symmetric PLE/AC/NaI/I₂ electrode supercapacitor shows a remarkable capacity increase from 90 F/g to 120 F/g in the first 200 cycles, then decrease from 120 F/g to 108 F/g after 1800 cycles. This slight capacitance decrease may be due to the irreversible side reaction of the mediator during cycling. The PEO/LiTFS based supercapacitor without mediator or pseudocapacitance exhibit slightly better cycling stability than the one with mediator. Although the initial capacity of the PEO/LiAlO₂ based supercapacitor is comparable to that of the PEO/LiTFS based supercapacitor at room temperature, it yields good cycling stability.

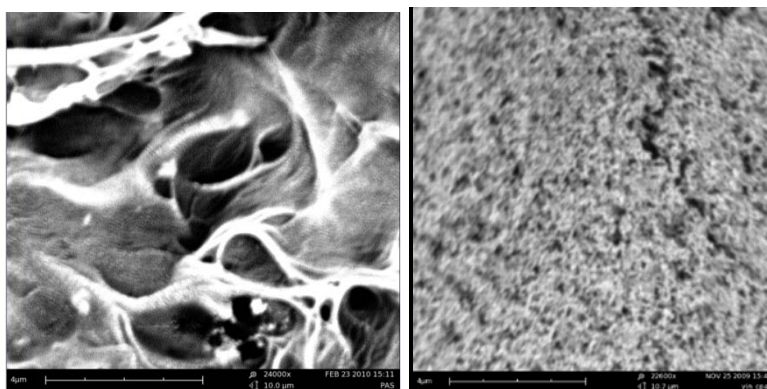
5.5 Surface morphology and chemical analysis

Figure 5.20 (a)-(f) are micrographs for of PEO/LiAlO₂/AC composite electrode samples [(b), (d), and (f)] and PEO/LiAlO₂ membrane samples [(a), (c), and (e)] for comparison. By comparing Figures 5.20 (a) and (b), the addition of activated carbon results in the amount and size of the spherulites of the PEO crystalline decreasing, and an increase in the amorphous phase is observed. The reason less crystalline phase is observed might be that the silica limits the formation of the

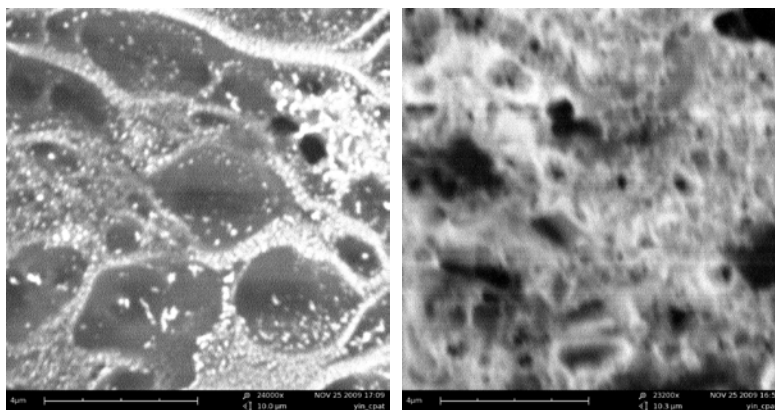
spherulites. This may result in a higher ionic conductivity in PEO-based polymers because the ionic conduction in the amorphous phase is much greater than that of the crystalline part [182]. From Figure 5.20 (d), it is easily observed that the addition of 1wt% of mesoporous SiO_2 impacts the structure of composite electrodes and essentially converts the macroporous structure into mesoporous structure (the diameter of the pore is around 10~50nm). However, as shown by Figure 5.20(e), the addition of a similar amount of TiO_2 cannot provide the same effect. The mesoporous TiO_2 randomly disperse in the continuous PEO's polymer matrix, but excessive TiO_2 particles exhibit aggregated morphologies on the edge of the porous structure. Comparing Figure 5.20(c) with (f), the addition of mediator can increase the porous size of PEO/ LiAlO_2 / SiO_2 /AC electrode, and part of the porous size could reach macro-scale. Compared to macroporous structure, the mesoporous structure provides more ion transfer tunnel so as to provide higher ion conductivity.



(a) PEO/LiAlO₂ (x24200); (b) CPA (x24200);



(c) PEO/LiAlO₂/SiO₂ (x24200); (d) CPAS (x24200);



(e) CPAT (x24200); (f) CPAS11 (x24200);

Figure 5. 20 SEM morphology of PEO/LiAlO₂/SiO₂ composite membrane and PEO/LiAlO₂/SiO₂(TiO₂)/AC composite electrode

5.6 Discussions

The three major effects of mediator in the PEO electrolyte are: 1) to significantly

increase the conductivity of the electrolyte through the fast electron/charge transfer among mediators; 2) to provide the supercapacitor with a pseudocapacitance; and 3) to mitigate the contact problem between the active material and the electrolyte material. The first effect is well manifested by the data shown in Table 4.10 and Figure 4.16.

The second effect can be observed in Table 5.5 and Table 5.10, showing that the addition of mediator can greatly increase the specific capacitance almost 30 fold and increase the specific power around 20 fold. The differences in specific capacitance and power between the supercapacitors with and without mediator clearly result from the pseudocapacitance of NaI/I₂ mediator. The theoretically calculated specific capacitance of NaI/I₂ mediator in the supercapacitor is about 172 F/g, which is higher than experimental specific capacitance (150 F/g) for PEO/LiAlO₂/AC/NaI/I₂-Nafion-PEO/LiAlO₂/AC/NaI/I₂ supercapacitors without filler in Table 5.10.

The cyclic voltammograms and charge/discharge cycle stability results reveal that these electrodes are stable in the selected potential window of 0.0-0.8 V. The CV curves in Figure 5.8 and 5.10 for electrodes loaded with I⁻/I₂ mediators have

one redox peak in the positive half cycle and another in the negative half cycle.

This indicates that the effect of the redox reactions of the mediators is the source of pseudocapacitance in the supercapacitors. These peaks in Figure 5.8 and 5.10 may be assigned to the formation of triiodide from iodide and iodine from triiodide. The peaks may be assigned to the redox reaction: $I_3^- + 2e^- = 3I^-$ [190-193, 197]. Interestingly, the peak in the negative half cycle in Figure 5.10 for an electrode without filler shows about 50 mV negative shifts with respect to the peak positions with the addition of SiO_2 and TiO_2 , revealing an interaction between SiO_2/TiO_2 and iodide/iodine redox pairs [198-200].

The realization of the third effect depends on the realization of two things: 1) dispersion of the mediator in the electrolyte and 2) high electron (charge) transfer rates between mediator and electrode (carbon) and between mediator and mediator. First of all, the XRD spectra in Figures 4.17 and 4.18 suggest that the mediators NaI and I_2 are highly dispersed in the PEO electrolytes. Secondly, a high electron transfer rate can be revealed by Nyquist plots for the PEO electrolyte based supercapacitors that are shown in Figure 5.7, Figure 5.9, and Figure 5.11. The charge transfer resistance at the electrolyte/electrode is dictated by the

interface area, adsorption, absorption, and double layer structures. For supercapacitors without mediator, the semicircle is too big to evaluate the actual value from the Nyquist plot. For the supercapacitor with the addition of mediator, the diameter of the semicircle in the Nyquist plot is 0.1 to 0.5 ohm. This suggests that the charge transfer or electron transfer rate between the mediator and electrode is high.

A high electron exchange rate between mediator and mediator is also important to realize a full charge of the mediators dispersed in the electrolytes. However, this cannot be directly verified with the available data. For most supercapacitors with pseudocapacitance, at potentials where the electron transfer reaction rate is faster than the diffusion rate, the reactants of the redox reaction will be depleted and the products will saturate the electrode surface. As a result, the current will become a function of the rate of product removal from the electrode surface or the rate of reactant replenishment. For such a diffusion control process, a peak current will appear and the peak current density is related to the square root of the scan rate, $v^{1/2}$, via Randles-Sevcik [2,3] equation (5.4),

$$I = (2.687 \times 10^5) C n^2 D^{1/2} v^{1/2} \quad (5.4)$$

where I [A/m²] is limiting current density, C [M] is mediator concentration, n is the number of electrons, D [m²/s] is the diffusion coefficient, and v [mv/s] is scan rate. However, for most CV curves at a scan rate from 20 to 200 mv/s, there is no typical current peak for the diffusion controlled cases. One of the possibilities is that both the electron transfer rate between the mediator and electrode and the electron transfer rate between the mediator and mediator in the electrolyte are sufficiently high and match. Therefore, the reduced or oxidized species at the electrode surface can quickly pass electrons to or gain electrons from the mediators in the electrolyte. This is equivalent to the effect of the products being quickly removed and the reactants being quickly replenished. If the diffusion is not dominant, the current peak may be absent. In addition, the behavior of the supercapacitor may be similar to that of an EDLC.

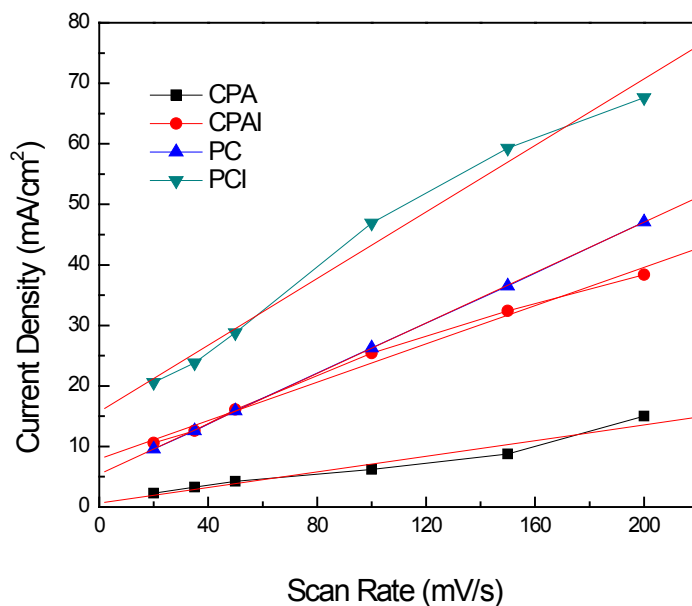


Figure 5. 21 Limiting current density plotted versus scan rate (the electrode potential is 0.8 V)

Table 5. 11 Linear fitting result for curve of current density versus scan rate in Figure 5.21

Sample label	a	b(slope)	Confidence number
CPA PEO/LiAlO ₂ /AC	0.65	0.06	0.97
CPAI PEO/LiAlO ₂ /AC/NaI/I ₂	7.94	0.16	0.99
PC PEO/LiTFS/AC	5.42	0.21	0.999
PCI PEO/LiTFS/AC/NaI/I ₂	15.76	0.27	0.99

Figures 5.12 to Figure 5.15 illustrate the CV curves for potential scan rates from 20-200 mV/s. The relationship between the scan rate and the maximum current density are illustrated in Figure 5.21. The data points in Figure 5.21 are fitted

using a linear equation $y=a+bx$ and the fitting results are listed in Table 5.11. The confidence for each fitting is about 99%. Thus for the range of scan rates of supercapacitors, the current can be described by:

$$I = \frac{dQ}{dt} = v \frac{dQ}{dE} = vC \quad (5.3)$$

where I is the maximum current density, v is the scan rate, dQ , dt , and dE are the differentials of charge, time, and potential. The charge current is a constant when the scan rate is given and is proportional to the scan rate, which is typical for an EDLC. It is unusual for a supercapacitor with pseudocapacitance to behave like an EDLC [19]. This is considered a benefit of pseudocapacitors including RuO_2 supercapacitors.

5.7 Conclusions

PEO/LiX/AC-Nafion-PEO/LiX/AC ($X=\text{AlO}_2^-$, ClO_4^- and CF_3SO_3^-) supercapacitors were fabricated by PEO/LiX/AC ($X=\text{AlO}_2^-$, ClO_4^- and CF_3SO_3^-) suspension depositing on carbon paper, then by assembling two identical electrodes on both side of Nafion 117 membrane. Effects of anions, mediator, fillers, and scan rate on the electrochemical performance of supercapacitors were studied. The cell resistance, specific capacitance, specific power, specific energy,

and cycle stability of PEO electrolyte based all-solid state supercapacitors were evaluated via EIS, CV, and galvanostatic charge/discharge methods, respectively.

The specific capacitance and specific power follow the order of $\text{PEO/LiAlO}_2/\text{AC} < \text{PEO/LiClO}_4/\text{AC} < \text{PEO/LiTFS}/\text{AC}$. The addition of filler in electrode material in the PEO electrolyte in the can increase the specific capacitance and specific power of the supercapacitors. However, the performance improvement can be achieved by varying lithium salt and the addition of filler is not significant.

With the addition of NaI/I_2 mediator, the specific capacitance increased more than 30 fold, specific power increased almost 20 fold, and specific energy increased around 10 fold. The stability of the corresponding supercapacitor is good within 2000 cycles. More than 90% of the original specific capacitance is maintained up to 2000 charge/discharge cycle. Further additions of filler to the electrodes with mediator can double the specific capacitor and specific power of the all-solid state supercapacitor. The addition of mediator not only increases the conductivity of the supercapacitor, but also provides the supercapacitor with pseudocapacitance. The specific capacitance of pseudocapacitance is around 30-50

fold greater than the electric double layer capacitance.

The ionic conductivity plays a major role in charge/discharge process. However, high ionic conductivity of electrolytes in the electrode material can enable a high discharge rate, or high power. A high conductivity in the PEO electrolyte with mediator is an indication of a high electron exchange rate between the mediator and mediator. The high electron exchange rates at mediator carbon interfaces and between mediator and mediator are essential to obtain a high response rate and high power.

REFERENCES

- [1] H. E. Becker, U.S. Patent 2 800 616 (1957)
- [2] G. V. Lagodzinskaya, N. G. Yunda, and G. B. Manelis, Labile supramolecular structures and their dynamics in associated liquids based on NMR data, *Russ.Chem.Bull., Int.Ed.*, 55 (2006) 597-623
- [3] Y. M. Volkovich, T. M. Serdyuk, Electrochemical capacitors, *Russian J. Electrochem.*, 38 (2002) 935–958
- [4] K. Chang, C. Hu, Textural and pseudocapacitive characteristics of sol–gel derived $\text{RuO}_2 \cdot x\text{H}_2\text{O}$: Hydrothermal annealing vs. annealing in air, *Electrochim. Acta*, 54 (2009) 978-983
- [5] B. Kumar, S. J. Rodrigues, S. Koka, The crystalline to amorphous transition in PEO-based composite electrolytes: role of lithium salts, *Electrochim. Acta*, 47 (2002) 4125-4131
- [6] M. Marzantowicz, J.R. Dygas, F. Krok, A. Łasińska, Z. Florjańczyk, E. Zygadło-Monikowska, A. Affek, *Electrochimica Acta*, 50 (2005) 3969-3977
- [7] I. Ruff and V.J. Friedrich, Transfer Diffusion. I. Theoretical, *J. Phys. Chem.*, 75 (1971) 3297-3302
- [8] I. Ruff, V.J. Friedrich, K. Demeter, and K. Caillag, Transfer diffusion II. kinetics of exchange reaction between ferrocene and ferricinium ion in alcohols, *J. Phy. Chem.*, 75 (1971) 3303-3309
- [9] D. Baril, M. Michot, and M. Armand, Electrochemistry of liquids vs. solids: polymer electrolytes, *Solid State Ionics*, 94 (1997) 35-47
- [10] R. Kötz, M. Carlen, Principles and applications of electrochemical capacitors, *Electrochim. Acta*, 45 (2000) 2483–2498
- [11] M. Winter, R. J. Brodd. What are batteries, fuel cells and supercapacitors? *Chem. Rev.*, 104(2004) 4245–4269.
- [12] A. Schneuwly, R. Gallay, Properties and applications of supercapacitors from the state-of-the-art to future trends, *PCIM Proceedings Europe Official Proceedings of the Forty-First International Power Conversion Conference (2000)* 115
- [13] S. G. Ekhanin, N. S. Nesmelov, I. V. Sveshnikov and L. Yu. Soldatova, Study of the spectral properties of alkali halide electroluminescence with plasma electrodes, *Russ. Phys. J.*, 40 (1997) 920-923
- [14] CAP-XX, Energy Storage Technologies: A Comparison, Articles and Reviews

- [15] Stanley Atcitty, Electrochemical Capacitor Characterization for Electric Utility Applications. Doctoral Dissertation, (2006)
- [16] T.C. Murphy, W.E. Kramer, Proceedings of the 4th International seminar on double layer capacitors and similar energy storage devices, Florida Educational Seminar, (1994)
- [17] M. Bärtsch, A. Braun, B. Schnyder, R. Kötz, O. Haas, Bipolar glassy carbon electrochemical double-layer capacitor: 100,000 cycles demonstrated, *J. New Mater. Electrochem. Sys.*, 2 (1999) 273-277
- [18] B. E. Conway, Transition from "Supercapacitor" to "Battery" behavior in electrochemical energy storage, *J. Electrochem. Soc.*, 138(1991) 1539-1548
- [19] B. E. Conway, Electrochemical supercapacitors, scientific fundamental and technological applications, Plenum Publishers (1999)
- [20] S. Sarangapani, B.V. Tilak, C. P. Chen, Materials for electrochemical capacitors theoretical and experimental constraints, *J. Electrochem. Soc.*, 143(1996) 3791-3799
- [21] T. C. Murphy, R. B. Wright, R. A. Sutula, in: F. M. Delnick, D. Ingersoll, X. Andrieu, K. Naoi, Electrochemical capacitors II, proceedings, The Electrochem. Soc., Pennington (1997)
- [22] C. Emmenegger, Ph. Mauron, P. Sudan, P. Wenger, V. Herman, R. Gallay, A. Zuttel; Investigation of Electrochemical Double Layer (ECDL) capacitors electrodes based on carbon nanotubes and activated carbon materials, *J. Power Sources*, 124 (2003) 321-329
- [23] R. J. Hunter, Foundations of colloid science, Oxford Univ. Press, Oxford (1989)
- [24] A. J. Bard, L. R. Faulkner, Electrochemical methods: fundamentals and applications, John Wiley & Sons, USA (2000)
- [25] C. M. Brett, A. M. O. Brett, Electrochemistry principles, methods and applications, Oxford Univ. Press, Oxford (1993)
- [26] J. O. Bockris, A. K. N. Reddy, M. Gamboa-Aldeco, Modern electrochemistry 2A: fundamentals of electrochemistry, Plenum Press, New York (2000)
- [27] J. Evans, C. A. Vincent, and P. G. Bruce, Electrochemical measurement of transference numbers in polymer electrolytes, *Polym.*, 28 (1987) 2324-2328
- [28] R. G. Linford, Electrical and electrochemical properties of ion conducting polymers, in Applications of Electroactive Polymers, Chapman & Hall, London, UK (1993)

- [29] S. Vorrey, D. Teeters, Study of the ion conduction of polymer electrolytes confined in microand nanopores, *Electrochim. Acta*, 48 (2003) 2137-2141
- [30] C. Bishop, Dale Teeters, Crystallinity and order of poly(ethylene oxide)/lithium triflate complex confined in nanoporous membranes, *Electrochim. Acta*, 54 (2009) 4084–4088
- [31] M. Marzantowicz, J. R. Dygas, F. Kroka, A. Tomaszewska, Z. Florjan'czyk, E. Zygadło-Monikowska, G. Lapienis, Star-branched poly(ethylene oxide) LiN(CF₃SO₂)₂: A promising polymer electrolyte, *J. Power Sources*, 194 (2009)51-57
- [32] G. D. Smith, R. L. Jaffe, D. Y. Yoon, A force-field for simulations of 1,2-dimethoxyethane and poly(oxyethylene) based upon ab-initio electronic-structure calculations on model molecules. *J. Phy. Chem.*, 97(1993) 12752-12759
- [33] M. Krishnan, S. Balasubramanian, Order-disorder transitions and melting in a helical polymer crystal: molecular dynamics calculations of model poly(ethylene oxide), *Chem. Phy. Lett.*, 385 (2004) 351-356
- [34] A. M. Stephan, Review on gel polymer electrolytes for lithium batteries, *Eur. Polym. J.*, 42 (2006) 21-42
- [35] W. Wieczorek, A. Zalewska, B. Raducha, Z. Florjańczyk, J.R. Stevens, Composite polyether electrolytes with lewis acid type additives, *J. Phys. Chem.*, 102 (1998) 352-360
- [36] L. Edman, A. Ferry and M.M. Doeff, Slow recrystallization in the polymer electrolyte system poly(ethylene oxide)_n-LiN(CF₃SO₂)₂, *J. Mater. Res.*, 15 (2000) 1950-1954
- [37] D. Golodnitsky, E. Livshits, Yu. Rosenberg, E. Peled, S.H. Chung, Y. Wang, S. Bajue, S. G. Greenbaum, A new approach to the understanding of ion transport in semicrystalline polymer electrolytes, *J. Electroanal. Chem.*, 491 (2000) 203–210
- [38] W. Lu, K. Henry, C. Turchi, J. Pellegrino, Incorporating ionic liquid electrolytes into polymer gels for solid-state ultracapacitors, *J. Electrochem. Soc.*, 155 (2008) A361-A367
- [39] A. Balducci, R. Dugas, P.L. Taberna, P. Simon, D. Plee, M. Mastragostino, S. Passerini, High temperature carbon-carbon supercapacitor using ionic liquid as electrolyte, *J. Power Sources*, 165 (2007) 922-927
- [40] J. H. Shin, W. A. Henderson, S. Passerini, Ionic liquids to the rescue? Overcoming the ionic conductivity limitations of polymer electrolytes, *Electrochem. Commun.*, 5 (2003) 1016-1020

- [41] M. Ue, M. Takeda, A. Toriumi, A. Kominato, R. Hagiwara, Y. Ito, Application of low-viscosity ionic liquid to the electrolyte of double-layer capacitors, *J. Electrochem. Soc.*, 150 (2003) A499-A502
- [42] P. Taberna, G. Chevallier, P. Simon, D. Plée, T. Aubert, Activated carbon–carbon nanotube composite porous film for supercapacitor applications, *Mater. Resear. Bull.*, 41 (2006) 478-484
- [43] S. Panero, A. Clemente, E. Spila, Solid state super capacitors using gel membranes as electrolytes, *Solid State Ionics*, 86-88 (1996) 1285-1289
- [44] A. Yamada, J. B. Goodenough, Keggin-Type heteropolyacids as electrode materials for electrochemical supercapacitors, *J. Electrochem. Soc.*, 145 (1998) 737-743
- [45] K. W. Park, H. J. Ahn; Y. E. Sung, All-solid-state supercapacitor using a Nafion(R) polymer membrane and its hybridization with a direct methanol fuel cell, *J. Power Sources*, 109 (2002) 500-506
- [46] P. Sivaraman, S. K. Rath, V. R. Hande, A. P. Thakur, M. Patri, A. B. Samui, All-solid-supercapacitor based on polyaniline and sulfonated polymers, *Synt. Metals*, 156 (2006) 1057–1064
- [47] F. Lufrano, P. Stati, Performance improvement of Nafion based solid state electrochemical supercapacitor, *Electrochimica Acta*, 49 (2004) 2683-2689
- [48] K. Ryu, Y. Hong, Y. J. Park, X. Wu, K. M. Kim, Y. Lee, S. H. Chang, S. J. Lee, Polyaniline doped with dimethylsulfate as a polymer electrode for all solid-state power source system, *Solid State Ionics*, 175 (2004) 759-763
- [49] Y.S. Yoon, W. I. Cho, J. H. Lim, D. J. Choi, Solid-state thin-film supercapacitor with ruthenium oxide and solid electrolyte thin films, *J. Power Sources*, 101 (2001) 126-129
- [50] Y. Wang, X. Zhang, All solid-state supercapacitor with phosphotungstic acid as the proton-conducting electrolyte, *Solid State Ionics*, 166 (2002) 61-67
- [51] A. White, R. Slade, Polymer electrodes doped with heteropolymetallates and their use within solid-state supercapacitors, *Synt. Metals*, 139 (2003) 123-131
- [52] A. Yamada, J. B. Goodenough, Keggin-Type Heteropolyacids as electrode materials for electrochemical supercapacitors, *J. Electrochem. Soc.*, 145 (1998) 737-743
- [53] K. W. Park, H. J. Ahn; Y. E. Sung, All-solid-state supercapacitor using a Nafion(R) polymer membrane and its hybridization with a direct methanol fuel cell, *J. Power Sources*, 109 (2002) 500-506
- [54] Y. Wang, Recent research progress on polymer electrolytes for dye-sensitized solar cells, *Sol. Energy Mater. Sol. Cells*, 93 (2009)1167-1175

- [55] F. B. Dias, L. Plomp, J. B. J. Veldhuis, Trends in polymer electrolytes for secondary lithium batteries, *J. Power Sources*, 88 (2000) 169-191
- [56] D. E. Fenton, J. M. Parker, P. V. Wright, Complexes of alkali metal ions with poly(ethylene oxide), *Polymer*, 14 (1973) 589
- [57] G. B. Appetecchi, F. Croce, B. Scrosati, High-performance electrolyte membranes for plastic lithium batteries, *J. Power Sources*, 66 (1997) 77-82
- [58] G. B. Appetecchi, G. Dautzenberg, B. Scrosati, A new class of advanced polymer electrolytes and their relevance in plastic-like, rechargeable lithium batteries, *J. Electrochem. Soc.*, 143 (1996) 6-12
- [59] M. B. Armand, J. M. Chabagno, and M. Duclot, Second international meeting on solid electrolytes, extended abstract, St. Andrews, Scotland (1978)
- [60] J. R. MacCallum and C. A. Vincent, *Polymer Electrolyte Reviews-2*, Elsevier Applied Science, London, UK (1989)
- [61] C. Berthier, W. Gorecki, M. Minier, M. B. Armand, J. M. Chabagno, P. Rigaud, Microscopic investigation of ionic conductivity in alkali-metal salts poly(ethylene oxide) adducts, *Solid State Ionics*, 11 (1983) 91-95
- [62] W. Wiczorek, J. R. Stevens, Impedance spectroscopy and phase structure of polyether-poly(methyl methacrylate)-LiCF₃SO₃ blend-based electrolytes, *J. Phys. Chem. B*, 101 (1997) 1529-1534
- [63] Y. Ito, K. Kanehori, K. Miyauchi, and T. Kudo, Ionic conductivity of electrolytes formed from PEO-LiCF₃SO₃ complex with low molecular weight poly(ethylene glycol), *J. Mater. Sci.*, 22 (1987) 1845-1849
- [64] J. F. LeNest, S. Callens, A. Gandini, and M. Armand, New polymer network for ionic conduction, *Electrochim. Acta*, 37 (1992) 1585-1588
- [65] Z. Wang, B. Huang, H. Huang, R. Xue, L. Chen, and F. Wang, A vibrational spectroscopic study on the interaction between lithium salt and ethylene carbonate plasticizer for PAN-based electrolytes, *J. Electrochem. Soc.*, 143 (1996) 1510-1514
- [66] F. Croce, S. D. Brown, S. G. Greenbaum, S. M. Slane, and M. Salomon, Lithium-7 NMR and ionic conductivity studies of gel electrolytes based on poly(acrylonitrile), *Chem. Mater.*, 5 (1993) 1268-1272
- [67] D. Peramunage, D. M. Pasquariello, and K. M. Abraham, Polyacrylonitrile-based electrolytes with ternary solvent mixtures as plasticizers, *J. Electrochem. Soc.*, 142 (1995) 1789-1798

- [68] H. S. Choe, B. G. Carroll, D. M. Pasquariello, and K. M. Abraham, Characterization of some polyacrylonitrile-based electrolytes, *Chem. Mater.*, 9 (1997) 369-379
- [69] G. Dautzenberg, F. Croce, S. Passerini, and B. Scrosati, Characterization of PAN-based gel electrolytes. Electrochemical stability and lithium cyclability, *Chem. Mater.*, 6 (1994) 538-542
- [70] B. Huang, Z. Wang, G. Li, H. Huang, R. Xue, and L. Chen, Lithium ion conduction in polymer electrolytes based on PAN, *Solid State Ionics*, 85 (1996) 79-84
- [71] Z. Wang, B. Huang, R. Xue, X. Huang, L. Chen, Spectroscopic investigation of interactions among components and ion transport mechanism in poly-acrylonitrile based electrolytes, *Solid State Ionics*, 121 (1999) 141-156
- [72] K. M. Abraham, H. S. Choe, D. M. Pasquariello, Polyacrylonitrile electrolyte-based Li ion batteries, *Electrochim. Acta*, 43 (1998) 2399-2412
- [73] O. Bohnke, G. Frand, M. Rezrazi, C. Rousselot, C. Truche, Fast ion transport in new lithium electrolytes gelled with PMMA. 2. Influence of lithium salt concentration, *Solid State Ionics*, 66 (1993) 105-112
- [74] E. Quartarone, C. Tomasi, P. Mustarelli, G. B. Appetecchi, F. Croce, Long-term structural stability of PMMA-based gel polymer electrolytes, *Electrochim. Acta*, 43 (1998) 1435-1439
- [75] T. Iijima, Y. Toyoguchi, N. Eda, Quasi-solid organic electrolytes gelatinized with polymethyl-methacrylate and their applications for lithium batteries, *Denki Kagaku*, 53 (1985) 619-623
- [76] O. Bohnke, G. Frand, M. Rezrazi, C. Rousselot, C. Truche, Fast ion transport in new lithium electrolytes gelled with PMMA. 1. Influence of polymer concentration, *Solid State Ionics*, 66 (1993) 97-104
- [77] G. Pistoia, A. Antonini, and G. Wang, Impedance study on the reactivity of gel polymer electrolytes towards a lithium electrode, *J. Power Sources*, 58 (1996) 139-144
- [78] M. Alamgir and K. M. Abraham, U.S. Patent 5,252,413 (1993)
- [79] M. Alamgir and K. M. Abraham, Li ion conductive electrolytes based on poly(vinyl chloride), *J. Electrochem. Soc.*, 140 (1993) L96-L97
- [80] S. Rajendran, Experimental investigations on PVC-LiAsF₆-DBP polymer electrolyte systems, *J. Power Sources*, 87 (2000) 218-222
- [81] Y. Wang, C. Wan, H. Y. Sung, U.S. Patent 5,874,185 (1999)

- [82] H. Sung, Y. Wang, C. Wan, Preparation and characterization of poly(vinyl chloride-co-vinyl acetate)-based gel electrolytes for Li-ion batteries, *J. Electrochem. Soc.*, 145 (1998) 1207-1211
- [83] A. M. Suresh, A. Nishimoto, M. Watanabe, Transport and electro-chemical characterization of plasticized poly(vinyl chloride) solid electrolytes, *Solid State Ionics*, 86-88, (1996) 385-393
- [84] K. Tsunemi, H. Ohno, E. Tsuchida, A mechanism of ionic-conduction of poly(vinylidene fluoride)-lithium perchlorate hybrid films, *Electrochim. Acta*, 28 (1983) 833-837
- [85] Z. Jiang, B. Carroll, and K. M. Abraham, Studies of some poly(vinylidene fluoride) electrolytes, *Electrochim. Acta*, 42 (1997) 2667-2677
- [86] P. Periasamy, K. Tatsumi, M. Shikano, T. Fujieda, T. Sakai, Y. Saito, M. Mizuhata, A. Kajinami, and S. Deki, An electrochemical investigation on poly(vinylidene fluoride)-based gel polymer electrolytes, *Solid State Ionics*, 126 (1999) 285-292
- [87] G. B. Appetecchi, F. Croce, A. De Paolis, B. Scrosati, A poly(vinylidene fluoride)-based gel electrolyte membrane for lithium batteries, *J. Electroanal. Chem.*, 463 (1999) 248-252
- [88] P. Mustarelli, E. Quartarone, C. Capiglia, C. Tomasi, A. Magistris, Cation dynamics in PVdF-based polymer electrolytes, *Solid State Ionics*, 122 (1999) 285-289
- [89] T. Michot, A. Nishimoto, M. Watanabe, Electrochemical properties of polymer gel electrolytes based on poly(vinylidene fluoride) copolymer and homopolymer, *Electrochim. Acta*, 45 (2000) 1347-1360
- [90] B. Lin, P.T. Boinske, J.W. Halley, A molecular dynamics model of the amorphous regions of polyethylene oxide, *J. Chem. Phys.*, 105 (1996) 1668-1681
- [91] N. Kobayashi, M. Uchiyama and E. Tsuchida. Poly[lithium methacrylate-co-oligo(oxyethylene)methacrylate] as a solid electrolyte with high ionic conductivity, *Solid State Ionics*, 17 (1985) 307-311
- [92] K. Ito, N. Nishina and H. Ohno, High lithium ionic conductivity of poly(ethylene oxide)s having sulfonate groups on their chain ends, *J. Mat. Chem.*, 7 (1997) 1357-1362
- [93] K. Ito, Y. Tominaga, H. Ohno, Polyether/salt hybrid (IV). Effect of benzenesulfonate group(s) and PEO molecular weight on the bulk ionic conductivity, *Electrochim. Acta*, 42 (1997) 1561-1570
- [94] H. Kim, J. Park. Effects of cations on ionic states of poly(oligo-oxyethylene methacrylate-co-alkali metal acrylamidocaproate) single-ion conductor, *Solid State Ionics*, 98 (1997) 237-244

- [95] H. Liang, X. Qiu, S. Zhang, W. Zhu, L. Chen, Study of lithiated Nafion ionomer for lithium batteries, *J. Appl. Electrochem.* 34 (2004) 1211–1214
- [96] Z. Lu, G. Polizos, D. Macdonald, E. Manias, State of water in perfluorosulfonic Ionomer (Nafion 117) proton exchange membranes, *J. Electrochem. Soc.*, 155 (2008) B163-B171
- [97] S. B. Ross-Murphy, Formation, structure and properties of physical networks. R.F.T. Stepto, Editor, *Polymer networks: principles of their formation, structure and properties*, Blackie Academic & Professional, New York (1992)
- [98] Y. Wang, J. Travas-Sejdic and R. Steiner, Polymer gel electrolyte supported with microporous polyolefin membranes for lithium ion polymer battery, *Solid State Ionics*, 148 (2002) 443-449
- [99] L. H. Sperling, *Introduction to physical polymer science*, Chap. 9, Wiley, New York, (1993)
- [100] H. Ohno, H. Matsuda, K. Mizoguchi, E. Tsuchida, Demonstration of solid-state cell based on poly(vinylidene fluoride) system containing lithium perchlorate, *Polym. Bull.*, 7 (1982) 271-275
- [101] R. Davidson, M. Sittig, *Water Soluble Resins*, Reinhold publishing Corporation, New York (1962)
- [102] A. Ferry, P. Jacobsson, J. D. Van Heuman, J. R. Stevens, Raman, infra-red and d.s.c. studies of lithium coordination in a thermoplastic Polyurethane, *Polymer*, 37 (1996) 737-744
- [103] H. Huang, L. Chen, X. Huang and R. Xue, Studies on PAN-based lithium salt complex, *Electrochim. Acta*, 37 (1992) 1671-1673
- [104] M. Wang, L. Qi, F. Zhao, S. Dong, A novel comb-like copolymer based polymer electrolyte for Li batteries, *J. Power Sources*, 139 (2005) 223-229
- [105] Z. Gadjourova, D. M. Marero, K. H. Andersen, Y. G. Andreev, P. G. Bruce, Structures of the Polymer Electrolyte Complexes $\text{PEO}_6:\text{LiXF}_6$ ($X = \text{P, Sb}$), Determined from Neutron Powder Diffraction Data, *Chem. Mater.*, 13 (2001) 1282–1285
- [106] F. M. Gray, *Solid polymer electrolytes: fundamentals and technological applications*, Scotland, UK: VIH Publishers, Inc. (1991)
- [107] J. A. Faucher, Glass transitions of ethylene oxide polymers. *J. Appl. Phys.*, 37 (1966) 3962-3964
- [108] F. M. Gray, *Polymer Electrolytes*, The Royal Society of Chemistry, Cambridge (1997)

- [109] G. L. Gutsev, A. I. Boldyrev, DVM- $X\alpha$ calculations on the ionization potentials of MX_{k+1}^- complex anions and the electron affinities of MX_{k+1} “superhalogens”, *Chem. Phys.*, 56 (1981) 277-283
- [110] I. Honma, Y. Takeda, J. M. Bae, Protonic conducting properties of sol-gel derived organic / inorganic nanocomposite membranes doped with acidic functional molecules, *Solid State Ionics*, 120 (1999) 255–264
- [111] C. Shen, J. Wang, Z. Tang, H. Wang, H. Lian, J. Zhang, C. Cao, Physicochemical properties of poly(ethylene oxide)-based composite polymer electrolytes with a silane-modified mesoporous silica SBA-15, *Electrochim. Acta*, 54 (2009) 3490–3494
- [112] P. C. Barbosa, M. M. Silva, M. J. Smith, A. Goncalves, E. Fortunato, Studies of solid-state electrochromic devices based on PEO/siliceous hybrids doped with lithium perchlorate, *Electrochim. Acta*, 52 (2007) 2938–2943
- [113] R. A. Zoppi, M. C. Goncalves, Preparation and characterization of polymeric electrolytes constituted by poly(ethylene oxide), sol–gel silica and lithium perchlorate, *Solid State Ionics*, 147 (2002) 157–170
- [114] Y. Wang, Recent research progress on polyelectrolytes for dye-sensitized solar cells, *Sol. Energy Mater. Sol. Cells*, 93 (2009) 1167-1175
- [115] L. Wang, W. Yang, J. Wang, D. G. Evans, New nanocomposite polymer electrolyte comprising nanosized $ZnAl_2O_4$ with a mesopore network and PEO- $LiClO_4$, *Solid State Ionics*, 180 (2009) 392–397
- [116] T. Yajima, US Patent 5672437 (1997)
- [117] G. D. Smith, R. L. Jaffe, D. Y. Yoon, A force-field for simulations of 1,2-dimethoxyethane and poly(oxyethylene) based upon ab-initio electronic-structure calculations on model molecules. *J. Phy. Chem.*, 97(1993) 12752-12759
- [118] M. Krishnan, S. Balasubramanian, Order-disorder transitions and melting in a helical polymer crystal: molecular dynamics calculations of model poly(ethylene oxide), *Chem. Phys. Lett.*, 385 (2004) 351-356
- [119] D. Golodnitsky, G. Ardel, E. Strauss, E. Peled, Y. Lareah, Y. Rosenberg, Conduction Mechanisms in Concentrated LiI -Polyethylene Oxide- Al_2O_3 -Based Solid Electrolytes, *J. Electrochem. Soc.*, 144 (1997) 3484-3491
- [120] C. D. Robitaille, D. Fauteux, Phase diagrams and conductivity characterization of some PEO- LiX electrolytes, *J. Electrochem. Soc.*, 133 (1986) 315-325
- [121] Z. Tao, Molecular Dynamics simulation study of PEO-based polymer electrolytes, Doctoral Thesis, Chemical Engineering, Nashville, Tennessee (05-2008)

- [122] H. Malmberg, Nanoscientific investigations of electrode materials for supercapacitors, Doctoral Thesis, KTH School of Chemical Science and Engineering, SWEDEN, (2007)
- [123] Y. Tominaga, N. Takizawa, H. Ohno, Effect of added salt species on the ionic conductivity of PEO/sulfonamide salt hybrids, *Electrochim. Acta*, 45 (2000) 1285-1289
- [124] W. Wiczorek, A. Zalewska, B. Raducha, Z. Florjańczyk and J. R. Stevens, Composite polyether electrolytes with lewis acid type additives, *J. Phys. Chem.*, 102 (1998) 352-360
- [125] Y. Geng, X. Wang, W. Chen, Q. Cai, C. Nan, H. Li, Synthesis, characterization and application of novel bicontinuous mesoporous silica with hierarchical pore structure, *Mater. Chem. Phys.*, 116 (2009) 254-260
- [126] L. Fan, C. Nan, S. Zhao, Effect of modified SiO₂ on the properties of PEO-based polymer electrolytes, *Solid State Ionics*, 164 (2003) 81-86
- [127] B. K. Choi, Optical microscopy study on the crystallization in PEO-salt polymer electrolytes, *Solid State Ionics*, 168 (2004) 123-129
- [128] B. K. Choi, Y. W. Kim, Conductivity relaxation in the PEO-salt polymer electrolytes, *Electrochim. Acta*, 49 (2004) 2307
- [129] C. J. Hawker, F. Chu, P. J. Pomery, D. Hill, Hyperbranched poly(ethylene glycol)s: A new class of ion-conducting materials, *Macromol.*, 29 (1996) 3831-3838
- [130] M. Watanabe, T. Endo, A. Nishimoto, K. Miura, M. Yanagid, High ionic conductivity and electrode interface properties of polymer electrolytes based on high molecular weight branched polyether, *J. Power Sources*, 81-82 (1999) 786-789
- [131] A. G. Ruzette, P. P. Soo, D. R. Sadoway, A. M. Mayes, Melt-Formable block copolymer electrolytes for lithium rechargeable batteries, *J. Electrochem. Soc.*, 148 (2001) A537-A543
- [132] P. P. Soo, B. Huang, Y. Jang, Y. Chiang, D. R. Sadoway, A. M. Mayes, Rubbery block copolymer electrolytes for solid-state rechargeable lithium batteries, *J. Electrochem. Soc.*, 146 (1999) 32-37
- [133] K. Inoue, H. Miyamoto, T. Itaya, Ionic conductivity of complexes of novel multiarmed polymers with phosphazene core and LiClO₄, *J. Polym. Sci. Polym. Chem.*, 35 (1997) 1839-1847
- [134] S. H. Chung, Y. Wang, S. G. Greenbaum, D. Golodnitsky, E. Peled, Uniaxial stress effects in poly(ethylene oxide)-LiI polymer electrolyte film A ⁷Li nuclear magnetic resonance study, *Electrochem. Solid State Lett.*, 2 (1999) 553-555

- [135] C. D. Robitaille, D. Fauteux, Phase diagrams and conductivity characterization of some PEO-LiX electrolytes, *J. Electrochem. Soc.*, 133 (1986) 315-325
- [136] D. Golodnitsky, E. Livshits, Y. Rosenberg, E. Peled, S.H. Chung, Y. Wang, S. Bajue, S. G. Greenbaum, A new approach to the understanding of ion transport in semicrystalline polymer electrolytes, *J. Electroanal. Chem.*, 491 (2000) 203–210
- [137] G. B. Appetecchi, F. Croce, J. Hassoun, B. Scrosati, M. Salomon, F. Cassel, Hot-pressed, dry, composite, PEO-based electrolyte membranes: I. Ionic conductivity characterization, *J. Power Sources*, 114 (2003) 105-112
- [138] G. B. Appetecchi, J. Hassoun, B. Scrosati, F. Croce, F. Cassel, M. Salomon, Hot-pressed, solvent-free, nanocomposite, PEO-based electrolyte membranes: II. All solid-state Li/LiFePO₄ polymer batteries, *J. Power Sources*, 124 (2003) 246-253
- [139] V. Danel, J. Flipo, X. Andrieu, B. Pichon, S. Barusseau, US Patent 6356432 (2002)
- [140] Y. Zhang, H. Feng, X. Wu, L. Wang, A. Zhang, T. Xia, H. Dong, X. Li, L. Zhang, Progress of electrochemical capacitor electrode materials: A review, *Int. J. Hydrogen Energy*, 34 (2009) 4889–4899
- [141] E. Frackowiak, F. Be'guin, Carbon materials for the electrochemical storage of energy in capacitors, *Carbon*, 39 (2001) 937–950
- [142] D. Qu, H. Shi, Studies of activated carbons used in double-layer capacitors, *J. Power Sources*, 74 (1998) 99–107
- [143] X. Andrieu, L. Josset, Proceedings of the Symposium on Electrochemical Capacitors, PV 95-29, *Electrochem. Soc.*, Pennington, (1997) 181-186
- [144] H. Shi, Activated carbons and double layer capacitance, *Electrochim. Acta*, 40(1996) 1633-1639
- [145] Y. Su, Y. Niu, Y. Xiao, M. Xiao, Z. Liang, K. Gong, Novel conducting polymer poly[bis(phenylamino)disulfide]: Synthesis, characterization, and properties, *J. Poly. Sci., Part A: Poly. Chem.*, 42 (2004) 2329-2339
- [146] C. Arbizzani, M. Mastragostino, L. Meneghello. Polymer-based redox supercapacitors: A comparative study, *Electrochim. Acta*, 41 (1996) 21-26
- [147] K. Naoi, Extended Abstracts, 49th Annual Meeting of the International Society of Electrochemistry, Kitakyushu, Japan (1998) 647
- [148] S. Trasatti, G. Lodi, in: S. Trasatti, *Electrodes of Conducting Metallic Oxides*, part B, Elsevier, Amsterdam, Chapter 10 (1981)
- [149] J. P. Zheng, T. R. Jow, A new charge storage mechanism for electrochemical capacitor, *J. Electrochem. Soc.*, L6 (1995) 142–145

- [150] S. Ardizzone, G. Fregonara, S. Trasatti, "Inner" and "outer" active surface of RuO₂ electrodes, *Electrochim. Acta*, 35 (1990) 263-267
- [151] R. Kötz, S. Stucki, Ruthenium dioxide as a hydrogen-evolving cathode, *J. Appl. Electrochem.*, 17 (1987) 1190-119
- [152] S. Trasatti and P. Kurzweil. Electrochemical supercapacitors as versatile energy stores, *Platinum Met. Rev.*, 38 (1994) 46-56
- [153] F. J. Liu, T. F. Hsu, C. H. Yang, Construction of composite electrodes comprising manganese dioxide nanoparticles distributed in polyaniline-poly(4-styrene sulfonic acid-co-maleic acid) for electrochemical supercapacitor, *J. Power Sources*, 191 (2009) 678-683
- [154] K. Lee, J. Lee, N. Wu, Electrochemical characterizations on MnO₂ supercapacitors with potassium polyacrylate and potassium polyacrylate-co-polyacrylamide gel polymer electrolytes, *Electrochim. Acta*, 54 (2009) 6148-6153
- [155] T.C. Liu, W.G. Pell, B.E. Conway, S.L. Roberson, Behavior of molybdenum nitrides as materials for electrochemical capacitors, *J. Electrochem. Soc.*, 145 (1998) 1882-1888
- [156] N. L. Wu. Nanocrystalline oxide supercapacitors, *Mater. Chem. & Phys.*, 75 (2002) 6-11
- [157] S. Wang, K. Ho, S. Kuo, N. Wu, Investigation on capacitance mechanisms of Fe₃O₄ electrochemical capacitors, *J. Electrochem. Soc.*, 153 (2006) A75-A80
- [158] P. Staiti, F. Lufrano, Study and optimisation of manganese oxide-based electrodes for electrochemical supercapacitors, *J. Power Sources*, 187 (2009) 284-289
- [159] J. A Dean.. *The Analytical Chemistry Handbook*. New York: McGraw Hill, Inc. (1995) 15.1-15.5
- [160] Y. Lin, H. Li, C. Liu, W. Xing, X. Ji, Surface-modified Nafion membranes with mesoporous SiO₂ layers via a facile dip-coating approach for direct methanol fuel cells, *J. Power Sources*, 185 (2008) 904-908
- [161] M. Le Granvalet-Mancini, T. Hanrath, D. Teeters, Characterization of the passivation layer at the polymer electrolyte/lithium electrode interface, *Solid State Ionics*, 135 (2000) 283-290
- [162] S. Ramesh, T. F. Yuen, C. J. Shen, Conductivity and FTIR studies on PEO-LiX [X: CF₃SO₃⁻, SO₄²⁻] polymer electrolytes, *Spectrochim. Acta: Part A*, 69 (2008) 670-675
- [163] Y. Wu, C. Wu, F. Yu, T. Xu, Y. Fu, Free-standing anion-exchange PEO-SiO₂ hybrid membranes, *J. Membr. Sci.*, 307 (2008) 28-36

- [164] M. Dissanayake, R. Frech, Infrared spectroscopic study of the phases and phase-transitions in poly(ethylene oxide) and poly(ethylene oxide)-lithium trifluoromethanesulfonate complexes, *Macromol.*, 28(1995) 5312-5319
- [165] S. Pavlidou, C. D. Papaspyrides, A review on polymer-layered silicate nanocomposites, *Prog. Polym. Sci.* 33 (2008) 1119–1198
- [166] Z. S. Mo, K.B. Lee, Y.B. Moon, M. Kobayashi, A.J. Heeger, F. Wudl, X-ray scattering from poly(thiophene): crystallinity and crystallographic structure, *Macromol.*, 18 (1985)1972-1977
- [167] Y. G. Andreev, P. Lightfoot and P. G. Bruce, Structure of the polymer electrolyte poly(ethylene oxide)₃: LiN(SO₂CF₃)₂ determined by powder diffraction using a powerful Monte Carlo approach, *Chem. Commun.*, 18 (1996) 2169-2170
- [168] S. Kim, E. J. Hwang, S. J. Park, An experimental study on the effect of mesoporous silica addition on ion conductivity of poly(ethylene oxide) electrolytes, *Curr. Appl. Phys.* 8 (2008) 729–731
- [169] K. Hanai, T. Maruyama, N. Imanishi, A. Hirano, Y. Takeda and O. Yamamoto, Enhancement of electrochemical performance of lithium dry polymer battery with LiFePO₄/carbon composite cathode, *J. Power Sources*, 178 (2008) 789–794
- [170] P. B. Bhargav, V. M. Mohan, A. K. Sharma, V. Rao, Investigations on electrical properties of (PVA:NaF) polymer electrolytes for electrochemical cell applications, *Curr. Appl. Phys.*, 9 (2009) 165–171
- [171] A. Vallée, S. Besner and J. Prud'homme, Comparative study of poly(ethylene oxide) electrolytes made with LiN(CF₃SO₂)₂, LiCF₃SO₃ and LiClO₄: Thermal properties and conductivity behavior, *Electrochim. Acta*, 37 (1992) 1579
- [172] N. Kobayashi, S. Sunaga, R. Hirohashi, Effect of additive salts on ion conductivity characteristics in solid polymer electrolytes, *Polym.*, 33 (1992) 3044-3048
- [173] D. R. Lide, *CRC handbook of chemistry and physics*, CRC, Boston, (2000) 12–20
- [174] B. L. Papke, M.A. Ratner, D.F. Shriver, Conformation and ion-transport models for the structure and ionic conductivity in complexes of polyethers with alkali metal salts, *J. Electrochem. Soc.*, 129 (1982) 1694-1701
- [175] M. G. Brik, C. N. Avram, I. Tanaka, Crystal field analysis of energy level structure of LiAlO₂:Cr₄₊ and LiGaO₂:Cr₄₊, *Phys. Stat. Sol. (b)* 241 (2004) 2501–2507
- [176] Z. Anorg, Crystal Structure of LiClO₄, *Allg. Chem.* 629 (2003) 1466-1468
- [177] M. Tremayne, P. Lightfoot, M. A. Mehta, P. G. Bruce, Ab Initio structure determination of LiCF₃SO₃ from X-ray powder diffraction data using entropy maximization and likelihood ranking, *J. Solid State Chem.*, 100 (1992) 191-196

- [178] M. A. Ratner, A. Nitzan, Conductivity in polymer ionics. dynamic disorder and correlation, *Faraday Discuss. Chem. Soc.*, 88 (1989) 19–42
- [179] M. J. Reddy, P. P. Chu, U.V. S. Rao, Study of multiple interactions in mesoporous composite PEO electrolytes, *J. Power Sources*, 158 (2006) 614-619
- [180] W. Wieczorek, D. Raducha, A. Zalewska, J. R. Stevens, Effect of salt concentration on the conductivity of PEO-based composite polymeric electrolytes, *J. Phys. Chem. B*, 102 (1998) 8725-8731
- [181] S. J. Wen, T. J. Richardson, D. I. Ghantous, K.A. Striebel, P.N. Ross, E.J. Cairns, FTIR characterization of PEO+LiN(CF₃SO₂)₂ electrolytes, *J. Electroanal. Chem.*, 408 (1996) 113-118.
- [182] J. Zhou, S. Fedkiw, Ionic conductivity of composite electrolytes based on oligo(ethylene oxide) and fumed oxides, *Solid State Ionics* 166 (2004) 275-293
- [183] L. Bandara, M. Dissanayake, B. Mellander, Ionic conductivity of plasticized (PEO)-LiCF₃SO₃ electrolytes, *Electrochim. Acta*, 43 (1998) 1447-1451
- [184] J. A. Forrest, K. Dalnoki-Veress, J. R. Dutcher, Interface and chain confinement effects on the glass transition temperature of thin polymer films, *Phys. Rev.*, E 56 (1997) 5705–5716
- [185] L. Fan, X. Wang, F. Long, X. Wang, Enhanced ionic conductivities in composite polymer electrolytes by using succinonitrile as a plasticizer, *Solid State Ionics*, 179 (2008) 1772-1775
- [186] Z.H. Li, H.P. Zhang, P. Zhang, G.C. Li, Y.P. Wu, X.D. Zhou, Effects of the porous structure on conductivity of nanocomposite polymer electrolyte for lithium ion batteries, *J. Membr. Sci.*, 322 (2008) 416–422
- [187] B. K. Choi, K. H. Shin, Effects of SiC and Si₃N₄ fillers on the electrical properties of (PEO)₁₆LiClO₄ electrolytes, *J. Appl. Electrochem.*, 27 (1997) 365-367
- [188] J. P. Lemmon, M. M. Lerner, Effect of salt concentration on the ionic conductivity of amorphous poly(ethylene oxide)-sodium salt complexes, *Macromol.*, 25 (1992) 2907–2909
- [189] J. Lee, Y. Lee, W. Chae, Y. Sung, Enhanced ionic conductivity in PEO-LiClO₄ hybrid electrolytes by structural modification, *J. Electroceram.*, 17 (2006) 941–944
- [190] G. W. Ehrenstein, *Polymeric materials : structure, properties, applications*, Hanser Gardner Publications, Cincinnati, Ohio (2001)
- [191] J. Xia, X. Qiu, S. Zheng and X. Tang, Nanocomposite polymer electrolyte comprising PEO/LiClO₄ and solid super acid: effect of sulphated-zirconia on the crystallization kinetics of PEO, *Polym.*, 20/ (2005) 5702-5706

- [192] R. Kawano, M. Watanabe, Equilibrium potentials and charge transport of an I^-/I_3^- redox couple in an ionic liquid, *Chem. Commun.*, 3 (2003), 330–331
- [193] S. L. Rosen, *Fundamental principles of polymeric materials*, Wiley, New York (1993)
- [194] R. Bonart, R. Hosemann, R.L. McCullough, The influence of particle size and distortions upon the X-ray diffraction patterns of polymers, *Polym.*, 4 (1963) 199-211
- [195] P. Sorensen, T. Jacobsen, Phase diagram and conductivity of the polymer electrolyte $(PEO)_xLiCF_3SO_3$. *Poly. Bull.*, 9 (1983) 47-51
- [196] Z. Huo, S. Dai, K. Wang, F. Kong, C. Zhang, X. Pan, X. Fang, Nanocomposite gel electrolyte with large enhanced charge transport properties of an I_3^-/I^- redox couple for quasi-solid-state dye-sensitized solar cells, *Sol. Energ. Mater. & Sol. Cells*, 91 (2007) 1959-1965
- [197] P. Maher, A. McNeil, N. Hampson, The electrochemistry of porous zinc—III. Plain and polymer-bonded porous microelectrodes in perchlorate solutions, *Electrochim. Acta*, 30(1985) 947-960
- [198] M. L. G. Mancini, T. Hanrath, D. Teeters, Characterization of the passivation layer at the polymer electrolyte/lithium electrode interface, *Solid State Ionics*, 135 (2000) 283–290
- [199] J. Xi, X. Qiu, T. X. Ma, M. Cui, J. Yang, X. Tang, W. Zhu, L. Chen, Composite polymer electrolyte doped with mesoporous silica SBA-15 for lithium polymer battery, *Solid State Ionics*, 176 (2005) 1249–1260
- [200] Y. Tominaga, S. Asai, M. Sumita, S. Panero, B. Scrosati, A novel composite polymer electrolyte: Effect of mesoporous SiO_2 on ionic conduction in poly(ethylene oxide)– $LiCF_3SO_3$ complex, *J. Power Sources*, 146 (2005) 402–406